Discovery of novel small molecule inhibitors of Bcl10-MALT1 interaction for the treatment of aggressive diffuse large B-cell lymphoma

by

Heejae Kang

BA, UC Berkeley, 2010

Submitted to the Graduate Faculty of the

School of Medicine in partial fulfillment

of the requirements for the degree of

Doctor of Philosophy

University of Pittsburgh

2020

UNIVERSITY OF PITTSBURGH

SCHOOL OF MEDICINE

This dissertation was presented

by

Heejae Kang

It was defended on

March 27, 2020

and approved by

Charleen Chu, Professor, Department of Pathology

Jian Yu, Professor, Department of Pathology & Department of Radiation Oncology

Bill Chen, Associate Professor, Department of Medicine

Melanie Scott, Associate Professor, Department of Surgery

Dissertation Director: Peter Lucas, Professor, Department of Pathology

Dissertation Director: Linda McAllister-Lucas, Professor, Department of Pediatrics

Discovery of novel small molecule inhibitors of Bcl10-MALT1 interaction for the treatment of aggressive diffuse large B-cell lymphoma

Heejae Kang, PhD

University of Pittsburgh, 2020

The CARMA1/Bcl10/MALT1 (CBM) signaling complex mediates antigen receptor-induced activation of the pro-survival NF-kB transcription factor in lymphocytes to support normal adaptive immunity. Gain-of-function mutations in the CARMA1 moiety or its upstream regulators trigger antigen-independent assembly of oligomeric CBM complexes, leading to constitutive activation of both the protease and scaffolding functions of MALT1, inappropriate NF-kB activity, and development of an aggressive Activated B-Cell subtype of Diffuse Large B-Cell Lymphoma (ABC DLBCL).

Since MALT1 activation relies on its recruitment to the CBM complex via its interaction with Bcl10, we sought to identify inhibitors of Bcl10-MALT1 interaction in order to target both the protease and scaffolding activities of MALT1 as a potential approach for treating ABC DLBCL. After confirming that Bcl10 residues 107-119 and the tandem Ig-like domains of MALT1 are critical for interaction, we performed a structure-guided *in silico* screen of 3 million compounds based on a computational model of the experimentally identified interaction interface.

Compound K691-0124 from the initial screening hits and its structural derivative, compound K691-0122, show dose-responsive inhibition of Bcl10-MALT1 interaction. Functionally, both compounds inhibit both the protease and scaffolding activities of MALT1 in Jurkat T cells, as demonstrated by its inhibition of CD3/CD28-induced RelB and N4BP1 cleavage, and inhibition of IKK phosphorylation, respectively. Both compounds also block *IL2* transcription

and IL-2 secretion by PMA/ionomycin-stimulated Jurkat T cells, as well as constitutive CBM-dependent secretion of IL-6 and IL-10 by ABC DLBCL cells. Accordingly, these two compounds selectively suppress the growth of ABC DLBCL cell lines, but does not affect the growth of MALT1-independent GCB DLBCL cell lines.

In conclusion, we have developed two early-stage small molecule compounds that inhibit Bcl10-MALT1 interaction, impair both protease and scaffolding activities of MALT1, inhibit secretion of cytokines encoded by MALT1-controlled downstream NF-kB target genes, and specifically inhibit proliferation of MALT1-driven ABC DLBCL cell lines. This new class of protein-protein interaction inhibitors has the potential for a more complete and efficacious blockade of MALT1, while offering protection from undesirable autoimmune side effects of unbalanced blocking of only the protease activity of MALT1, in the treatment of this aggressive form of lymphoma.

Table of Contents

List of Tables

List of Figures

Preface

I would like to express my sincerest gratitude to my advisors, Peter and Linda, for their mentorship, bottomless enthusiasm and drive for new discoveries, and the incredible amount of time and commitment that they have invested into my scientific and personal growth during my PhD training. I would also like to thank all the talented members of the Lucas lab, especially Dong Hu, Jing Cheng, Lisa Maurer, Linda Klei, Matthew Trotta, Prasanna Ekambaram, and Kelly Bailey for their intellectual and technical contributions and countless discussions on the best way forward in continuously developing this project. I also thank my collaborators at University of Michigan, Zaneta Nikolovska-Coleska, Marcelo Murai, and Ahmed Mady, as well as Bill Chen for extending their expertise and support for this project.

I am grateful for the support within the MD-PhD program, School of Medicine, Department of Cellular and Molecular Pathology, Department of Pediatrics, Children's Hospital of Pittsburgh Foundation, and the Institute of Precision Medicine, including Richard Steinman, Gwen Sowa, Joan Harvey, Wendy Mars, Amanda Bytzura, Carla Clarke, and Carol Ashby, as well as the members of my committee, Charleen Chu, Bill Chen, Melanie Scott, and Jian Yu, for their invaluable insight, discussions, and guidance.

I am grateful for the Conover family, Noelle, David, and Megan, whose generosity and passion for cancer research has supported this work. I would like to thank Matt Conover and all the patients and their families whose courage and heart in the face of devastating experiences are my greatest inspiration and drive in my career.

I sincerely thank all of my family and friends who have been unwavering sources of laughter, joy, and love through the highs and lows, especially my mom and dad, my best friend

and sister, Stephen, Max, Jenny, Patricia, and Aaron. I would not be here today without your love and encouragement. Thank you.

1.0 Introduction

The cancer death rate declined by 29% from 1991 to 2017, including a 2.2% drop from 2016 to 2017, the largest single-year drop in cancer mortality ever reported (1). This improvement was in significant part due to advances in treatment – mainly immunotherapy and targeted therapies – which has improved the conventional foundation of cancer treatment of chemotherapy, surgery, and radiation therapy. These advances in precision medicine have helped transform cancer treatment: patients with leukemia, melanoma, as well as breast, lung, and colorectal cancers routinely undergo molecular testing in order to select treatments tailored to the genetic profile of an individual's tumor that improve survival and reduce adverse systemic effects. For example, the 5-year relative survival rate for chronic myeloid leukemia increased from 22% in the mid-1970s to 70% for those diagnosed during 2009-2015, and most people treated with tyrosine kinase inhibitors now have nearly normal life expectancy (1). Despite the profound declines in *overall* mortality, a lack of improvement in survival rates in many cancers largely reflect a lack of major treatment advances, and cancer remains the second leading cause of death globally, responsible for an estimated 9.6 million deaths in 2018 (World Health Organization).

This thesis aims to investigate a largely unexplored area in targeted cancer therapy development: inhibition of protein-protein interactions. The majority of intracellular drug targets in targeted drug discovery field have focused on enzymes, such as kinases, that catalyze reactions. Enzymatic targets have proven easier to develop drugs against, primarily due to the ease of screening against enzymes in high-throughput biochemical assays and due to the fact that enzymes already have discrete active sites with small pockets or grooves for binding substrates. Protein-protein interactions (PPIs), on the other, have long been considered "undruggable" until recently,

because of the relatively flat, large, and featureless interface between interacting protein partners, seemingly rendering them unable to bind small molecule drugs. Despite these challenges, 650,000 PPIs have been estimated by proteomics studies, compared to only 20,000 protein coding genes (2, 3), and PPIs have always been highly desirable targets in cancer therapy development, as the structured assembly of protein complexes and its regulation are of critical importance in nearly all normal cellular functions, including gene expression, cell division, protein homeostasis, and modulating key signaling pathways in the cell. Correspondingly, this organized coordination of assembly and dynamics of multi-protein complexes is hijacked in many pathologies, including cancer and autoimmune disorders. Importantly, because the assembly process of multi-protein complex has evolved as a strategy that uses sequential obligate steps in space and time to increase selectivity in molecular recognition, PPI interfaces tend to be less conserved and more diverse than active sites of enzymes. Moreover, the requirement of multiple constituent proteins coming together to initiate a signal in and of itself allows for greater specificity and signal-to-noise ratio (4, 5). Thus, PPI inhibitors are generally thought to have a greater opportunity for being selective compared to enzymatic inhibitors. In addition, advances in highly sensitive methods, such as NMR, X-ray diffraction, electron microscopy, and surface plasmon resonance, have improved our structural and biological understanding of PPIs, facilitating the discovery and development of small molecule PPI-targeting drugs. Finally, the declining cost of computational power has led to wider accessibility and routine use of virtual screening with increasing number of compounds from in silico libraries, greatly accelerating the pace of PPI therapeutic development over the past few years. Although more challenging to develop compared to enzymatic inhibitors, targeting PPIs has a tremendous potential for therapeutic intervention in cancer.

Since the discovery of Bcl10-MALT1 protein-protein interaction in MALT lymphoma two decades ago, we have gained detailed understanding of the critical importance of NF-kB-activating signaling complex comprising the CARMA1, Bcl10, and MALT1(CBM) proteins in a variety of B-cell and T-cell lymphomas and leukemias. Although the function of CBM complex is best known in the context of TCR and BCR signaling in adaptive immune cells, more recent studies have discovered that the multimeric CBM complex containing CARMA3 instead of CARMA1 is ubiquitously expressed and operates downstream of various receptors in non-lymphoid cells. A variety of G-protein-coupled receptors (GPCRs) (e.g. AGTR1, PAR1, CXCR4) and receptor tyrosine kinases (RTKs) (e.g. EGFR, HER2/neu) have been shown to rely on the CBM complex to mediate NF-kB activation. Accordingly, CBM hyperactivity due to inappropriate overexpression or activation of GPCRs or RTKs is attributed to various oncogenic processes in solid tumors, including tumor growth, epithelial-mesenchymal transition, angiogenesis, and metastasis. (6-10) Moreover, aberrant overaction of MALT1 has been implicated in multiple sclerosis and other Th17-dependent autoimmune inflammatory disorders.

Thus, deregulated CBM signaling is a common factor underscoring major subsets of hematological malignancies, solid tumors, and autoimmune diseases. Given this broad range of therapeutic applicability of CBM-specific targeted therapies, there has been considerable interest and effort in the field to develop drugs to target MALT1 activity. Although this thesis focuses on the efficacy of two promising lead compounds to terminate inappropriate CBM activity in a specific model of diffuse large B-cell lymphoma, we see substantial potential in multiple disease models.

1.1 Diffuse large B-cell lymphoma (DLBCL)

Diffuse large B-cell lymphoma (DLBCL) is the most common type of non-Hodgkin lymphoma (NHL), accounting for roughly 40% of newly diagnosed NHL cases globally. (Sehn et al Blood 2015) According to the US National Cancer Institute's SEER database, the estimated incidence of DLBCL is 7 per 100,000, affecting approximately 20,000 people every year in the US. The current standard of care, R-CHOP, consists of a chimeric monoclonal antibody against CD20 expressed on the surface of B cells (Rituximab), a combination of three chemotherapy drugs (cyclophosphamide, doxorubicin hydrochloride, vincristine), and a corticosteroid (prednisolone). Approximately 40% of patients with DLBCL who are treated with R-CHOP will relapse or develop refractory disease (11). There are two major molecularly distinct subtypes of DLBCL identified by gene expression profiling: **a**ctivated **B**-**c**ell (ABC) and **g**erminal **c**enter **B**-cell (GCB). This molecular classification of DLBCL carries important prognostication difference, with the ABC subtype being associated with significantly lower survival compared to the GCB subtype (35% 5-year OS in ABC subtype vs. 60% in GCB subtype). Despite this significant difference in prognosis, the current R-CHOP regimen has remained the same between two distinct molecular subtypes, and thus, subtype testing for frequently recurring mutations are currently not routinely used. These two subtypes are driven by distinct intracellular oncogenic signaling pathways, which can be differentially targeted as a therapeutic approach. Novel therapies targeting mutations that occur in the ABC type is needed to improve patient outcome and survival.

1.1.1 Germinal center B-cell diffuse large B-cell lymphoma (GCB DLBCL)

Using cell of origin (COO) as a subtype classification, approximately 40-50% of DLBCL are classified as germinal center B-cell subtype (12-14). GCB DLBCLs are derived from lymphoid cells in the germinal center. Approximately 30-40% of GCB DLBCLs have a t(14;18) translocation, 30% have c-rel amplification, 20% have mutations of the histone methyltransferase EZH2, and deletion of tumor suppressor PTEN is observed in 55% of GCB DLBCL (15), all of which are typically not seen in ABC DLBCL. Constitutive activation of phosphatidylinositol 3 kinase (PI3K)/AKT/MTOR signaling pathway in GCB DLBCL lacking PTEN drives the growth and metabolism of tumor cells, spurring development of multiple inhibitors against this pathway.

1.1.2 Activated B-cell diffuse large B-cell lymphoma (ABC DLBCL)

ABC DLBCL is the more aggressive and chemoresistant subtype with poor prognosis, accounting for 30-40% of DLBCL (12-14). ABC DLBCL is derived from B cells at a plasmablastic stage, just before exiting the germinal center, and therefore display gene expression profile of mature plasma cells. The pathogenic hallmark of ABC DLBCL is the antigen-independent, constitutive activation of the NF-kB pathway in B lymphocytes, largely due to inappropriate activation of the CBM signaling complex (composed of proteins **C**ARMA1, **B**cl10, and **M**ALT1), which is normally only transiently active following antigen stimulation. A loss-of-function RNA interference (RNAi) screening by Ngo et al in 2006 revealed that all(16) genes critical for the survival of ABC DLBCL are involved in regulating NF-kB activity. These genes included *CARMA1, BCL10*, *MALT1*, and *IKKβ*. Silencing individual CBM proteins using RNAi was toxic to ABC DLBCL cell lines, but not to GCB-DLBCL cell lines. Subsequent studies found that

approximately 10% of ABC DLBCLs harbor activating mutations of CARMA1, and 20% of cases harbor mutations in the components of the BCR complex, CD79A/B, thereby engaging the CBM pathway downstream. Mutations in MYD88 have been identified in ~30% of ABC DLBCL, leading to upregulation of both NF-kB and Janus kinase-signal transducer and activator of transcription (JAK/STAT) pathways. Of note, the activating missense mutations within the coiled-coil domain of CARMA1 disrupt the intra-and intermolecular interactions that are critical for maintaining its autoinhibition by the ID domain of CARMA1, resulting in constitutive assembly of the CBM complex and constitutive activation of NF-kB (17).

In ABC DLBCL, autocrine IL-6 production has been shown to provide proliferative and antiapoptotic signals, and elevated IL-6 levels in patient serum correlate with adverse outcome (18, 19). Previous studies have shown that ABC DLBCL cell lines, OCI-Ly3 and TMD8, spontaneously secrete IL-6 and IL-10 (20), and that transcription and expression of these two cytokines depend on MALT1 protease activity (21).

Considerable knowledge has been gained in the field of CBM biology in the context of not only ABC DLBCL, but also in increasing number of T and B cell malignancies recognized to trigger CBM assembly to drive chronic antigen receptor signaling. Disrupting the intra- and intermolecular interactions within the CBM complex can modulate downstream NF-kB signaling in ABC DLBCL as well as various hematologic malignancies whose pathogenic hallmark is constitutive NF-kB activation.

1.2 The CARMA1-Bcl10-MALT1 (CBM) signaling complex

The CBM signaling complex, which is composed of proteins Caspase recruitment domain-containing MAGUK protein1 (CARMA1, also known as CARD11), B-cell lymphoma 10 (Bcl10) and Mucosa-associated lymphoid tissue lymphoma translocation protein 1 (MALT1), is a critical signaling complex that mediates T-cell receptor (TCR) and B-cell receptor (BCR)-dependent NF-κB activation. T and B cells isolated from mice deficient in *CARMA1*, *BCL10*, or *MALT1* display impaired cellular activation and proliferation, aberrant cytokine secretion, and defective cell differentiation, resulting in diminished immunity. *CARMA1*, *BCL10*, and *MALT1* are bona fide oncogenes: mutations, chromosomal translocations, and overexpression of CBM component proteins have shown to directly lead to multiple lymphoid malignancies, including activated B-cell diffuse large B-cell lymphoma (ABC DLBCL). In resting cells, the CBM members exist in an inactive form in the cytoplasm. CARMA1 is kept in an inactive monomeric form, whereas the catalytically inactive paracaspase MALT1 is constitutively bound to Bcl10. Upon receptor ligation, TCR or BCR engages the proximal antigen receptor signaling cascades that converge in the activation of protein kinase C (PKC) θ or β, respectively, leading to phosphorylation-dependent activation of CARMA1 and the subsequent recruitment of Bcl10 and MALT1 to form the CBM complex (22-24). This inducible assembly of the CBM complex involves the formation of a high-order filamentous structure that serves as a docking surface for the recruitment of downstream signaling mediators of NF-κB. MALT1, the effector molecule of the CBM complex, promotes downstream NF-kB signaling via both its scaffolding and protease functions.

Then, given the critical role that the CBM complex plays in normal adaptive immune response as well as inappropriate CBM hyperactivation in oncogenic settings that needs to be

dampened, disrupting this complex for cancer therapeutic purpose requires a consideration of delicate immunomodulation.

1.2.1 The role of the CBM complex in hematological malignancies

Since the discovery of Bcl10-MALT1 interaction in MALT 1ymphoma two decades ago, multiple groups have identified constitutive CBM signaling in an increasing number of B and T cell lymphomas, including diffuse large B-cell lymphoma (DLBCL), mantle cell lymphoma (MCL) (25-27), acute T-cell leukemia/lymphoma (ATLL) (28), chronic lymphocytic leukemia (CLL) (29), cutaneous T-cell lymphoma (CTCL) (30, 31), peripheral T-cell lymphomas (PTCL) (32), and B-cell expansion with NF-kB and T-cell anergy (BENTA) disease (33-35).

In addition to ABC DLBCL (detailed in section 1.1), in which the pathogenic role of CBM signaling is best described, a subset of MCL has been shown to depend on chronic BCR-driven constitutive MALT1 signaling and NF-kB activation (26). Germline gain-of-function mutations in the CARD or between the CARD and coiled-coil domain of CARMA1 were identified in patients with BENTA disease. Of note, patients with BENTA have an increased risk of developing lymphoma, which suggests that CARMA1 mutations are predisposing, but not sufficient for lymphomagenesis by itself (33-35). Beyond B-cell malignancies, gain-of-function mutations in CARMA1 (in the coiled-coil domain and in the linker domain) or in upstream TCR signaling components, such as PLCγ1, PKCβ, CD28 were also identified in adult T-cell leukemia/lymphoma (ATLL) (28) and in an aggressive leukemic form of cutaneous T-cell lymphoma called Sezary syndrome (30, 31). Taken together, the CBM complex represents a critical hub for oncogenic signaling pathway in an increasing number of B-cell and T-cell malignancies.

1.2.2 The role of the CBM complex in inflammatory autoimmune diseases

As expected, MALT1-deficient mice display general immunodeficiency with defects in B and T cell activation, B1 and marginal zone B cell development (36, 37). These mice fail to produce detectable amounts of antigen-specific IgM or IgG antibodies. Total number and distribution of CD4+ and CD8+ T cells in the spleen or lymph node are unaffected, but there is complete absence of regulatory T cells (Tregs) in the thymus and periphery. Moreover, MALT1 KO mice were found to be protected from induction of multiple sclerosis model of experimental autoimmune encephalitis (EAE) (38, 39), highlighting the fact that CBM signaling mediates both protective and pathologic immune responses.

In MALT1 protease-dead knock-in mice (MALT1 PD mice), where a catalytically inactive MALT1 is expressed by replacing the active site cysteine with alanine ($MALT1^{C472A/C472A}$), the MALT1 protease function is lost, while the scaffold function for NF-kB activation is preserved. These MALT1 PD mice were found to phenocopy most of the immune defects of completely MALT1-deficient mice, but an unexpected destructive autoimmunity with inflammation of several organs with immune cell infiltration was also observed, including the development of spontaneous autoimmune gastritis (40-43). These animals displayed a severe deficiency in the development of FoxP3+ regulatory T cells (Tregs), and adoptive transfer of functional Tregs reduced autoimmune symptoms (41). Although MALT1 KO mice are characterized by even more severe deficiency of Tregs, they are protected from the development of autoimmunity, because they also lack the immune activation from the loss of both the protease and scaffold functions of MALT1. To recap, the inflammatory phenotype of MALT1 PD mice is believed to be caused by residual immune activation in which T cells are still able to activate NF-kB by the preserved MALT1 scaffold

function, combined with defective peripheral tolerance from impaired Treg development, resulting in T cell activation that cannot be checked by Tregs.

Moreover, MALT1-deficient mice also show severe impairment in the differentiation of T helper 17 (Th17) cells and loss of MALT1 has been shown to interfere with IL-17 and GM-CSF production, indicating that MALT1 signaling is necessary for Th17 differentiation and function (39, 44). Th17 cells are key inflammatory drivers characterized by their production of IL-17, IL-21, IL-22, TNF, and GM-CSF, and they are regarded as the main effector/pathogenic cell type in multiple sclerosis and other autoimmune diseases. The MALT1 protease cleaves and inactivates a number of mRNA stability regulators, including Regnase-1, Roquin-1, and Roquin-2, such that inactivation of MALT1 protease leads to excessive interferon gamma (IFN-γ) secretion by effector lymphocytes, contributing to the observed destructive autoinflammation in MALT1 PD mice (40, 45). MALT1 protease-mediated cleavage of A20, RelB, CYLD, and Regnase-1 have also been shown to contribute to TCR-induced IL-2 secretion in mouse T cells (46), which is essential for Treg development and function. Accordingly, T cells deficient in CARMA1, Bcl10, or MALT1 which leads to impairment in NF-kB activation downstream, each exhibits defective TCR-mediated IL-2 production (36, 47-51). Cleavage of Regnase-1, Roquin-1, and Roquin-2 also stabilize several mRNAs of c-Rel, IRF-4, IL-6, IL-12b, and ICOS, that encode proteins important for optimal Th17 differentiation (45, 52, 53). The observation that MALT1-deficient mice are completely protected against the induction of EAE (38, 39), combined with another study that the MALT1 protease inhibitor, Mepazine, is able to partially attenuate EAE induction and progression (54), supports the therapeutic potential of MALT1 inhibitors in the treatment of MS, especially of an inhibitor that can block both the protease and scaffold activity of MALT1 in its entirety to suppress both effector T cells and regulatory T cells.

Thus, beyond its key role in lymphomagenesis and anti-cancer target, MALT1 also plays an essential role in differentiation and function of Th17 cells, making it an attractive therapeutic target for chronic, T-cell mediated autoimmune inflammatory disorders, including multiple sclerosis, as well as other Th17-mediated diseases, such as rheumatoid arthritis, psoriasis, ulcerative colitis, etc.). MALT1 has been associated with multiple sclerosis in humans from a genome-wide association study (55).

1.2.3 The role of the CBM complex in solid tumors

Given the ubiquitous expression of CARMA1/3, Bcl10, and MALT1 in multiple cell types and its critical role in normal adaptive immunity under multiple types of receptors in both lymphoid and non-lymphoid cells, deregulated CARMA3, Bcl10, and MALT1 (C3BM) complex has also been implicated in multiple solid tumors, including breast cancer (6, 9, 10), osteosarcoma (7), ovarian cancer (56), oral squamous cell carcinoma (57), and lung cancer (8, 58).

1.3 Structural architecture of the CBM signaling complex

1.3.1 CARMA1 – a multi-modular scaffold protein

CARMA1, a member of the caspase recruitment domain (CARD)-containing membrane-associated guanylate kinase (MAGUK) family, is an essential signaling component that mediates antigen receptor-induced NF-kB activation in lymphocytes. CARMA1 contains an N-terminal CARD, a coiled-coil (CC) domain, a linker region, and a MAGUK signature motif comprising a

PDZ domain, a Src homology 3 (SH3) domain and a GUK domain in the C-terminus (59) (Figure 1). In its resting state, CARMA1 is kept inactive in a closed, auto-inhibited conformation via intramolecular interactions. Upon antigen receptor engagement, phosphorylation of the CARMA1 linker region (also referred to as the Inhibitory Domain) converts CARMA1 to an active, open conformation, allowing it to associate with signaling proteins and leading to IKK activation (17, 60, 61).

CARD of CARMA1 has been shown to associate directly with the CARD of Bcl10 (62, 63). The CARMA1 CARD, like all CARDs, possesses acidic and basic surfaces which carry opposite charges to mediate their interactions. The CC domain of CARMA1, which contains approximately four discontinuous coiled-coil motifs, mediates the oligomerization that is required for TCR-induced NF-kB activation. A CARMA1 construct comprising the N-terminal CARD and the first coiled-coil segment exists in solution as a trimer, while a CARMA1 construct with two CC motifs produces a soluble protein with a higher oligomerization state, and CARMA1 constructs containing more than the first two coiled-coil segments produced only insoluble proteins, indicating even higher-order oligomerization and aggregation. Intra- and inter-molecular interactions of the SH3 and GUK domains of CARMA1 also play a role in the oligomerization and membrane recruitment of CARMA1 and CARMA1 microcluster formation.

Gain-of-function mutations within the CARD and CC domains of CARMA1 occur in a variety of lymphoid neoplasms, including activated B-cell diffuse large B-cell lymphoma (ABC DLBCL), and these mutations disrupt multiple repressive elements in the linker region to allow partial conversion of CARMA1 to an open, active state (60, 61, 64). Taken together, CARMA1 is a multi-modular scaffold protein, and only carefully coordinated conformational changes of distinct domains are able to drive the formation of the CBM complex. Accordingly, disruption of

intra- and inter-molecular interactions within CARMA1 via gain-of-function mutations leads to dysregulation of CBM assembly and NF-kB signaling, and inappropriate proliferation and survival of lymphoma cells.

1.3.2 Bcl10 – a filamentous adapter

Bcl10 contains an N-terminal CARD domain and an unstructured C-terminal serine/threonine-rich motif (Figure 1). The key function of Bcl10 is to serve as the linker within the CBM complex. Endogenous Bcl10 displays a diffuse cytosolic distribution, whereas overexpression of Bcl10 in the cell induces formation of filament-like structures shown by fluorescence microscopy. The CARD of Bcl10 is necessary and sufficient to promote filamentous oligomerization, evidenced by the ability of C-terminal-truncated forms of Bcl10 to still self-aggregate (65, 66). Bcl10 oligomerization through its CARD (AA 1-119) is able to strongly induce NF-kB activation (67). In T cells, TCR stimulation can induce formation of punctate and filamentous structures called POLKADOTS (punctuated and oligomeric killing or activating domains transducing signals), which are cellular foci of enriched interactions between Bcl10 and partner signaling proteins that mediate NF-kB activation (68, 69).

Unlike the CARMA1 CARD, purified Bcl10 CARD has a tendency to aggregate and does not remain in a soluble state. Since Bcl10 CARD forms filaments spontaneously in vitro and in cells, solving the crystal structure of Bcl10 has proven to be a challenge. However, the E53R mutation within the Bcl10 CARD generates monomeric Bcl10, allowing for its structural determination in solution using nuclear magnetic resonance (NMR) (Protein Data Bank (PDB) ID: 2MB9). NMR analysis of this monomeric mutant of Bcl10 CARD revealed that the Bcl10 CARD is quite different from other DD superfamily structures, with unusually long α1 and α6 helices.

Negative-staining EM reconstruction of Bcl10 CARD (AA 1-115) filament showed that there are two major types of interfaces between Bcl10 subunits within the filament: interstrand and intrastrand interfaces (70). Subsequent cryo-EM analyses of the Bcl10 (AA 1-205) filament (PDB ID: 6BZE) and full length Bcl10 (PDB ID: 6GK2) identified three distinct types of Bcl10 CARD-CARD interactions: type I and II interactions represent interstrand contacts between adjacent Bcl10 monomers, whereas the type III interaction facilitates the charge-charge intrastrand contacts (71, 72). The Bcl10 E53R mutant, which involves the type III interaction, completely disrupted filament formation. On the other hand, Bcl10 with mutations targeting type I and II interfaces (Bcl10 R62E and R36E, respectively) still formed filaments at high protein concentrations, suggesting that the type III charge-charge intrastrand contacts facilitate the strongest interaction for filament formation (71).

Through CARD-CARD interactions, Bcl10 assembles into a hollow helical filament with a left-handed symmetry and three to four Bcl10 subunits per helical turn. Time-lapse confocal microscopy showed that Bcl10 polymerization occurs in a unidirectional manner. When the cryo-EM structure of Bcl10 CARD in filament form was superimposed with the previous NMR structure of monomeric Bcl10 CARD in solution, the most notable mismatches occurred at α2, α3-α4 loop, and α5-α6 loop. These misaligned regions coincide with the positively charged surfaces on the growing end of the filament that interact with the negatively charged surfaces on the next Bcl10 monomer joining the filament. Compared to the negatively charged surface, the positively charged surface in a Bcl10 filament showed greater conformational difference between monomeric solution form and the filament form. These differential conformational changes govern the unidirectional polymerization of Bcl10 (71).

1.3.3 MALT1 – a protease and a scaffold

The human paracaspase, MALT1, is a caspase-like Bcl10-binding protein that is integral to CBM-dependent NF-kB activation by acting as the effector protein of the complex. MALT1 is characterized by an N-terminal death domain (DD) followed by two immunoglobulin (Ig)-like domains (Ig1 and Ig2), a C-terminal caspase-like enzymatic domain and a third Ig-like domain (Ig3) (Figure 1). MALT1 and Bcl10, both independent targets of chromosomal translocation in MALT lymphoma, were first discovered to interact with each other to mediate synergistic activation of the NF-kB signaling pathway (73). MALT1 has been shown to constitutively associate with Bcl10 in cells without stimulation (73, 74). Mutational analyses coupled with co-immunoprecipitation suggest that a small region at the C-terminal end of the Bcl10 CARD extending into the serine/threonine-rich motif and N-terminal region of MALT1 containing the DD and the two Ig-like domains mediate their association (69, 73, 75). Recently, Schlauderer et al examined the cryo-EM structure of the complex of full-length Bcl10 and MALT1 (AA 29-722). This Bcl10-MALT1 complex showed a helical arrangement that is similar to that of the overall Bcl10 CARD core filament. Remarkably, the MALT1 DD rigidly attached to Bcl10 at the rim of the Bcl10 CARD core filament in a 1:1 stoichiometry with the C-termini of MALT1 DDs pointing away from the core filament (Figure 1). MALT1 binds to the C-terminal end of helix α6 of Bcl10 CARD, forming a distinct interface that is separate from the above mentioned Bcl10 filament interfaces I-III. In the Bcl10-MALT1 interaction, residues V81 and L82 in helix α4 of MALT1 are located at the center of the interacting site I (BM-I). The opposing hydrophobic surface in Bcl10 is formed by V103 and L104 in helix α6 and V83 and I96 in helices α5 and α6, respectively. Mutation in either MALT1 (V81R or L82D) or Bcl10 (L104R) completely blocks the constitutive

binding of Bcl10 and MALT1 in resting cells. Interestingly, these mutations at the Bcl10-MALT1 interface also impaired the binding of Bcl10 to CARMA1, which suggests that constitutive association of Bcl10 and MALT1 may be a prerequisite for recruitment to CARMA1 and thus the assembly of the CBM complex (72).

At a lower resolution of the EM density, MALT1 Ig1 domain is shown to be pointing away from the Bcl10 core-MALT1 DD filament, thus separating the MALT1 C-terminal domains from the inner core of the filament (Figure 1). The top view of the EM structure illustrates a "paddle wheel-like" architecture of the Bcl10-MALT1 complex with the MALT1 Ig1-Ig2 and paracaspase domains forming a more adaptable periphery of the filament. This structural arrangement facilitates the anti-parallel dimerization of the MALT1 paracaspase domains, which is required for MALT1 protease activation (76, 77).

As the effector protein of the CBM signalosome, MALT1 carries out two known functions: 1) scaffolding activity to recruit key downstream signaling mediators, and 2) protease activity to cleave and inactivate specific cellular proteins, notably negative regulators of downstream NF-kB signaling (Table 1) (78, 79). Protein-protein interactions facilitated by MALT1 scaffolding function lead to the recruitment and activation of several ubiquitin ligases and kinases, including inhibitor of kB kinase (IKK) complex. This MALT1 scaffold-dependent IKK activation rapidly but transiently leads to NF-kB activation, and MALT1 protease-dependent cleavage of negative regulators of NF-kB, including RelB and A20 (Table 1 for comprehensive list of MALT1 substrates) ensures sustained and amplified NF-kB activation (52, 80, 81). The protease activity of MALT1 modulates NF-kB activation independently of the IKK complex, evident by the observations that 1) catalytically inactive MALT1-Cys464Ala knock-in mice and 2) inhibition of MALT1 protease in vitro both affect NF-kB activation without noticeable effect on the

phosphorylation of IkBα or IkBβ and p65 (78, 82, 83). Thus, MALT1 scaffolding activity to recruit IKK complex is largely independent of MALT1 proteolytic activity.

Although the protease activity of MALT1 is dispensable for canonical NF-kB signaling, it supports the direct scaffolding activity by modulating the intensity and persistence of the NF-kB response, and the protease activity is also required for optimal T cell activation (78, 81, 82). The active site of MALT1, which includes C464 located in the paracaspase domain, is structurally related to the enzymatic domains of the caspase family of proteins. Unlike true caspases, which specifically cleave their substrates after aspartic acid, MALT1 cleaves its substrates after arginine. Activation of MALT1 is thought to occur through a two-step process: dimerization of the MALT1 paracaspase domain followed by structural rearrangement in the active site that could be induced by substrate binding to stabilize the active site conformation. The first step, dimerization of MALT1 paracaspase domains, is a necessary step toward MALT1 activation, evidenced by complete loss of proteolytic activity with site-specific mutation R551E at the homodimer interface. Crystal structures of the MALT1 paracaspase and Ig3 domains (339-719 or 334-719) in either the active conformation (PDB ID 3UOA, 3UO8, or 3V4L) or the inactive conformation (PDN ID 3V55) both show the paracaspase domains of two monomers forming an antiparallel homodimer. This antiparallel homodimer is formed through interactions between β6 strands and α5 helices of each monomer. However, dimerization by itself is not sufficient for MALT1 activation. The second step in MALT1 activation depends on specific conformational changes that alter the interface between the paracaspase domain and the Ig3 domain of MALT1. Most notably, the L2 loop, which contains the catalytic cysteine, is disordered in the inactive, ligand-free conformation, but becomes substantially stabilized in the active conformation upon binding of the covalent peptidic inhibitor that mimics MALT1 substrate at the active site (76). In this active conformation,

the α2 helix and β2 strand of the paracaspase domain interact with β5/β6 and β2/β3 loops within the Ig3 domain (84).

In addition to promoting MALT1 protease activity, the assembled CBM complex also serves as a docking surface for the recruitment of downstream signaling mediators via MALT1 scaffolding activity. Binding the C-terminal region of MALT1 proteins within the filament induces the oligomerization of the E3 ligase, tumor necrosis factor receptor (TNFR)-associated factor 6 (TRAF6), leading to polyubiquitination of MALT1 and recruitment of the IKK complex to culminate in NF-kB activation (85, 86).

Table 1. Known MALT1 substrates and effects of proteolysis by MALT1.

Substrate	Role	Cleavage site	Effect of proteolysis by MALT1	Reference
A20	Deubiquitinase	Arg439	Enhances NF-kB activation	(80)
RelB	Non-canonical NF-kB transcription factor	Arg85	Enhances NF-kB activation	(52)
MALT1	CBM complex protein	Arg149	Dissociation from Bcl10	(87, 88)
CYLD	Deubiquitinase	Arg324	AP-1 transcription factor activation, endothelial cell permeability	(46)
Regnase-1	RNase	Arg111, Arg510	Stabilizes T-cell effector mRNAs and Th17 differentiation factors	(45, 53)
Roquin-1/2	RNA binding protein	Arg579	Stabilizes T-cell effector mRNAs and Th17 differentiation factors	(45)
Bcl10	CBM complex protein	Arg228	Promotes leukocyte adhesion to fibronectin	(78)

HOIL1	Subunit of LUBAC, E3 ubiquitin ligase for linear ubiquitination	Arg165	Enhances NF-kB activation	(83, 89)
N4BP1	RNase	Arg509	Promotes viral reactivation	(90)

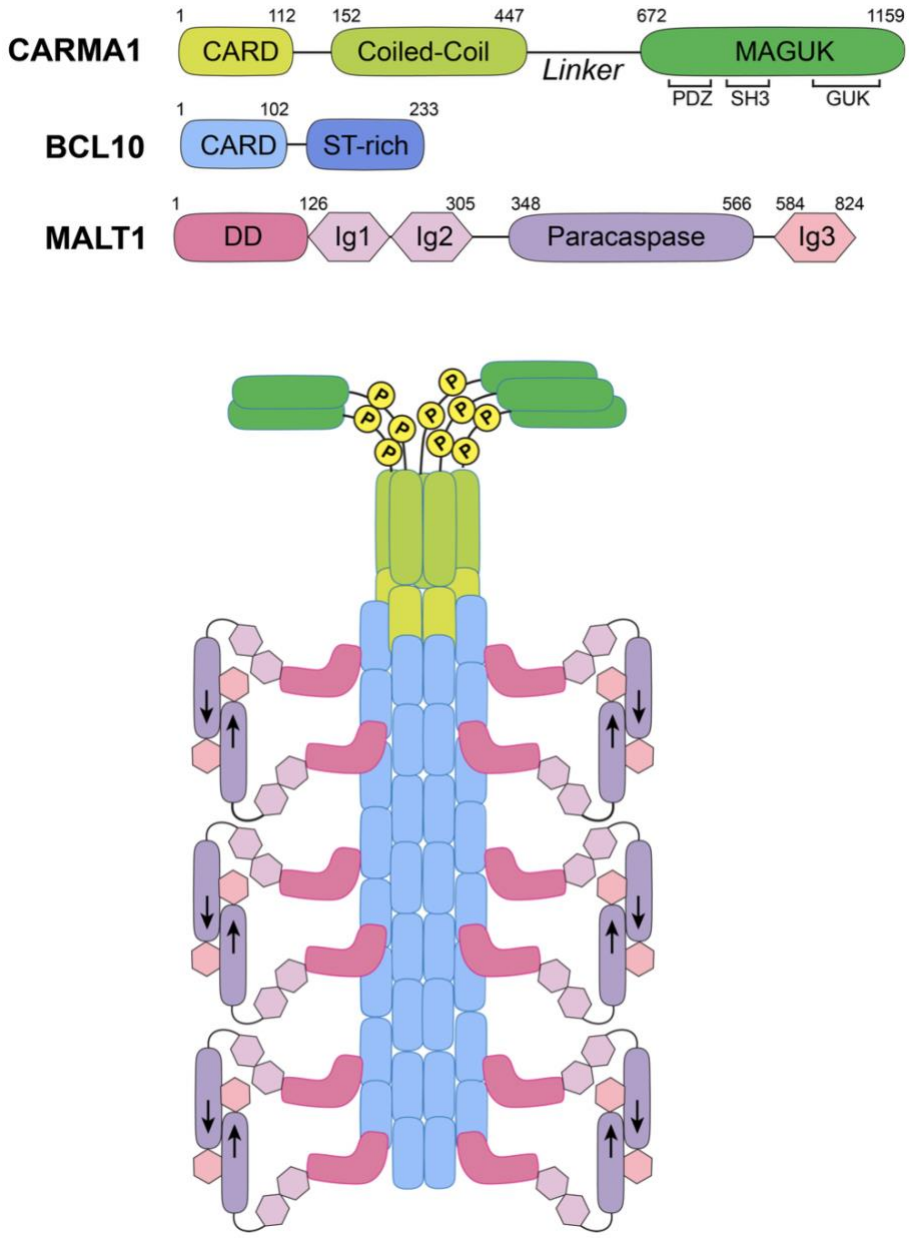

Figure 1. Domain structures of CARMA1, Bcl10, and MALT1 and overall supramolecular filamentous organization of the CBM complex.

Upon PKC-dependent phosphorylation, CARMA1, with its multiple coiled-coil motifs, forms short helical segments to nucleate Bcl10 filaments through heterotypic CARD-CARD interactions. Bcl10 CARD, which is constitutively associated with MALT1 at the DD interface, polymerizes to form a helical filament, with the Ig domains of MALT1 pointing away from the Bcl10 core. This filamentous structural arrangement enables the antiparallel dimerization of MALT1 caspase domains, leading to MALT1 activation.

1.4 A review of novel targeted drugs for ABC DLBCL and the current state of the MALT1 inhibitor field as a therapeutic approach to treating ABC DLBCL

Diffuse large B cell lymphoma (DLBCL) is a molecularly heterogeneous disease with identifiable subsets that are at high risk for treatment failure with standard immunochemotherapy, R-CHOP. Gene expression profiling has led to the categorization of DLBCL subtypes, ABC and GCB, and has identified driver mutations that represent the critical Achilles heel of these tumors. The majority of patients who fail to respond to, or relapse after the standard R-CHOP treatment, have the ABC subtype of DLBCL, whose pathogenic hallmark is the constitutive activation of NF-kB. Recurrent genetic alterations that drive constitutive activation of the NF-kB pathway include mutations in CARMA1 and CD79A/B downstream of BCR, and MYD88 downstream of the toll-like receptor, and biallelic deletion of TNFAIP3 (A20) (91). Mutations in CARMA1 are found in 10% of cases of ABC DLBCL, and mutations in the B cell co-receptor CD79A/B occur in 21% of cases of ABC DLBCL. Thus, approximately 30% of patients with ABC DLBCL may benefit from MALT1 blockade. Screening patient tumors for the presence of these identified driver mutations (CARMA1 and CD79A/B) that induce constitutive MALT1 activity in this subset of patients will be a crucial counterpart to targeted therapy development in this field.

The NF-kB pathway was first validated in 2005 as a selective therapeutic target in ABC DLBCL by an inhibitor of IkB kinase (IKK) complex (92). Bortezomib, which targets the chymotrypsin-like activity of the proteasome and blocks the degradation of the inhibitory protein IkBα, has been shown to selectively sensitize patients with ABC DLBCL to chemotherapy (93). However, bortezomib often induces dose-limiting toxicity, including painful peripheral neuropathy in approximately 30-40% of patients (94). Carfilzomib is a second-generation proteasome inhibitor with higher selectivity and better tolerated than the first-generation

proteasome inhibitors (95). A combinatorial therapy of carfilzomib with a histone deacetylase (HDAC) inhibitor, Vorinostat, was shown to have synergistic activity in vitro and in vivo for both ABC and GCB DLBCL, but failed to correlate with clinical response in a phase 1 study of patients with relapsed or refractory B-cell lymphomas (96). Lenalidomide, an analogue of thalidomide, is an oral immunomodulatory drug with multiple direct and indirect anti-tumor mechanisms, including natural killer cell- and monocyte-mediated antibody-dependent cell-mediated cytotoxicity, impairment of pro-inflammatory cytokines, as well as decreased NF-kB activity and DNA synthesis arrest (97, 98). Lenalidomide has been shown to selectively kill ABC DLBCL cells by downregulating IRF-4, leading to increased production of toxic IFN-β and decreased NF-kB activity (99, 100). Lenalidomide has shown single-agent activity in multiple relapsed or refractory aggressive and indolent B-cell NHL, including mantle cell lymphoma (MCL) and follicular lymphoma, in addition to DLBCL. Lenalidomide has been approved by the FDA for the treatment of relapsed or refractory MCL, and the feasibility of combinatorial therapy of lenalidomide with R-CHOP in previously untreated ABC DLBCL has been demonstrated in phase II trials (101). However, in a phase III trial of lenalidomide with R-CHOP vs placebo with R-CHOP in previously untreated ABC DLBCL, the primary endpoint of progression-free survival (PFS) was not met (102).

In addition to the direct NF-kB pathway inhibitors, therapeutic strategies to target the BCR signaling pathway for NF-kB pathway regulation in ABC DLBCL have led to drugs that target Bruton tyrosine kinase (BTK) and PKC-β (103). Knocking down BTK using short hairpin RNAs (shRNA) was shown to be highly toxic to ABC DLBCL cell lines with wildtype CARMA1 (HBL-1, TMD8, U2932, OCI-Ly10), but not to ABC DLBCL cell line with mutant CARMA1 (OCI-Ly3) (104). Ibrutinib is an oral small molecule that irreversibly inhibits BTK by covalently binding

cystine-481. A phase III trial of R-CHOP with or without ibrutinib in patients with newly diagnosed non-GCB DLBCL did not meet its primary end point of event-free survival in the intent-to-treat (ITT) population and the ABC DLBCL subgroup (105). PKC-β is a serine/threonine kinase with an essential role of phosphorylating CARMA1 in BCR signaling and required for activation of the NF-kB pathway and survival in DLBCL (106). Sotrastaurin, a PKC-β inhibitor, has been shown to selectively inhibit the growth of CD79 mutant DLBCL in vitro and in vivo. Mutations in CD79B correlated with sensitivity to sotrastaurin, but CARMA1 mutations resulted in resistance to the PKC-β inhibitor, similar to a BTK inhibitor (107). A phase I study in patients with relapsed or refractory DLBCL that harbor CD79A or CD79B mutation was started by Novartis, but terminated due to enrollment challenges and availability of other options for DLBCL patients. Another phase I trial of sotrastaurin and everolimus in patients with DLBCL harboring the CD79A/B mutation or with the ABC DLBCL subtype did not progress into phase II due to suboptimal tolerability of the combination treatment.

MALT1, as the effector signaling component of the CBM complex that is critical for upstream activation of NF-kB, and downstream of the recurrently mutated CARMA1, has been an attractive new therapeutic target that has garnered considerable attention recently. ABC DLBCL tumors with CARMA1 mutations would be expected to be sensitive to MALT1 inhibitors, unlike inhibitors of BTK or PKC-β. Inhibitors of MALT1 has shown promising preclinical effects in ABC DLBCL that rely on MALT1 for BCR signaling. To date, termination of MALT1 signaling as a therapeutic approach has focused on blockade of only the protease activity of MALT1. Several MALT1 protease inhibitors have been developed preclinically over the last decade, and these agents have been shown to dampen MALT1-dependent NF-kB signaling and to inhibit proliferation of ABC DLBCL cells (21, 108).

The first reported MALT1 protease inhibitor, z-VRPR-fmk (78), is a peptide that irreversibly binds to the active site in the MALT1 paracaspase domains. X-ray crystallography studies show that the P1 arginine of the inhibitor interacts with the MALT1 active site residues, including C464 (76, 84). Although z-VRPR-fmk inhibitor exerts selective toxicity in ABC DLBCL cells, and not in GCB DLBCL cells, its use in humans is limited due to low potency and low cell permeability, which is thought to be due to the two arginine residues (21, 108). Subsequent high-throughput screening identified the small molecule MI-2 as an irreversible MALT1 inhibitor (109). Docking studies suggest that similar to z-VRPR-fmk, MI-2 also binds to the active site within the paracaspase domain. MI-2 has been shown to inhibit the growth of ABC DLBCL cells at a significantly higher potency compared to z-VRPR-fmk. However, there is a concern for lack of specificity and toxicity with MI-2. Given this concern, structure-activity relationship (SAR) studies were used recently to develop a new MALT1 active site inhibitor, "compound 3," with *in vitro* and *in vivo* activity against ABC DLBCL (110). X-ray crystallography of MALT1 paracaspase-Ig3 (AA 339-719) with compound 3 demonstrates that unlike z-VRPR-fmk, which promotes MALT1 paracaspase domain dimerization, compound 3 promotes the formation of larger MALT1 oligomers. Oligomerization occurs secondary to covalent binding of compound 3 to C464 in the active site of one MALT1 fragment and Y389 in an adjacent MALT1 fragment (110). The final MALT1 active site inhibitor, β-lapachone, was identified from a high-throughput screen of a small molecule library followed by chemical synthesis. Modeling experiments suggest that β-lapachone and its structural derivatives covalently bind to C464 within the MALT1 protease domain in a manner similar to z-VRPR-fmk or MI-2 (111). Additional studies showed that incorporating electron-withdrawing substituents at the C8 position of β-lapachone improved its potency (111).

In addition to direct inhibitors of the active site of the MALT1 protease domain, allosteric inhibitors of MALT1 protease function have also been reported. Phenothiazine derivatives, namely mepazine, thioridazine, and promazine, were identified as MALT1 protease domain inhibitors after a screen of 18,000 compounds in the ChemBioNet library (112). Phenothiazines have been known as first generation antipsychotics and were in clinical use for treatment of psychiatric disorders since the 1950s (113). Mepazine, under the brand name Pacatal, was in clinical use as an antipsychotic drug, but was removed from market in the 1960s after failing to show significant antipsychotic response in clinical trials (114). Phenothiazines have now been repurposed as noncompetitive reversible inhibitors of MALT1 protease function with selective toxicity in ABC DLBCL *in vitro* and *in vivo*. X-ray crystallography showed that phenothiazines bind to a hydrophobic pocket located between the paracaspase and Ig3 domains of MALT1 (115). Binding of phenothiazines to this allosteric site prevents a conformational change in MALT1 that is required for activation. More recently, two additional allosteric MALT1 inhibitors with nanomolar potency, MLT-748 and MLT-747, were identified using a high-throughput screen of more than a million compounds in the Novartis compound library. These inhibitors bind to the same allosteric sites as the phenothiazines, between the paracaspase and Ig3 domains, locking the catalytic residue C464 into an inactive conformation. Interestingly, these allosteric MALT1 inhibitors were used as a molecular corrector to rescue MALT1 function in an immunodeficient patient's $MALT1^{mut/mut}$ lymphocytes (116).

Most recently, a preclinical development of a series of proteolytic targeting chimera (PROTAC) compounds against MALT1 has been reported by the same group that has developed MI-2 and compound 3. PROTACs induce selective proteolysis by targeting proteins of interest to E3 ligases for directed proteasomal degradation. By fusing their parental MALT1-targeting

allosteric compound with a Cereblon (CRBN) binding moiety, the CRBN E3 ligase complex is brought to close proximity of MALT1, promoting its ubiquitination and proteasomal degradation, and effectively targeting both the protease and scaffolding activities of MALT1 (117).

1.5 Study Overview

Given the critical role CBM plays in lymphomagenesis, the pharmaceutical industry has shown considerable interest in developing inhibitors of MALT1 activity, with potential initial application in the treatment of various types of lymphoma. Currently, inhibition of the CBM signalosome as a therapeutic approach for the treatment of ABC DLBCL and potentially other MALT1-addicted neoplastic and inflammatory diseases have focused almost exclusively on blockade of MALT1 protease activity (118). However, inhibiting the MALT1 protease activity only partially interferes with the CBM signalosome and is not expected to impair MALT1 scaffolding activity, which is integral to downstream NF-kB signaling. As reviewed above, an intact high order filamentous structure is essential for the activation of MALT1 and MALT1-mediated NF-kB signaling. Thus, protein-protein interactions within the CBM complex itself could be targeted at three levels: CARMA1-Bcl10, Bcl10-Bcl10, and Bcl10-MALT1 interactions, in order to block both the protease and scaffolding activities of MALT1.

While the development of small molecule inhibitors of protein-protein interaction (PPI) has proven difficult in cases where interactions occur over broad surfaces, there are many successful examples of PPI inhibitors when the targeted interaction interface is more defined (3, 119-128). Whereas the interaction between the CARD domains of CARMA1 and Bcl10 involves broad regions of contact, previous studies suggest that the interaction between Bcl10 and MALT1

occurs through a small and limited interface. The two immunoglobulin (Ig)-like domains of MALT1 are similar to the antigen recognition domains in antibodies. Previous studies have reported that these Ig-like domains of MALT1 mediate interaction with Bcl10 (69, 73, 74). In addition, a small internal peptide (AA 107-119) within Bcl10 serves as the site of recognition for the MALT1 Ig domains (69, 73).

Thus, we hypothesize that this limited and well-defined antibody-epitope-like site of Bcl10-MALT1 interaction is druggable, sharing properties with other PPIs that have been successfully targeted with small molecule PPI inhibitors, and that an inhibitor of the Bcl10-MALT1 interaction will inhibit CBM-dependent signaling and selectively kill ABC DLBCL cells. This new class of CBM inhibitors hold promise as novel therapeutic options for the treatment of MALT1-dependent neoplastic and inflammatory disorders associated with deregulated NF-kB signaling.

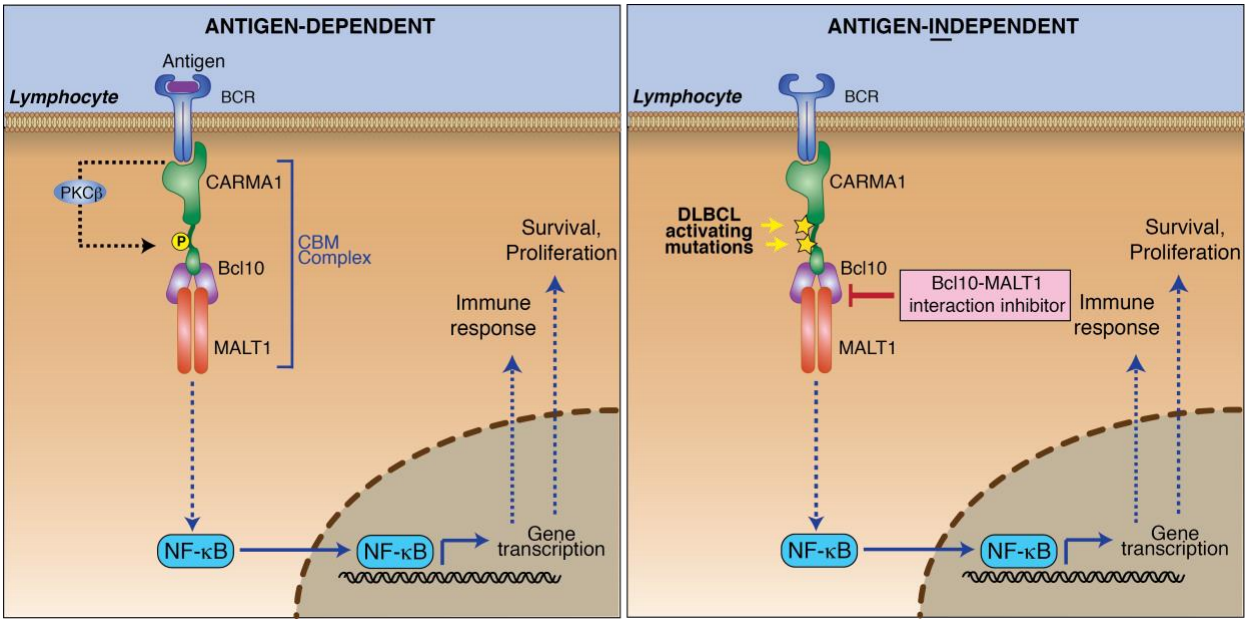

Figure 2. Graphical abstract showing a strategy of inhibiting the critical Bcl10-MALT1 interaction.

Inhibition of Bcl10-MALT1 interaction is proposed as a therapeutic approach to treating diffuse large B-cell lymphomas where activating mutations in the CARMA1 moiety of the CBM complex leads to antigen-independent constitutive CBM complex assembly and constitutive NF-kB activation.

2.0 Materials and Methods

2.1 Cell lines and reagents

The DLBCL cell lines, OCI-Ly1, OCI-Ly3, and OCI-Ly7, were provided by Dr. Mark Minden (University Health Network, Toronto, Ontario, Canada). TMD8 cells were provided by Dr. Louis Staudt (NCI, NIH). OCI-Ly1 and OCI-Ly7 cells were cultured in Iscove's Modified Dulbecco's Medium (IMDM) supplemented with 10% FBS. OCI-Ly3 cells were cultured in IMDM supplemented with 20% FBS. TMD8 and Jurkat T cells were cultured in RPMI1640 medium with 10% FBS. HEK293T cells were cultured in DMEM medium with 10% FBS. All media were supplemented with 100 U/ml penicillin streptomycin. Stimulation of Jurkat cells was conducted by adding 5 ng/ml of phorbol 12-myristate13 acetate (PMA) (Sigma-Aldrich) and 1 μM ionomycin (Calbiochem), or by adding 5-10 μL/mL of ImmunoCult Human CD3/CD28 (STEMCELL Technologies). Proteasome inhibitor MG132 (Calbiochem) was used at a final concentration of 5uM for RelB cleavage detection.

2.2 Antibodies

Rabbit Phospho-IKKa/b antibody (Cell Signaling #2078)

Rabbit IKKa/b antibody (H-470) (Santa Cruz #sc-7607)

Rabbit Phospho-p44/42 MAPK (Erk1/2) antibody (Cell Signaling #9101)

Rabbit P44/42 MAPK (Erk1/2) antibody (Cell Signaling #9102)

Rabbit RelB antibody (C1E4) (Cell Signaling #4922)

Rabbit N4BP1 antibody (Cohesion Biosciences #CPA2415)

Mouse GAPDH antibody (6C5) (Santa Cruz #sc-32233, Lot# H0411)

Rabbit MALT1 (Cell Signaling #2494)

Mouse Bcl10 (331.3) (Santa Cruz Cat# sc-5273)

2.3 In vitro experimental methods

Mammalian Two-Hybrid system

In the Mammalian Two-Hybrid system, wildtype full-length Bcl10 (AA 1-233), and two Bcl10 deletion mutants (Bcl10Δ107-119 and Bcl10Δ90-119) were cloned into the pBIND vector containing the yeast GAL4 DNA-binding domain. MALT1 (AA 1-330) containing both the death domain and the Ig1-Ig2 domains were cloned into the pACT vector containing the herpes simplex virus VP16 activation domain. The pG5luc vector containing five GAL4 binding sites upstream of the firefly luciferase gene and pEF1-BOS-β-gal vector were co-transfected along with pACT-MALT1 and pBIND-Bcl10 constructs into HEK293T cells using Lipofectamine 3000 (Thermo Fisher Cat# L3000001) in 24-well, 96-well, or 384-well plates. Two to three days after transfection, the cells were lysed, and the amount of firefly luciferase and β-galactosidase are quantitated using the Luciferase Reporter Assay system (Promega Cat# E1501) and the β-galactosidase enzyme assay system (Promega Cat# E2000). The pBIND-Id and pACT-MyoD vectors that encode and express two proteins known to interact in vivo were used as positive controls. The pM3-VP16 vector (Takara Cat# 630305), which expresses a fusion of the GAL4

DNA binding domain to the VP16 activation domain, was used as an additional positive control vector.

Surface Plasmon Resonance (SPR)

SPR is a real-time, label-free optical technique to detect biomolecular interactions. All SPR experiments were performed on Biacore 2000. Full-length Bcl10 molecules were immobilized on a gold sensor chip surface and analyte solution containing MALT1 DD+Ig1-Ig2, MALT1 Ig1-Ig2, or MALT1 DD protein was injected over the surface through a series of flow cells. During the course of the interaction, polarized light is directed toward the sensor surface and the angle of minimum intensity reflected light is detected. This angle changes as molecules bind and dissociate and the interaction profile is recorded in real time in a sensorgram. The binding kinetic parameters were obtained using the Langmuir model (129) for global fitting 1:1 binding ratio where one ligand molecule interacts with one analyte molecule. To verify the binding constants, additional local fitting was performed.

ELISA-based protein-protein interaction assay

On a high-binding 96-well ELISA microplate (Greiner Cat# 655061), 100 ng of His-tagged recombinant human full-length Bcl10 protein (ProteinTech Cat# Ag12162) in 100 ul PBS was allowed to adhere overnight in 4°C. The plate was blocked with 5% BSA in PBS for 1 hour at room temperature. After washing twice with PBS-T, a mixture of 100 ng of GST-tagged recombinant human full-length MALT1 protein (Novus Biologicals Cat# H00010892-P01) and compound that was preincubated for 1 hour in 100 ul PBS was added to the plate for 1 hour at room temperature. After washing three times with PBS-T, anti-MALT1 antibody in 5% BSA in

PBS was added at 1:1000 dilution for 1 hour at room temperature. After washing three times with PBS-T, HRP-conjugated secondary antibody in 5% BSA in PBS was added at 1:5000 dilution for 1 hour at room temperature. After washing three times with PBS-T, 100ul of TMB was added for 5 minutes, and 100ul of 2M sulfuric acid was added to stop the reaction. The plate was read at 450 nm using a spectrophotometer (Molecular Devices SpectraMax i3).

In silico screening

LibDock program from Discovery Studio 3.5 was used to perform a structure-guided in silico screen of 3 million compounds to identify candidate molecules that could potentially fit within the identified groove of MALT1 Ig1-Ig2 domain and disrupt the interaction between the Bcl10 helix and MALT1. Lipinski's rule of five filters were applied to enrich for compounds with drug-like properties.

qRT-PCR

Total RNA extraction was performed using RNeasy Plus Mini Kit (Qiagen Cat# 74136). RNA was transcribed into cDNA using High-Capacity cDNA Reverse Transcription Kit (Applied Biosystems Cat# 4368814) according to manufacturer's instructions. The following probes were used for qRT-PCR: IL2 TaqMan probe Hs00174114_m1 (Cat# 4331182), CXCL8 Taqman probe Hs00174103_m1 (Cat# 4331182).

ELISA

Expression of cytokines from cell culture supernatants was measured 24h after treatment with 0, 0.01, 0.03, 0.1, 0.3, 1, or 3 uM of compounds using the following ELISA kits according to

the manufacturer's instructions: Human IL-2 ELISA (BioLegend Cat# 431804), Human IL-6 ELISA (BioLegend Cat# 430504), and Human IL-10 ELISA (BioLegend Cat# 430604).

Immunoprecipitation and Western blot analysis

For immunoprecipitation, cells were rinsed in PBS and lysed in buffer (150mM NaCl, 2mM EDTA, 10% glycerol, 1% Nonidet P-40, 20mM Tris Hcl, pH 7.4) containing protease and phosphatase inhibitors. Supernatants were incubated with specific antibody for 1 hour at 4C followed by 30ul protein A/G beads overnight at 4C. with gentle rotation. Beads were then pelleted at 1000 rpm for 2 min and washed 3 times with buffer. Antibody-protein conjugates were removed from beads by boiling for 5 minutes, and samples were then subjected to SDS-PAGE and immunoblotting.

Cell proliferation, viability, and cell cycle arrest assays

Cell number was counted using the trypan blue dye exclusion method with Vi-CELL cell viability analyzer (Beckman Coulter) at days 7, 10, and 12 of treatment with compounds.

CellTrace Violet reagent (ThermoFisher Cat# C34571) was used as a cell division tracking dye for OCI-Ly3 and OCI-Ly1 cells treated with 1uM of compound K691-0124, where the intensity of the staining decreases with each round of cell division. At days 0, 3, and 6 after staining of DMSO- and compound-treated cells, CellTrace Violet fluorescence was measured by flow cytometry and analyzed by FlowJo.

CellTiter-Glo luminescence assay (Promega Cat# G7570) was used to quantify ATP levels in DLBCL cells treated with compounds for 48 hours or 96 hours as a surrogate marker of metabolic viability

Annexin V FITC and SYTOX Blue Dead Cell stains were used to detect apoptosis in DLBCL cells treated with 1uM compounds for 6 days and analyzed with flow cytometry.

Cellular Thermal Shift Assay (CETSA)

CETSA assesses drug-protein interaction in the protein's native cellular environment, based on ligand-induced changes in protein thermal stability. To evaluate target engagement by the compounds within cells, HEK293 cells were treated with 1 uM compounds for 30 minutes to 1 hour, then harvested, washed with PBS, and suspended in 1mL PBS supplemented with Halt protease and phosphatase inhibitor cocktail, and the same dose of compounds or DMSO as initial treatment. 100ul volume of cell suspension from different samples was aliquoted into a PCR tube for each temperature to be tested. Samples were heated at their designated temperatures for 2 minutes in Applied Biosystems Veriti 96-well thermal cycler with six independent temperature blocks. Immediately after heating, tubes were removed and incubated on ice for 3 minutes Then, in order to lyse cells, three freeze-thaw cycles in liquid nitrogen was performed. The tubes were briefly vortexed after each thawing. Cell debris along with precipitated and aggregated proteins were removed by centrifuging samples at 20,000 g for 20 minutes at 4C. Loading buffer was added to the cell lysate samples and boiled for 5 minutes at 90C for Western blot analysis. Both Bcl10 and MALT1 was probed with anti-Bcl10 (Santa Cruz H-197) and anti-MALT1 (Cell Signaling #2494) antibodies.

Proximity ligation assay (PLA)

Duolink in situ detection reagents Orange kit (Sigma-Aldrich DUO92102) was used to perform PLA. TMD8 cells were treated with 1uM compounds or equivalent volume of DMSO for

30 minutes, and plated onto a 15 well ibiTreat chamber slide (Ibidi) and allowed to adhere to the surface for 30 minutes at 37C. Cells were fixed with 4% paraformaldehyde for 20 minutes at room temperature, then washed with PBS. Cellular membranes were labelled with 5 ug/ml Wheat Germ Agglutinin (WGA) conjugated to Alex Fluor 488 (Invitrogen) for 10 minutes at room temperature. Cells were permeabilized in cold methanol for 10 minutes, washed with PBS, then blocked in Duolink Blocking buffer for 30 minutes at room temperature. Primary antibodies were diluted in Duolink Antibody Diluent and incubated overnight at 4C. Cells were then washed for 20 minutes in PBS with 1% BSA, followed by incubation with Duolink mouse and rabbit secondary antibodies for 1 hour at 37C, then washed with TBST with 0.5% Tween-20 for 10 minutes. Ligation and amplification steps were performed according to the manufacturer's instruction. Cells were mounted in Duolink mounting medium with DAPI. Images were acquired using Zeiss LSM confocal microscope and PLA spots were counted using CellProfiler.

Statistical Analysis

All values are represented as mean ± SEM. Data were analyzed, and statistics performed using GraphPad Prism 8 software. Student's t-test was used for comparing two groups and ANOVA test was used for comparing three or more groups. Dose-response curves were fitted using the following equation: Y = bottom + (top-bottom)/(1+10^(X-LogIC50), with the top and bottom representing the plateaus in the units of Y axis. In vivo tumor growth curve was evaluated using two-way ANOVA and Sidak's multiple comparison tests.

2.4 In vivo mouse model

Pharmacokinetic study

Preliminary pharmacokinetic bioanalysis was done by Touchstone Biosciences. Male CD-1 mice were fasted overnight before being dose with compound K691-0124 via intraperitoneal injection in the lower right quadrant of the abdomen at 20 mg/kg. All blood samples (30-50ul per sample) are taken via tail vein at 5, 15, and 30 minutes, and 1, 2, 4, 6, 8, and 24 hours after dosing. Blood samples are collected in Greiner MiniCollect K_2EDTA tubes, placed on ice, and within 30 minutes, centrifuged at 15,000g for 5 minutes to obtain plasma samples. All plasma samples are stored at -70C until analysis. Plasma samples were prepared for analysis by LC-MS/MS, and key PK parameters, including terminal half-life ($t_{1/2}$), initial plasma concentration (C_0), area under the plasma concentration vs. time curve (AUC), volume of distribution at steady-state (V_{ss}), total plasma clearance (CL_p), and mean residence time (MRT), were measured.

Xenograft model of DLBCL

Tumors were engrafted into 8-week old female SCID NOD.CB17-Prkdc$_{scid}$/J (nonobese diabetic/severe combined immunodeficiency) mice from Jackson Laboratory by subcutaneous injection of 10x10_6 TMD8 cells resuspended in Matrigel (Cultrex Basement Membrane Extract, type 3, Pathclear; Trevigen) into the right flank of individual mice, with 10 mice for DMSO vehicle control, 10 mice for compound K691-0124, and 10 mice for compound K691-0122. After visual appearance of tumor (i.e. when tumors reach an average volume of 100 mm_3), mice were randomized to DMSO vehicle control or K691-0124 or K691-0122, and received once daily intraperitoneal injection of 50 mg/kg of K691-0124 (corresponding to 42 ul for a 25g mouse) or equivalent volume of DMSO for up to 12 days. Tumor size was measured three times a week using

a caliper and calculated using the formula: (smallest diameter^2 x largest diameter)/2. Mice were sacrificed 24 hours after the 12th injection. Tumors and various organs, including lung, heart, liver, and kidney were collected for histological analyses. Mice were sacrificed when tumors reached 2500 mm^3. All experimental procedures involving animals have been approved by University of Pittsburgh IACUC.

3.0 Results

3.1 Bcl10 AA 107-119 and MALT1 Ig1-Ig2 domains are critical regions that mediate Bcl10-MALT1 interaction.

Previous studies have indicated that a small region at the C-terminal end of the Bcl10 CARD and extending into the serine/threonine-rich motif between amino acids 107 and 119 is necessary for binding MALT1 and critically important for NF-kB activation (69, 73). On the MALT1 side, several papers have reported that the tandem Ig1 and Ig2 domains are critical for binding Bcl10, mostly through co-immunoprecipitation analyses (69, 73, 74). To confirm these previous reports of the regions important in mediating Bcl10-MALT1 interaction and for potential use as a high-throughput screening assay, a mammalian two-hybrid system was developed. One major advantage of the mammalian two-hybrid system over the yeast system is that mammalian protein interactions can be studied in an environment that is more conducive to that in vivo, such as post-translational modifications, folding, and localization of eukaryotic proteins. In this system, the modular DNA-binding domain and the transcriptional activation domain, produced by separate plasmids, are able to associate closely when one protein fused to a DNA binding domain interacts with a second protein fused to a transcriptional activation domain, resulting in the transcription of the firefly luciferase reporter gene.

Human MALT1 (AA 1-330), which includes both the death domain and the tandem Ig1 and Ig2 domains, was cloned into pACT vector, which contains the herpes virus VP16 activation domain. Three different Bcl10 constructs were cloned into pBIND vector, which contains the yeast GAL4 DNA-binding domain: full-length wild-type Bcl10, Bcl10 deletion mutant lacking the

aforementioned putative MALT1-binding residues 107-119, and Bcl10 deletion mutant lacking residues 90-119 that cuts into the C-terminal end of the CARD domain (Figure 3). Interaction between the two test protein partners expressed as GAL4-Bcl10 and VP16-MALT1 fusion constructs, results in an increase in luciferase expression over the background negative controls. MyoD, a myogenic regulatory protein expressed in skeletal muscle and the Id protein are known to interact in vivo, and are used as positive controls in this system (130). For negative controls, the background level of luciferase is measured in the presence of GAL4 and VP16 (from empty vectors pBIND and pACT, respectively), as well as in the presence of an empty vector and its partner plasmid with either Bcl10 or MALT1 (e.g. pACT with pBIND-Bcl10 or pBIND with pACT-MALT1). The level of interaction was assessed by measuring firefly luciferase activity normalized for β-galactosidase expression in cell extracts 2-3 days after transfection.

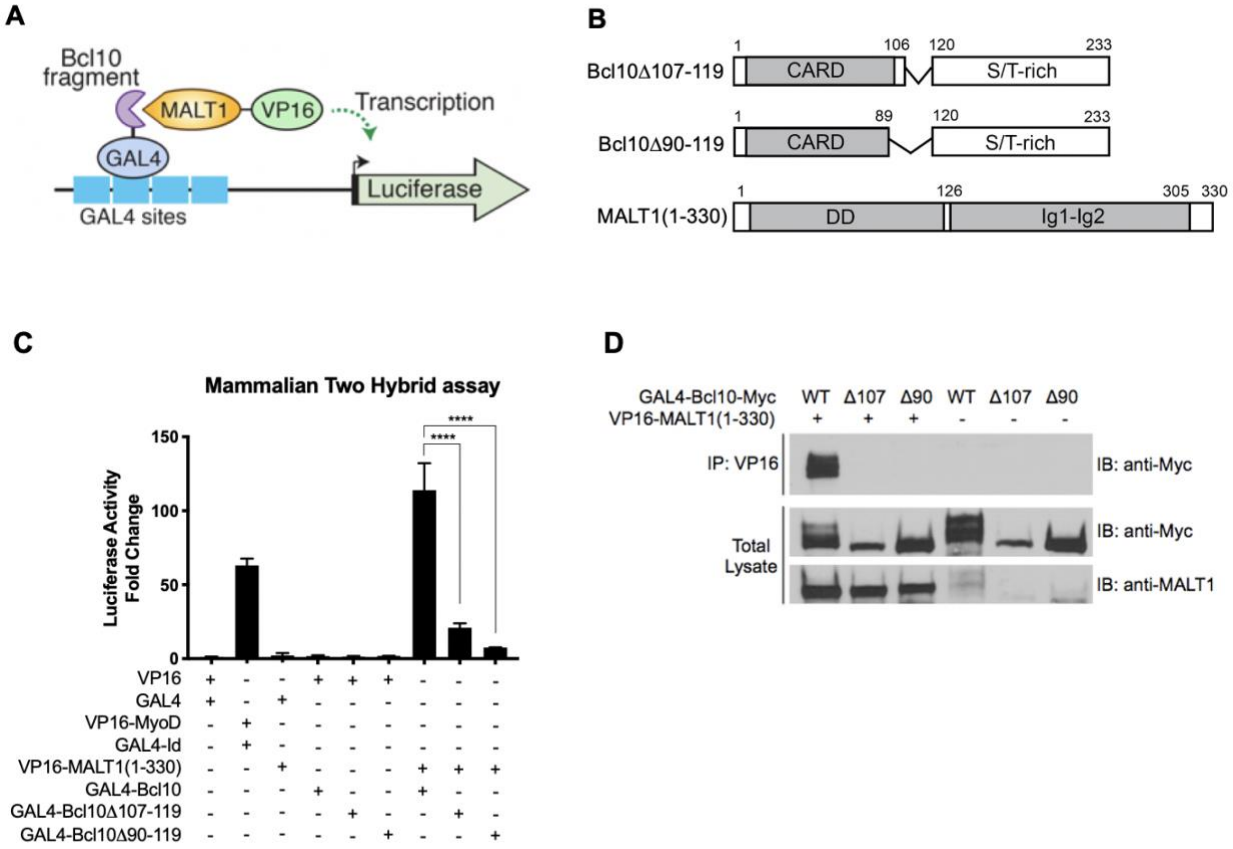

Figure 3. Deletion of Bcl10 residues 107-119 significantly impairs its ability to bind MALT1(1-330) using the mammalian two-hybrid system in HEK293 cells.

A schematic representation of the mammalian two-hybrid assay system (A) with Bcl10 mutants and MALT1 construct used are shown (B). 2.5 x 10_5 HEK293 cells were transfected with 400 ng of pACT-MALT1(1-330) and either 100ng of pBIND-Bcl10-Myc, 500ng of pBIND-Bcl10Δ107-119-Myc, or 100ng of pBIND-Bcl10Δ90-119-Myc. WT Bcl10 displays robust interaction with MALT1, while the interaction is significantly impaired with Bcl10 lacking AA 107-119 and with Bcl10 lacking AA 90-119 (C). VP16-MALT1 fusion protein was immunoprecipitated using anti-VP16 antibody, and both total lysates and immunoprecipitated products were analyzed by Western blot (D). Statistical analysis was performed using one-way ANOVA and Dunnett test to correct for multiple comparisons in GraphPad Prism software (**** $p < 0.0001$).

As shown in Figure 3, interaction between wild-type Bcl10 and MALT1 (AA 1-330) increased the luciferase activity by approximately 100-fold. Consistent with previous reports, deletion of only 13 amino acids in Bcl10 between residues 107-119 drastically reduced its ability to bind MALT1 (AA 1-330). In co-immunoprecipitation analysis, VP16-MALT1 (AA 1-330) construct was again shown to efficiently bind GAL4-Bcl10, while GAL4-Bcl10Δ107-119 and GAL4-Bcl10Δ90-119 showed absolutely no interaction with MALT1 (AA 1-330) (Figure 3). With the intention of using the mammalian two-hybrid system as a high-throughput compound screening platform, we successfully miniaturized the assay system into 384-microwell plates with similar robust signal (Figure 4).

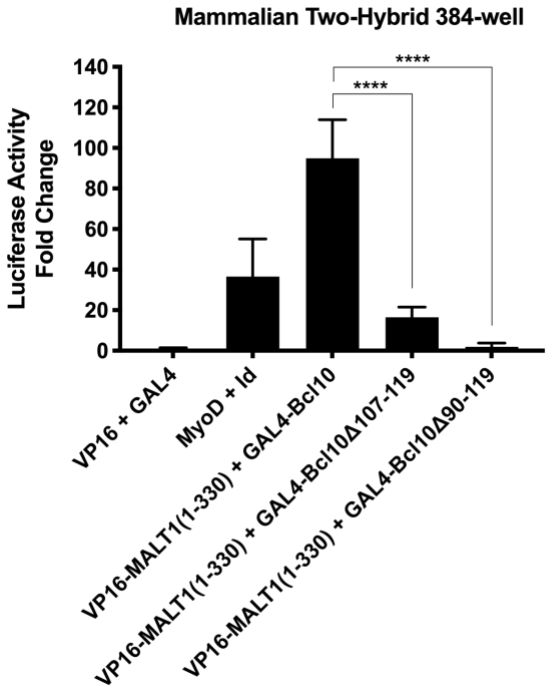

Figure 4. Miniaturization of the mammalian two-hybrid system in a 384-well microplate platform for high-throughput screening.

Mammalian two-hybrid system was successfully miniaturized to a 384-well microplate with luciferase activity signals that are comparable to that in a 24-well plate. Statistical analysis was performed using one-way ANOVA and Dunnett test to correct for multiple comparisons in GraphPad Prism software (mean ± SEM; N = 6; **** $p < 0.0001$).

Previous studies have performed co-immunoprecipitation studies to show that MALT1 DD by itself cannot bind Bcl10 (69, 73), while MALT1 Ig1-Ig2 domain by itself is sufficient to bind Bcl10 (69). To evaluate whether MALT1 DD or MALT1 Ig1-Ig2 by itself is able to bind Bcl10 in the mammalian two-hybrid system, MALT1 DD construct (AA 2-124) and MALT1 Ig1-Ig2 construct (AA 128-330) were cloned into the pACT vector, and co-transfected with pBIND-Bcl10. Neither MALT1 DD-only nor MALT1 Ig1-Ig2-only constructs showed interaction with Bcl10 in the mammalian two-hybrid system (Figure 5A). Interestingly, upon Western blot analysis to check for expression of these proteins, it was evident that MALT1 Ig1-Ig2 construct failed to express,

while MALT1 DD construct expressed well (Figure 5B). Thus, from the mammalian two-hybrid experiments, we are only able to conclude that MALT1 DD by itself is not sufficient to interact with Bcl10.

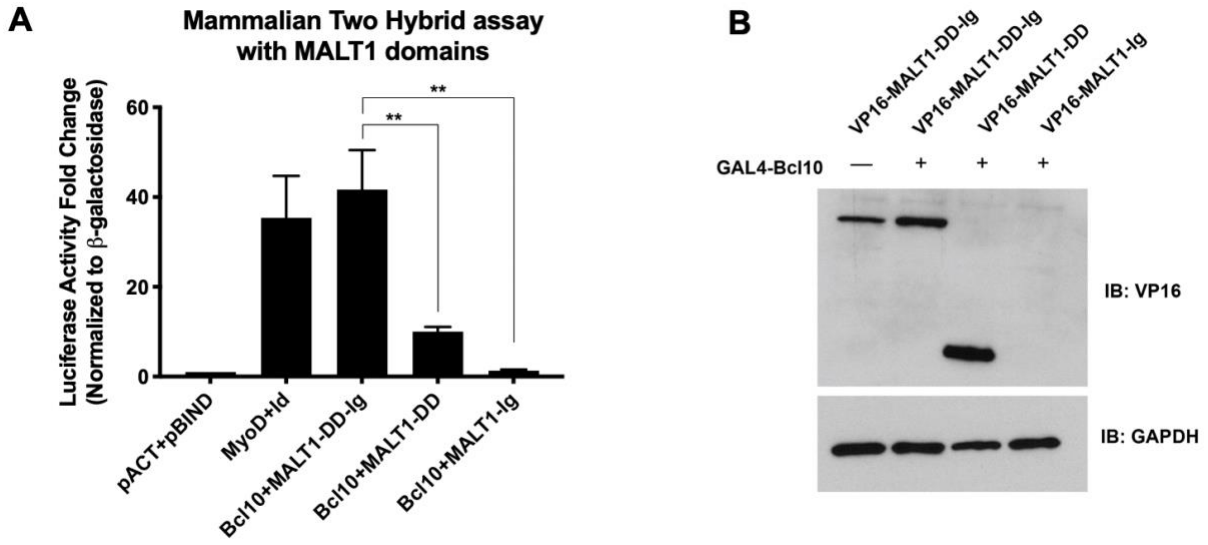

Figure 5. Mammalian Two-Hybrid assay with MALT1 domain constructs and corresponding protein expression of MALT1 domain constructs.

A) MALT1 DD alone and MALT1 Ig domain alone showed significantly reduced interaction with GAL4-Bcl10, compared to MALT1 DD+Ig in the mammalian two-hybrid system. Statistical analysis was performed using one-way ANOVA and Dunnett test to correct for multiple comparisons in GraphPad Prism software (mean ± SEM; N = 3; ** $p < 0.01$). B) Protein expression of VP16-MALT1-DD was robust, whereas VP16-MALT1-Ig domain was not detected by Western blot.

Next, surface plasmon resonance (SPR) analysis of Bcl10-MALT1 binding was performed in collaboration with the laboratory of Zaneta Nikolovska-Coleska at University of Michigan. For SPR, one interaction partner, Bcl10 is immobilized onto a gold-plated chip, and the other partner, MALT1, is injected over the chip in liquid phase. Interaction between the ligand and analyte

molecules alters the resonance of polarized light that is directed at the chip, and data is converted into real-time kinetic measurements that can precisely quantify binding affinity (K_D) and other kinetic parameters, such as association and dissociation constants (k_{on}, k_{off}).

The Langmuir model, which describes a 1:1 interaction where one ligand molecule (e.g. Bcl10) interacts with one analyte molecule (e.g. MALT1), was used to globally fit the data. This model assumes that the binding is equivalent and independent for all binding sites in first-order kinetics, and that the reaction is not limited by mass transport (129). Interestingly, in a cell-free environment with purified recombinant proteins, MALT1 Ig1-Ig2 domain showed strong binding with Bcl10 (Figure 6B), with similar binding kinetic parameters as that of MALT1 protein that contains both DD and Ig1-Ig2 domains (Figure 6A). Both MALT1 DD + Ig1-Ig2 and MALT1 Ig1-Ig2 constructs displayed rapid association, with the plateau of association being reached within 200 seconds. The dissociation constant, k_D, for MALT1 DD + Ig1-Ig2 is 25nM, and for MALT1 Ig1-Ig2 is 29nM, representing similarly high affinity between the two interacting proteins (Figures 6A, 6B). Consistent with previously published reports (69, 73) and the mammalian two-hybrid results, MALT1 DD by itself showed no binding to Bcl10 (Figure 6C). Thus, the SPR analysis indicates that the Ig1-Ig2 domains are required for interaction with Bcl10.

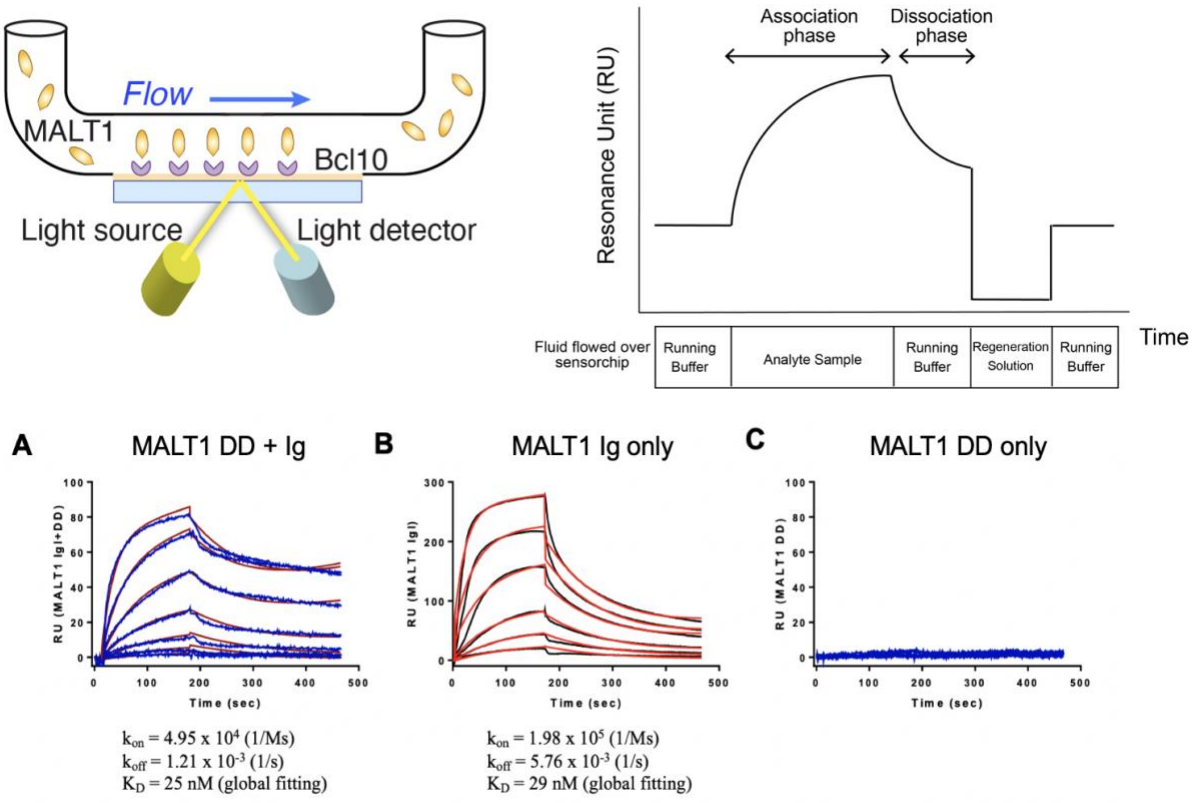

Figure 6. MALT1 Ig domain is sufficient and necessary to bind Bcl10 by surface plasmon resonance (SPR).

A schematic of surface plasmon resonance (SPR) platform is shown. Bcl10 proteins are immobilized on the sensor chip and a range of concentrations of three MALT1 domains in liquid phase are flowed over the sensor chip to detect real-time binding. Association between the two proteins occurs during analyte (MALT1) injection onto ligand (Bcl10) surface until equilibrium is reached, when the rate of association equals the rate of dissociation. In the dissociation phase, the analyte is removed from the flow and comes to a concentration of zero. Association and dissociation are measured in arbitrary Response Unit (RU) in a typical SPR sensorgram. SPR interaction was fitted using the Langmuir model for 1:1 interaction in which one ligand molecule interacts with one analyte molecule, follows pseudo-first-order kinetics, binding is assumed to be equivalent and independent for all binding sites, and reaction is assumed to be not limited by mass transport. The rate of formation of the complex is represented by the association constant k_{on}, the rate of complex decay is represented by the dissociation constant k_{off}, and the equilibrium constant is represented by K_D.

Taken together, different assay environments have revealed the complexity of Bcl10-MALT1 interaction. As detailed before, Schlauderer et al has reported their cryo-EM study that shows the N-terminal MALT DD serving as the rigid Bcl10-binding interface, while the Ig1-Ig2 and the paracaspase domains flexibly protrude at the filament periphery (72). They have also demonstrated that the mutation of key residues in the MALT1 DD (V81R and L82D) completely blocks constitutive Bcl10-MALT1 interaction in resting cells. They concluded that the Ig1-Ig2 domains, although outside the direct Bcl10-MALT1 interface, are critical for the conformation of the protein complex, and are thus indirectly involved in facilitating the interaction, as well as enabling an arrangement that allows for dimerization of MALT1 paracaspase domains, which is necessary for MALT1 protease activation (115). Indeed, the crystal structure of the MALT1 DD alone shows that the α6 helix is not kinked in the absence of the Ig1-Ig2 domains, which could prevent Bcl10 from binding or paracaspase dimerization (131). Moreover, although an interaction between the MALT1 DD and Bcl10 was not observed by immunoprecipitation of overexpressed proteins in HEK293T cells (69, 73), FRET analysis suggests that the MALT1 DD certainly contributes to Bcl10-MALT1 interaction directly or indirectly. Deletion of both the DD and Ig1-Ig2 domains has consistently been shown to abolish the interaction.

Bcl10 constitutively forms a heterodimer complex with MALT1, and this interaction has been observed to stabilize each other, as knockout of *BCL10* or *MALT1* reduces MALT1 or Bcl10 levels, respectively (132), and shown by Western blot analysis in Figure 5, where co-expression of Bcl10 stabilizes MALT1, bolstering its protein expression level. It has also been previously shown that either deletions in the DD or Ig1-Ig2 domains in MALT1 or mutations and deletions in the CARD and serine/threonine-rich C-terminus region of Bcl10 impair the interaction (69, 73, 75, 133). In Figure 5, we speculate that the deletion of Ig1-Ig2 domains, which may have triggered

complete loss of the stabilizing force of Bcl10 binding, in turn destabilized the MALT1 protein and targeted for degradation. Thus, despite the apparently conflicting results on which domain is necessary or sufficient, efficient interaction between Bcl10 and MALT1 seems to rely on the overall conformation of both proteins, with contributions from both DD and Ig1-Ig2 domains of MALT1.

3.2 Computational modeling of Bcl10-MALT1 interaction and in silico screening of compounds with potential for inhibition of Bcl10-MALT1 interaction.

Before the cryo-EM study by Schlauderer et al was published, we had proceeded to focus on targeting the MALT1 Ig1-Ig2 domains for an in silico compound screening based on previous co-immunoprecipitation analyses and our current SPR results (Figure 7A). In collaboration with Dr. Bill Chen, we first used the crystal structure data of MALT1 Ig1-Ig2 (PDB ID: 3K0W) to guide our screening approach. Electrostatic surface representations revealed that a region at the junction of the two Ig domains has a highly negative charge and forms a linear and hydrophobic groove, features strongly suggestive of an interaction pocket (Figure 7B). The structure of Bcl10 (AA 1-119) was modeled based on the NMR structure of Bcl10 CARD (AA 1-115) (PDB ID: 2MB9) (70) with the α6 helix extended to include the entirety of the putative MALT1-binding peptide residues 107-119 (RNIKLEHLKGLKC) (73). Since this stretch of the peptide is rich in positively charged lysine residues and forms an elongated α-helix (70, 71), we speculated that the identified groove in MALT1 Ig1-Ig2 crystal structure may serve as the docking site for Bcl10. Subsequent computer modeling to identify best-fit docking positions for Bcl10-MALT1 interaction supports this model (Figure 7C).

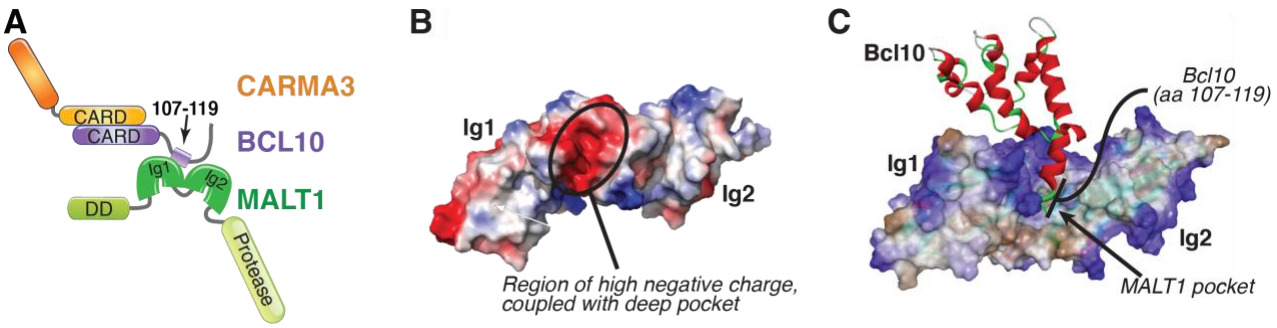

Figure 7. Bcl10 and MALT1 interaction interface models.

A) Model of Bcl10-MALT1 interaction domains based on previous co-immunoprecipitation analyses and our SPR study, which indicate that MALT1 Ig1-Ig2 domains are necessary and sufficient to bind Bcl10.

B) Electrostatic surface representation of the Ig1-Ig2 domains of MALT1. A region of high negative charge is highlighted in red. This region also displays a linear groove-like feature at the junction of the two Ig domains.

C) Best fit docking of Bcl10 (AA 1-119) onto MALT1 Ig1-Ig2 suggests that the region between residues 107-119 of Bcl10 forms an α-helix and fits into the identified MALT1 groove.

Next, the LibDock program from Discovery Studio 3.5 was used to perform a structure-guided in silico screen of 3 million compounds from ChemDiv chemical libraries in order to identify candidate molecules that could potentially fit within the identified groove of MALT1 Ig1-Ig2 domain and disrupt the interaction between the Bcl10 helix and MALT1. To enrich for compounds with drug-like properties, the traditional Lipinski's rule of five filters were applied to the screening process. Lipinski's rule of five applies to a molecule with: 1) a molecular mass less than 500 Da, 2) no more than 5 hydrogen bond donors, 3) no more than 10 hydrogen bond acceptors, and 4) a partition coefficient between octanol and water ($LogP_{o/w}$) not greater than 5 (134). Two decades ago, Lipinski et al proposed that the rule of five could predict the likelihood that a given small molecule will be orally active, such that early prioritization for compounds that do not violate these criteria will increase the likelihood of developing a successful drug. Their proposal was based on their analyses of properties and descriptors of 341 FDA-approved oral drugs

from 1900 to 1997 (134), and that these parameters correlated with the permeability and solubility needed for a molecule to be orally absorbed, since 90% of oral drugs abided by these guidelines. Although Lipinski's rule of five is predictive of oral bioavailability, and has become a standard metric in the drug discovery field to filter libraries of compounds, there are many examples of FDA-approved drugs that violate the rule (16% of oral drugs violate at least one criterion and 6% fail two or more), notably atorvastatin (Lipitor) and montelukast (Singulair), both of which fail more than one of the five rules (135). Moreover, the molecular weight and number of hydrogen bond acceptors have increased substantially over the past 20 years, and the new generation of molecules derived from combinatorial chemistry is seeing decreasing resemblance to the traditional parameter distribution of previously approved oral drugs (136, 137).

3.3 Dose-dependent inhibition of Bcl10-MALT1 interaction by initial screening hits.

With these considerations in mind, we assembled a group of 9 candidate compounds with top docking scores and screened them for activity in three complementary biochemical assays to each quantitate Bcl10-MALT1 interaction. We first attempted to use the mammalian two-hybrid assay in HEK293 cells to test the ability of the screening hits to inhibit the interaction between the fusion constructs of Bcl10 and MALT1. However, the nine compounds showed the same profile of effects on both Bcl10-MALT1 interaction and control MyoD-Id interaction in the mammalian two-hybrid system (Figure 8A, B), indicating that the apparent inhibition of Bcl10-MALT1 interaction by these compound hits are nonspecific in this particular assay, as they are also inhibiting an unrelated protein-protein interaction. Therefore, we decided to test the effect of these compounds on additional control protein-protein interaction, between a fusion construct of the

GAL4 DNA binding domain and mouse p53 and a fusion construct containing VP16 activation domain and SV40 large T-antigen, which is known to interact with p53 (138). Again, the compounds displayed a similar profile of effects on the control pM53 and VP16-T interaction, suggesting that these compounds may be promiscuously inhibiting multiple protein-protein interactions (Figure 8D). Finally, we tested the effect of these compounds in the presence of a single construct that expresses a fusion of the GAL4 DNA binding domain to the VP16 activation domain to test whether these compounds are interfering with any process other than protein-protein interaction in the mammalian two-hybrid system, such as transcription of the luciferase gene or translation of the luciferase reporter protein. Because this positive control plasmid pM3-VP16 expresses a single fusion protein with both the GAL4 DNA binding domain and VP16 activation domain, this construct does not depend on any protein-protein interaction for the expression of the luciferase reporter. If the compounds show inhibition of luciferase activity in the presence of this single control construct, then it is indicative that the compounds are affecting some common process in the mammalian two-hybrid assay that is independent of any protein-protein interaction. Indeed, the compounds displayed a similar inhibitory profile in the presence of this pM3-VP16 positive control (Figure 8E). Thus, we concluded that the mammalian two-hybrid assay system is unsuitable for testing our screened compounds, as they were interfering with certain aspects of the assay that are independent of our desired readout and we sought to develop a cell-free assay system to test these compounds.

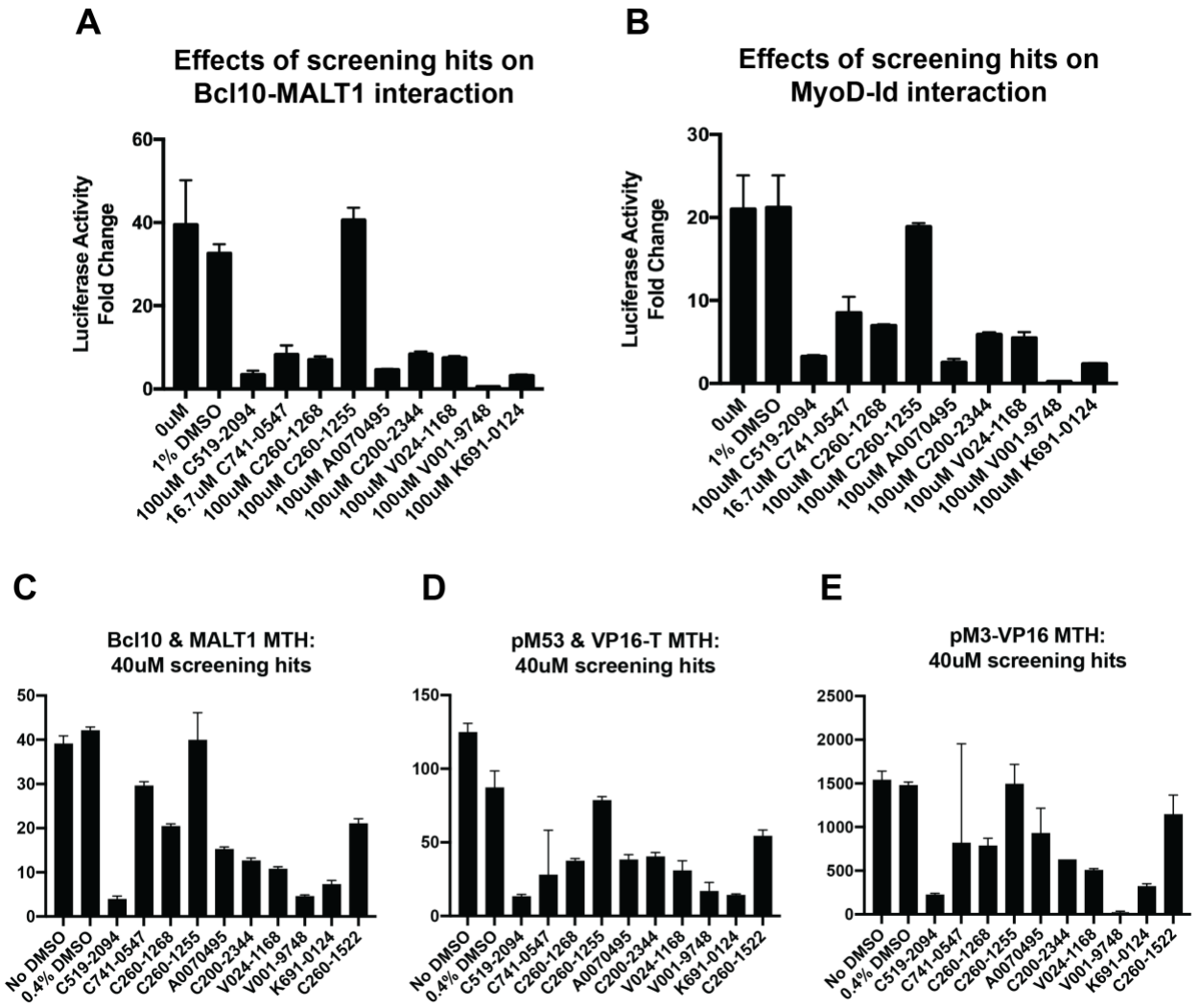

Figure 8. Screening hits display off-target effects in the luciferase assay of the mammalian two-hybrid system. Compounds inhibit luciferase activity induced by Bcl10-MALT1 interaction in the mammalian two-hybrid system (A). Compounds display similar profiles of inhibitory effect for two control protein-protein interactions: MyoD and Id interaction (B), as well as pM53 and VP16-T interaction (C). Compounds also inhibit luciferase activity in the presence of a single fusion construct pM3-VP16, which contains both the GAL4 DNA binding domain and the VP16 activation domain and thus does not depend on protein-protein interaction (E).

Given the off-target effects of these compound hits in the mammalian two-hybrid system, we proceeded to test the candidate molecules using purified recombinant Bcl10 and MALT1 in two different cell-free platforms: surface plasmon resonance (SPR) and an ELISA-based assay for

Bcl10-MALT1 interaction. First, in the SPR platform, full-length Bcl10 is immobilized and a preincubated mixture of 50 nM MALT1 Ig1-Ig2 construct and 100 uM compound is flowed over the Bcl10-bound chip. In this platform, two compounds, K691-0124 and C260-1255, showed complete blockade of Bcl10-MALT1 interaction at 100 uM concentration (Figure 9A, B). Next, these two compounds were tested at different concentrations and shown to demonstrate dose-dependent inhibition of Bcl10-MALT1 interaction, with an IC50 of approximately 20 uM for each compound (Figure 9C, D).

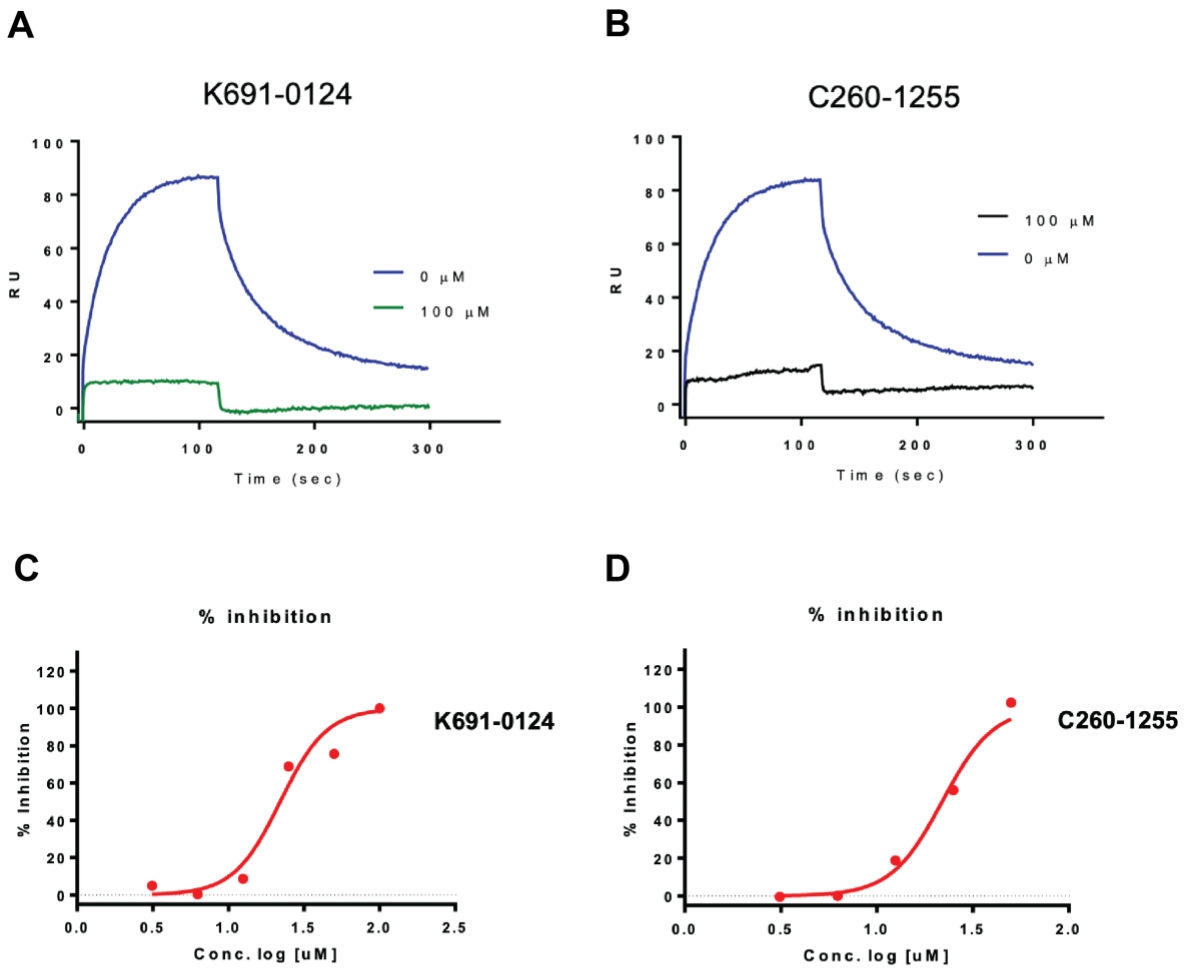

	K691-0124
Bottom	0
Top	100
LogEC50	1.343
Hill slope	2.820
EC50	22.02 uM

	C260-1255
Bottom	0
Top	100
LogEC50	1.341
Hill slope	3.249
EC50	21.91 uM

Figure 9. Compounds K691-0124 and C260-1255 show dose-dependent inhibition of Bcl10-MALT1 interaction by surface plasmon resonance (SPR).

The in silico screening hits, compounds K691-0124 (A) and C260-1255 (B), display complete inhibition of Bcl10-MALT1 binding in SPR at 100uM. Compound K691-0124 shows dose-dependent inhibition of Bcl10-MALT1 interaction, with an EC50 of 22uM (C), and compound C260-1255 shows similar dose-dependent inhibition of Bcl10-MALT1 interaction with an EC50 of 21.9uM (D).

Early efforts to optimize drug-like physicochemical properties of lead compounds are crucial for successful progression to drug candidates, and consensus optimal ranges and limits for key molecular properties are routinely used in ADME prediction models (139, 140). The predicted bioavailability by SwissADME predictive modeling (141) and structures of our two compounds are shown in Figure 10. This modeling was used in order to assess the predicted absorption, distribution, metabolism, and excretion (ADME) parameters, pharmacokinetic properties, drug-like nature and medicinal chemistry friendliness of these two hits from SPR and ELISA-based PPI assays (141). The six physicochemical properties of the compound, including lipophilicity, size, polarity, solubility, flexibility, and saturation, are displayed in hexagonal axes, called "bioavailability radar," for rapid appraisal of drug-likeness. The pink shaded area within the hexagon represents the optimal range for each property that contribute to optimal oral bioavailability (141-143) (Figure 10).

Compound K691-0124 violates one criterion of Lipinski's rule of 5, in that its molecular weight is >500 Da, at 594.66 g/mol. In terms of lipophilicity, the consensus estimation of $LogP_{o/w}$ (octanol-water partition coefficient log P) for compound K691-0124 is 3.77, which generally represents a compound of intermediate polarity, balanced aqueous and lipid solubility, and medium absorption and distribution. Reduced molecular flexibility, as measured by the number of rotatable bonds, is found to be an important predictor of good bioavailability (144). Compound K691-0124 has 10 rotatable bonds, deviating slightly from the optimal "flexibility" property of no more than 9 rotatable bonds in the SwissADME model. Other models suggest 10 or fewer rotatable bonds for high probability of good oral bioavailability (142, 144). Rotatable bonds are defined as any single bond not in a ring, bound to a non-terminal heavy (i.e. non-hydrogen) atom, with the amide C-N bonds excluded due to their high rotational energy barrier. In general, the number of

rotatable bonds increases with molecular weight, and it has been found to be one of the effective predictors of oral bioavailability. The Abbott bioavailability score, which represents the probability that a compound will have >10% bioavailability in a rat (139) is 0.55. The optimal carbon bond "saturation" property, which denotes that the fraction of sp^3 hybridized carbons over the total carbon count of the molecule (Fsp^3 = number of sp^3 hybridized carbons/total carbon count), must not be less than 0.25 (141, 142). This property has been shown to correlate with solubility, and also represents one surrogate measure of the complexity of molecules, which is often associated with target selectivity (142, 145). Thus, Fsp^3 is an important physical property for predicting successful progression of compounds from discovery into clinical development. Compound K691-0124 displays a lower than optimal carbon bond saturation of 0.17. The synthetic accessibility characterizes the estimated ease of synthesis of drug-like molecules, scored from 1 (easy to make) to 10 (very difficult to make). This estimation of the synthetic accessibility score is based on 1) a combination of fragment contributions obtained by analyzing the chemical structures of a million synthesized PubChem molecules and 2) a complexity penalty, which takes into account the presence of non-standard structural features, such as large rings, ring fusions, high number of stereocenters, and molecule size (146). Compound K691-0124 displays an optimal synthetic accessibility score of 3.9.

Compound C260-1255 violates the same criterion of Lipinski's rule of 5, in that its molecular weight is >500 Da, at 518.54 g/mol. The consensus $LogP_{o/w}$ is 3.19, representing intermediate polarity with better aqueous solubility, compared to compound K619-0124. From its bioavailability radar, C260-1255 also deviates from optimal "flexibility" property of no more than 9 rotatable bonds, with 12 rotatable bonds. The Abbott bioavailability score (139) is also 0.55 for C260-1255. The Fsp^3 of C260-1255 is 0.21, slightly lower than the optimal carbon bond

"saturation" fraction of 0.25. The synthetic accessibility score is 3.52, representing optimal estimated ease of synthesis.

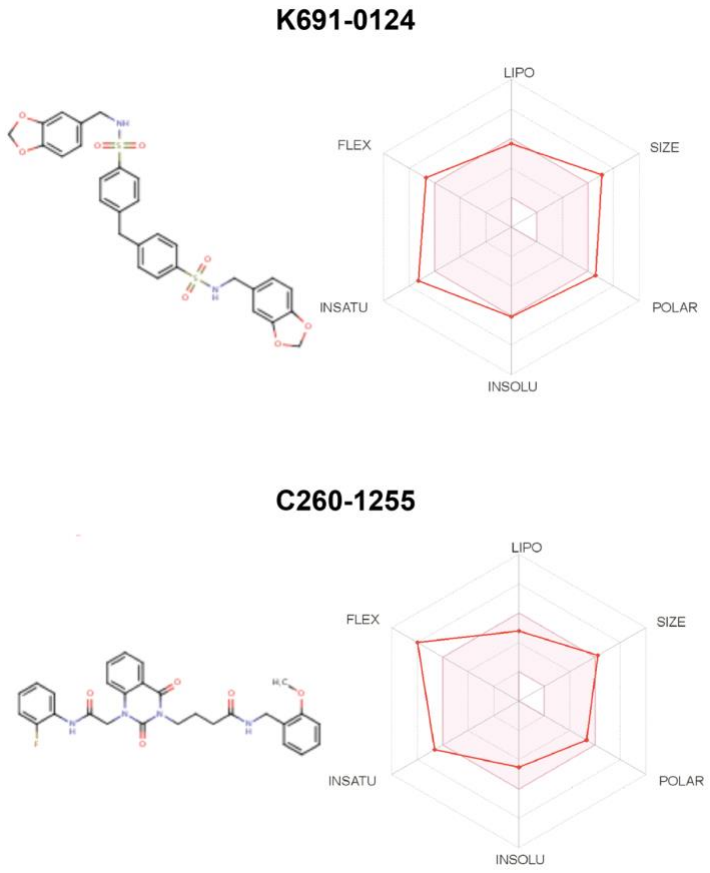

Figure 10. Structures and graphical representation of predicted bioavailability of two compound hits from in vitro protein-protein interaction screening assays.

This "bioavailability radar" shows a first glance look at the drug-likeness of these two molecular structures. The pink area illustrates the optimal range of oral bioavailability for each physicochemical property (lipophilicity, MW, polarity, solubility, saturation, and flexibility). To be estimated as drug-like, the red line of the compound should ideally be included within the pink area. Properties that could be improved in compound K691-0124 for optimal bioavailability includes reducing the size, reducing the number of rotatable bonds, and increasing the ratio of sp3 hybridized carbons over the total carbon count. Properties that could be improved in compound C260-1255 for optimal bioavailability similarly includes decreasing the number of rotatable bonds and increasing the ratio of sp3 hybridized carbons.

In order to corroborate that these two SPR hits inhibit Bcl10-MALT1 interaction, a second cell-free ELISA-based protein-protein interaction (PPI) assay was developed, modified from those previously described (147-150). As shown in Figure 11A, the ELISA-based PPI assay was validated with negative controls that contain only one interacting protein partner as well as a pair of proteins known to not interact with each other (Bcl10 and GRK2). First, 50uM of K691-0124 and C260-1255, two compounds that showed dose-dependent inhibition of Bcl10-MALT1 by SPR, along with one other compound, V001-9748, which did not show inhibition by SPR, were each preincubated with full-length recombinant purified human MALT1 protein for an hour. The preincubated mixtures were allowed to interact with full-length recombinant purified human Bcl10 immobilized on a plate. After washing away unbound proteins, the samples were probed with anti-MALT1 antibody, followed by HRP-conjugated secondary antibody, and TMB substrate solution was added for reaction to occur. Consistent with the SPR findings, both compounds K691-0124 and C260-1255 showed inhibition of Bcl10-MALT1 interaction compared to control Bcl10-MALT1 reaction without any compounds. Also consistent with SPR, compound V001-9748 did not show inhibition of Bcl10-MALT1 interaction in the ELISA platform (Figure 11B).

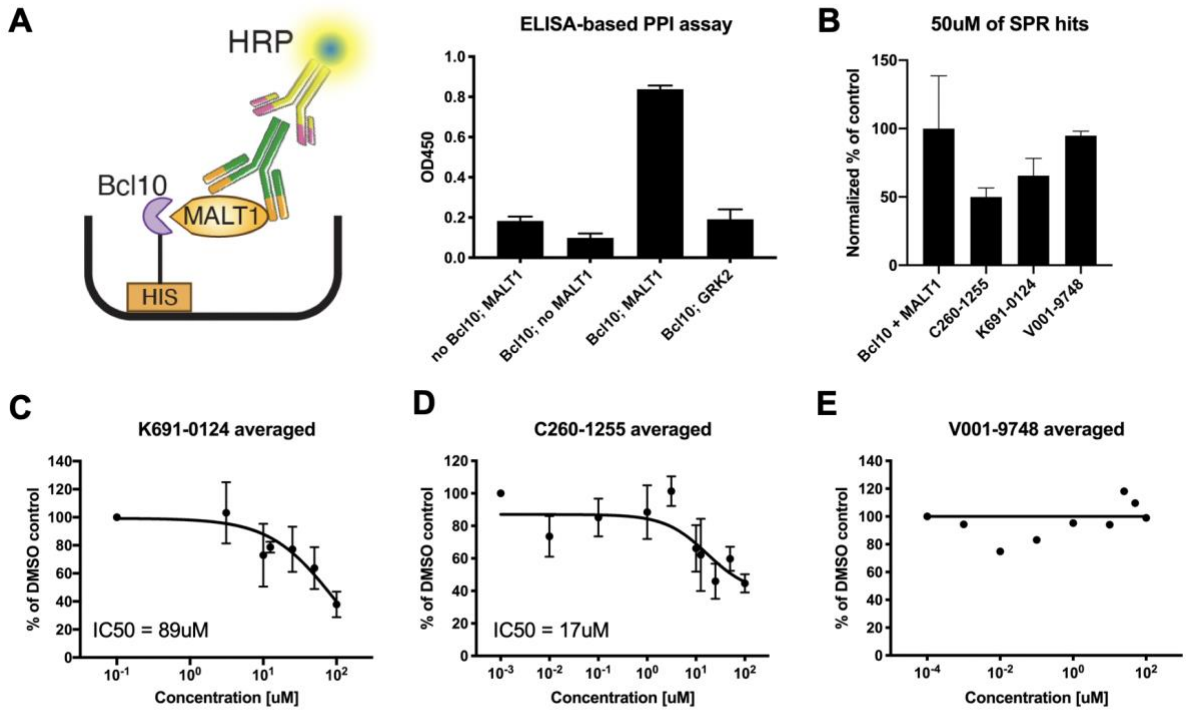

Figure 11. Compounds K691-0124 and C260-1255 show dose-dependent inhibition of Bcl10-MALT1 interaction by ELISA-based protein-protein interaction assay.

Schematic of ELISA-based protein-protein interaction (PPI) assay and validation of the assay are shown (A). SPR hits, C260-1255 and K691-0124, show reduction in the level of Bcl10-MALT1 interaction at 50uM, compared to DMSO control interaction in the ELISA-based PPI assay. Compound V001-9748, which did not show inhibition of Bcl10-MALT1 interaction by SPR, also does not reduce binding in the ELISA (N = 2, not significant) (B). Dose-dependent inhibition of Bcl10-MALT1 interaction by compounds in the ELISA was determined using the following equation: Y = bottom + (top-bottom)/(1+10^(X-LogIC50), with the top and bottom representing the plateaus in the units of Y axis, and with the assumption of one-site binding that is reversible and at equilibrium. Compounds K691-0124 and C260-1255 display dose-dependent inhibition of Bcl10-MALT1 binding with an IC50 of 89 uM and 17 uM, respectively. Compound V001-9748, which failed to show inhibition of the interaction by SPR, also does not display dose-dependent inhibition in the ELISA.

Next, dose-response inhibition of Bcl10-MALT1 interaction shown in SPR was confirmed in the ELISA platform. Compound K691-0124 demonstrated an IC50 of 89 uM, and compound C260-1255 had an IC50 of 17 uM. Again, compound V001-9748 did not show inhibition of Bcl10-MALT1 interaction at 100 uM, the highest concentration tested (Figure 11C, D, E).

As alluded to previously, although the complexity of a molecule can confer greater target selectivity and potency, unnecessarily complex substructures of a starting compound can render it unsuitable for lead optimization, as synthetic accessibility decreases (146). Compounds have been shown to become more complex as they advance through sequential stages of drug development to increase potency, solubility, and other physicochemical properties or improve ADME properties (142, 151). With these considerations, we decided to pursue the development of compound K691-0124 with a simpler backbone.

3.4 Structure-activity relationship (SAR) study of compound K691-0124.

Next, we identified three derivative compounds that have modification of specific chemical groups of compound K691-0124 for an initial structure-activity relationship (SAR) study for the purpose of improving in vitro potency. The structures of three derivative compounds, K691-0122, K691-0185, and K691-0182 are shown, with regions of structural alteration from the parent compound K691-0124 indicated with red arrows in Figure 12. Either the replacement of the 1,3-dioxolane group at the terminal end of the compound with a 4-methoxy group or the removal of the carbon linker in the middle of the compound effectively change the length of the compound and potentially the fit into the linear groove that was identified in MALT1 Ig1-Ig2 domain.

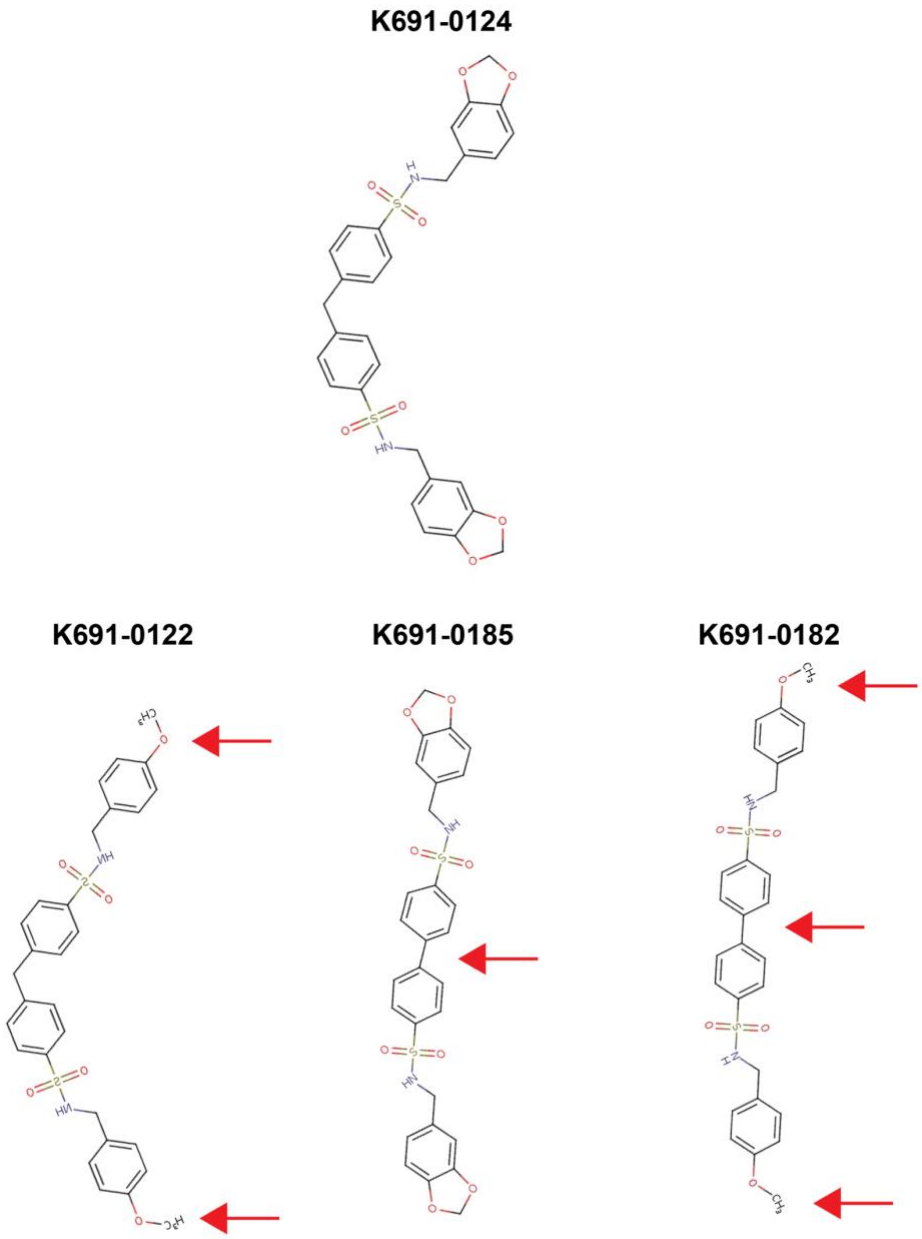

Figure 12. Structures of K691-0124 and its three derivative compounds.

Red arrows indicate regions of structural alteration that differ from the parent compound K691-0124.

Again, the potency of these three derivative compounds in inhibiting in vitro Bcl10-MALT1 interaction was tested in the ELISA-based PPI assay. Remarkably, we observed increased potency as the length of the compounds decreased and the overall conformation became more

linear. One site-fit logIC50 model was used to fit the data on GraphPad Prism. The relative IC50 values of compounds K691-0122, K691-0185, and K691-0182 are 8.45uM, 0.71uM, and 0.40uM, respectively (Figure 13), representing substantial improvement from the IC50 value of 89uM for compound K691-0124.

The structures of additional analogue compounds derived from C260-1255 and their inhibitory effects on Bcl10-MALT1 interaction measured by ELISA is shown in Appendix Figures 2 and 3.

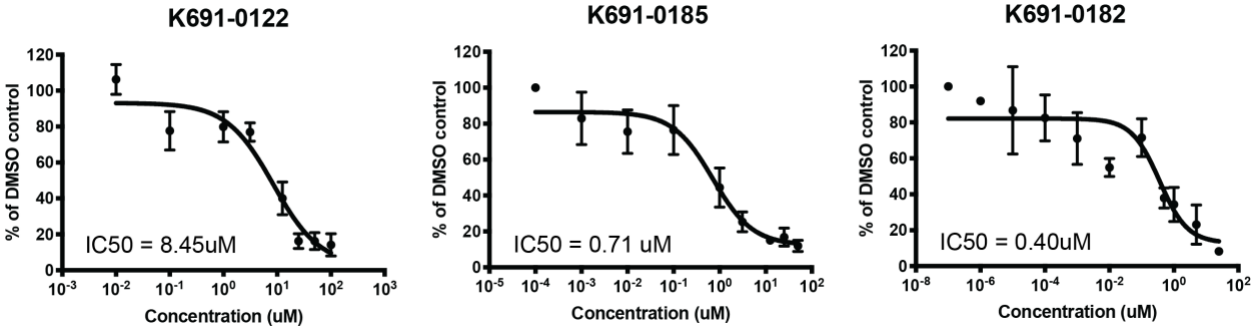

Figure 13. Derivative compounds show dose-dependent inhibition of Bcl10-MALT1 interaction with increasing potency.

Dose-dependent inhibition of Bcl10-MALT1 interaction by compounds in the ELISA was determined using the following equation: Y = bottom + (top-bottom)/(1+10^(X-LogIC50), with the top and bottom representing the plateaus in the units of Y axis, and with the assumption of one-site binding that is reversible and at equilibrium. All three structural analogues of K691-0124 display dose-dependent inhibition of Bcl10-MALT1 binding with increased potency.

3.5 Compounds K601-0124 and K601-0122 show dose-response inhibition of MALT1-dependent IL-2 production by Jurkat T cells.

With these four related candidate molecules (K691-0124, K691-0122, K691-0185, and K691-0182) that show dose-response inhibition of Bcl10-MALT1 interaction in vitro, we proceeded to validate the downstream impact of these compounds on MALT1-dependent signaling, which is vital for T cell activation. To that end, we tested for any changes in the transcription of interleukin-2 (IL-2) gene and secretion of IL-2 cytokine after PMA/ionomycin stimulation in Jurkat T cells treated with these compounds for 24 hours. We chose to focus on IL-2 as one functional readout of the cellular effects of compounds because IL-2 is an NF-kB-inducible cytokine produced in activated T cells after T-cell receptor ligation and thus, its production is dependent on MALT1 activity (36, 82, 152). We found that both compounds K691-0124 and K691-0122 show profound inhibition of IL-2 gene transcription as well as cytokine secretion (Figure 14A, B), resulting from impaired MALT1-dependent canonical NF-kB activation. Compound K691-0185 showed a modest reduction in IL-2 gene transcription, but no significant inhibition of IL-2 production, while compound K691-0182 showed a modest inhibition of IL-2 production, but no inhibition of IL-2 transcription (Figure 14A, B). Compound K691-0124 inhibited PMA/ionomycin-induced IL-2 secretion in a dose-responsive manner with an IC50 of 13nM (Figure 14C). Similarly, compound K691-0122 also displayed dose-dependent inhibition of IL-2 secretion with an IC50 of 19nM (Figure 14C, D). Thus, these two compounds effectively disrupt MALT1 function, evident in the dampened level of secreted IL-2 in the media of K691-0124- or K691-0122-treated Jurkat T cells after PMA/ionomycin stimulation.

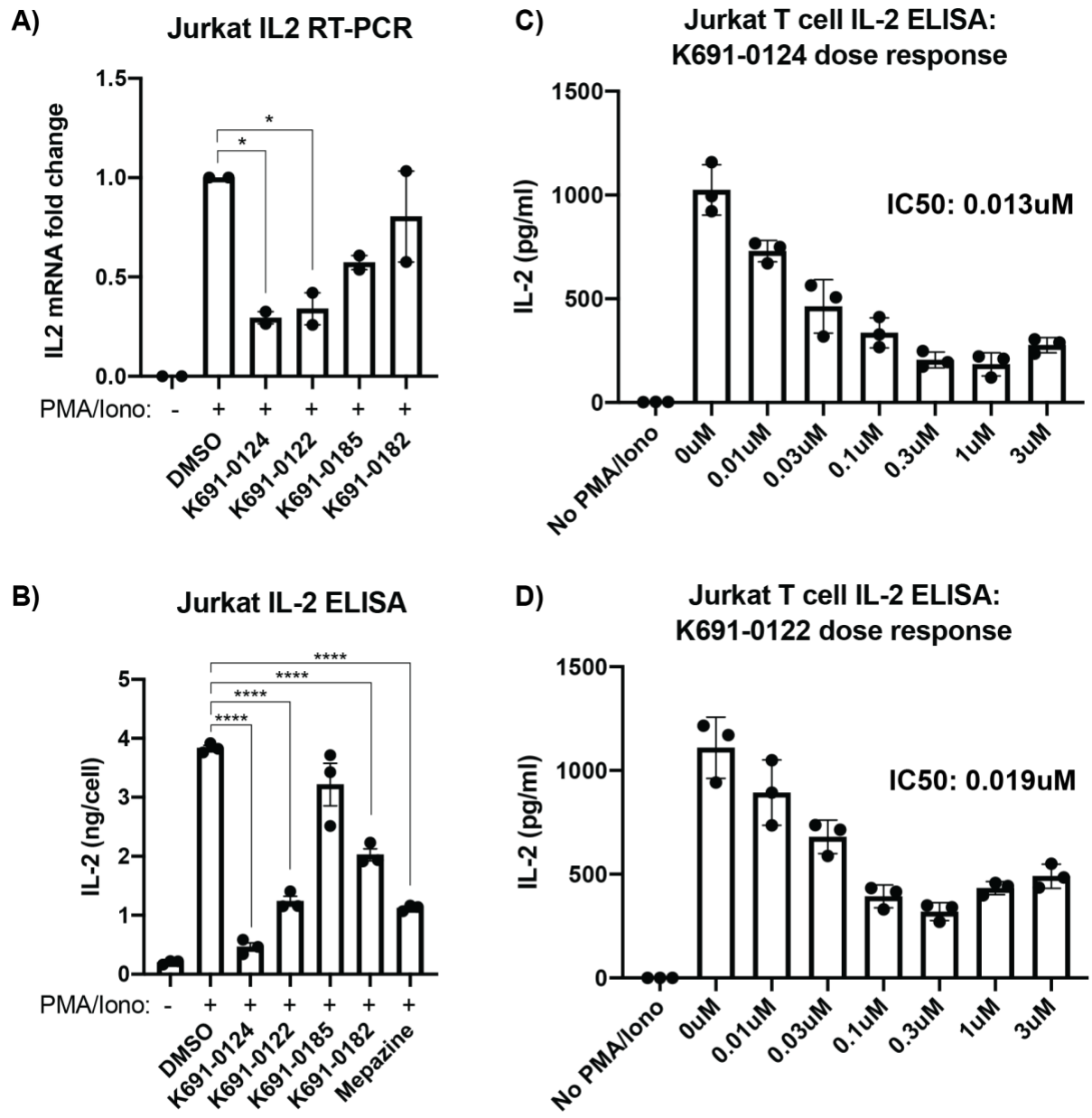

Figure 14. Compounds K691-0124 and K691-0122 inhibit antigen receptor-induced MALT1-dependent signaling in Jurkat T cells.

Compounds K691-0124, K691-0122, and K691-0185 impair PMA/ionomycin-induced IL-2 transcription in Jurkat T cells at 1uM (A). Compounds K691-0124 and K691-0122, at 1uM, significantly reduce the level of PMA/ionomycin-induced IL-2 secretion in media normalized to live Jurkat T cell count, similar to known MALT1 protease inhibitor, Mepazine (B). Compound K691-0124 exhibits dose-response inhibition of IL-2 secretion with a relative IC50 of

0.013uM (C) and compound K691-0122 exhibits dose-response inhibition of IL-2 secretion with a relative IC50 of 0.019uM (D). Statistical analysis was performed using one-way ANOVA and Dunnett test to correct for multiple comparisons in GraphPad Prism software (* $p < 0.05$, **** $p < 0.0001$).

3.6 Compounds K691-0124 and K691-0122 inhibit CBM-dependent secretion of NF-kB targets, IL-6 and IL-10, in ABC DLBCL cells.

Next, in order to determine the downstream impact of these compounds on MALT1-dependent signaling in ABC DLBCL cells, we tested their effects on the constitutive secretion of cytokines IL-6 and IL-10 from two different ABC DLBCL cell lines. IL-6 and IL-10 are cytokines present in the lymphoma tumor microenvironment, and are known to promote the proliferation and survival of malignant B cells. NF-kB-dependent gene expression of these cytokines are critical for ABC DLBCL cell survival and growth (27). The autocrine IL-6 production contributes to the oncogenic process in ABC DLBCL by providing proliferative and anti-apoptotic signals (20), and both IL-6 and IL-10 are secreted by malignant cells purified from patients, with elevated IL-6 levels in patient serum correlating with adverse outcomes (18, 19). Previous studies have demonstrated that ABC DLBCL cells, including OCI-Ly3 and TMD8, spontaneously secrete substantial levels of IL-6 and IL-10, whereas GCB DLBCL cell lines express a negligible amount of IL-6 and IL-10 (112, 153, 154). The transcription and expression of these two cytokines have been shown to depend on MALT1 protease activity, and thus inhibition of MALT1 paracaspase impairs the expression of IL-6 and IL-10 in ABC DLBCL cells (21).

Two ABC DLBCL cell lines, OCI-Ly3 and TMD8, were treated with 1 uM K691-0124, K691-0122, K691-0185, or K691-0182 for 20 hours and the concentrations of secreted IL-6 and

IL-10 in supernatants were determined by ELISA as previously described (112). Both K691-0124 and K691-0122 showed significant reduction in constitutively secreted IL-6 and IL-10 in both OCI-Ly3 and TMD8 cell lines that harbor different CBM-dependent mutations (Figure 15) (Table 3). Despite the fact that compounds K691-0185 and K691-0182 showed the highest potency in Bcl10-MALT1 interaction in vitro, they both failed to affect MALT1-dependent secretion of IL-6 or IL-10 in ABC DLBCL cells.

Moving forward, we decided to pursue the two compounds with the strongest effects on MALT1 function and signaling in lymphocytes: K691-0124 and K691-0122.

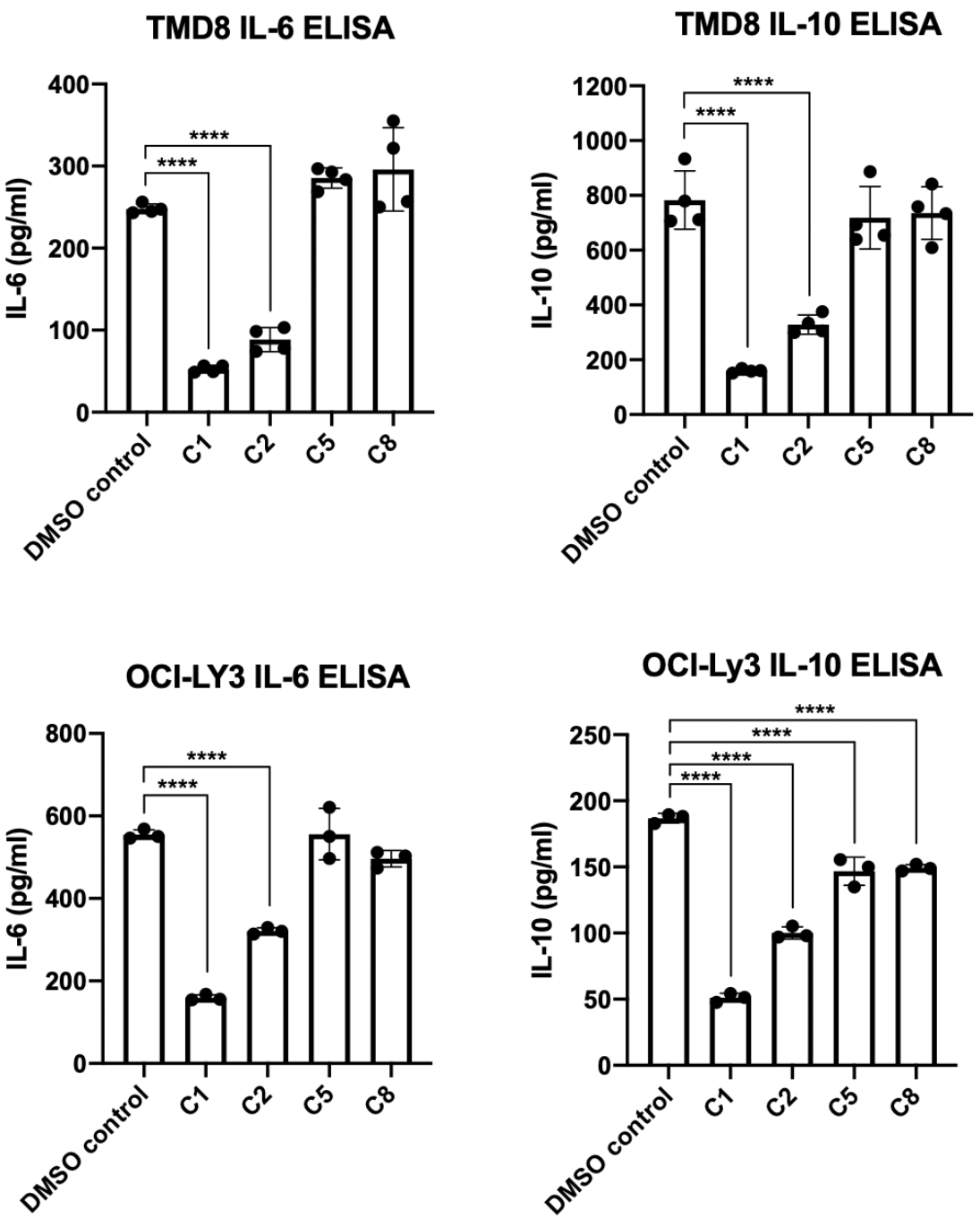

Figure 15. Treatment with K691-0124 or K691-0122 impairs MALT1-dependent expression of NF-kB targets, IL-6 and IL-10, in ABC DLBCL cells.

Two ABC DLBCL cell lines were treated with 1uM K691-0124, K691-0122, K691-0185, or K691-0182 for 20 hours and the levels of secreted IL-6 and IL-10 in the cell culture media were analyzed via ELISA (mean ± SD; N = 3-4).

Statistical analysis was performed using one-way ANOVA and Dunnett test to correct for multiple comparisons in GraphPad Prism software (**** $p < 0.0001$).

Focusing on K691-0124 and K691-0122, we show dose-dependent reduction of both IL-6 and IL-10 in both ABC DLBCL cell lines, TMD8 and OCI-Ly3 (Figure 16). IC50 values for each compound, each cytokine, and each cell line are reported in Table 3. Following constraints were applied for IC50 calculation: Minimum = 0, Maximum = y at x=0.001. With the exception of a weak inhibition of IL-6 secretion in OCI-Ly3 cells by compound K691-0122, all other settings showed remarkably robust blockade of MALT1-dependent constitutive secretion of IL-6 and IL-10 in ABC DLBCL cells.

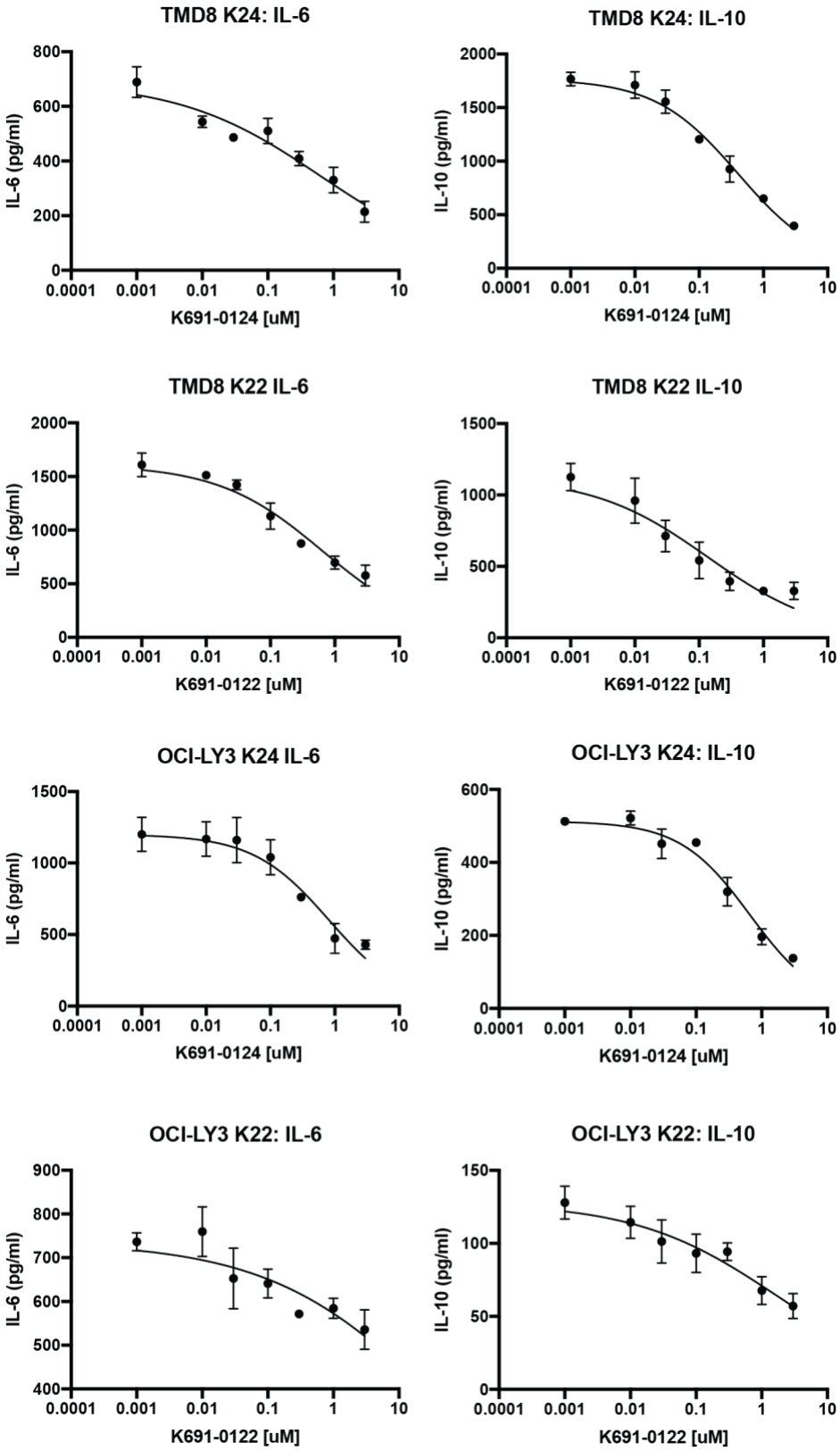
TMD8 K24: IL-6
IL-6 (pg/ml)
800
600
400
200
0
0.0001 0.001 0.01 0.1 1 10
K691-0124 [uM]
TMD8 K24: IL-10
IL-10 (pg/ml)
2000
1500
1000
500
0
0.0001 0.001 0.01 0.1 1 10
K691-0124 [uM]
TMD8 K22 IL-6
IL-6 (pg/ml)
2000
1500
1000
500
0
0.0001 0.001 0.01 0.1 1 10
K691-0122 [uM]
TMD8 K22 IL-10
IL-10 (pg/ml)
1500
1000
500
0
0.0001 0.001 0.01 0.1 1 10
K691-0122 [uM]
OCI-LY3 K24 IL-6
IL-6 (pg/ml)
1500
1000
500
0
0.0001 0.001 0.01 0.1 1 10
K691-0124 [uM]
OCI-LY3 K24: IL-10
IL-10 (pg/ml)
600
400
200
0
0.0001 0.001 0.01 0.1 1 10
K691-0124 [uM]
OCI-LY3 K22: IL-6
IL-6 (pg/ml)
900
800
700
600
500
400
0.0001 0.001 0.01 0.1 1 10
K691-0122 [uM]
OCI-LY3 K22: IL-10
IL-10 (pg/ml)
150
100
50
0
0.0001 0.001 0.01 0.1 1 10
K691-0122 [uM]

Figure 16. Compounds K691-0124 and K691-0122 show dose-response inhibition of IL-6 and IL-10 secretion in ABC DLBCL cells.

Dose-dependent inhibition of cytokine secretion by compounds was determined using the following equation: Y = bottom + (top-bottom)/(1+10^(X-LogIC50), with the top and bottom representing the plateaus in the units of Y axis, and with the assumption of a standard slope equal to a Hill slope of -1.0. Compounds K691-0124 and K691-0122 display dose-dependent inhibition of both IL-6 and IL-10 secretion in two different ABC DLBCL cell lines.

Table 2. IC50 values of compounds K691-0124 and K691-0122 in inhibiting IL-6 and IL-10 secretion in ABC DLBCL cell lines

Cell line	Compound	IL-6	IL-10
TMD8	**K691-0124**	0.64 uM	0.4 uM
	K691-0122	0.65 uM	0.14 uM
OCI-Ly3	**K691-0124**	0.82 uM	0.66 uM
	K691-0122	40.6 uM	1.72 uM

3.7 Compounds K691-0124 and K691-0122 impair both MALT1 protease and scaffolding activities in Jurkat T cells.

Since the activation of MALT1 functions relies on its recruitment to the CBM complex via its interaction with Bcl10, both the protease and scaffolding activities of MALT1 are expected to be impaired if the interaction between Bcl10 and MALT1 is truly blocked by these compounds in cells. Thus, we first tested the ability of compounds K691-0124 and K691-0122 to inhibit the cleavage of certain MALT1 substrates, RelB and N4BP1, upon T cell activation (52, 90, 155)

(Table 1), to test their effects on MALT1 protease activity. Both compounds K691-0124 and K691-0122 show effective inhibition of RelB cleavage and N4BP1 cleavage in Jurkat T cells stimulated with CD3/CD28. Compound V001-9748 is one of the 9 hits from the in silico screen that did not show inhibition of in vitro Bcl10-MALT1 interaction on SPR or ELISA-based PPI assays. Accordingly, compound V001-9748 does not show inhibition of either RelB cleavage or N4BP1 cleavage by MALT1. Known protease inhibitor of MALT1, Mepazine, is included as a positive control (112). Compounds K691-0124 and K691-0122 inhibited RelB cleavage to a similar degree as Mepazine, but both compounds showed enhanced inhibition of N4BP1 cleavage compared to Mepazine (Figure 15A, B).

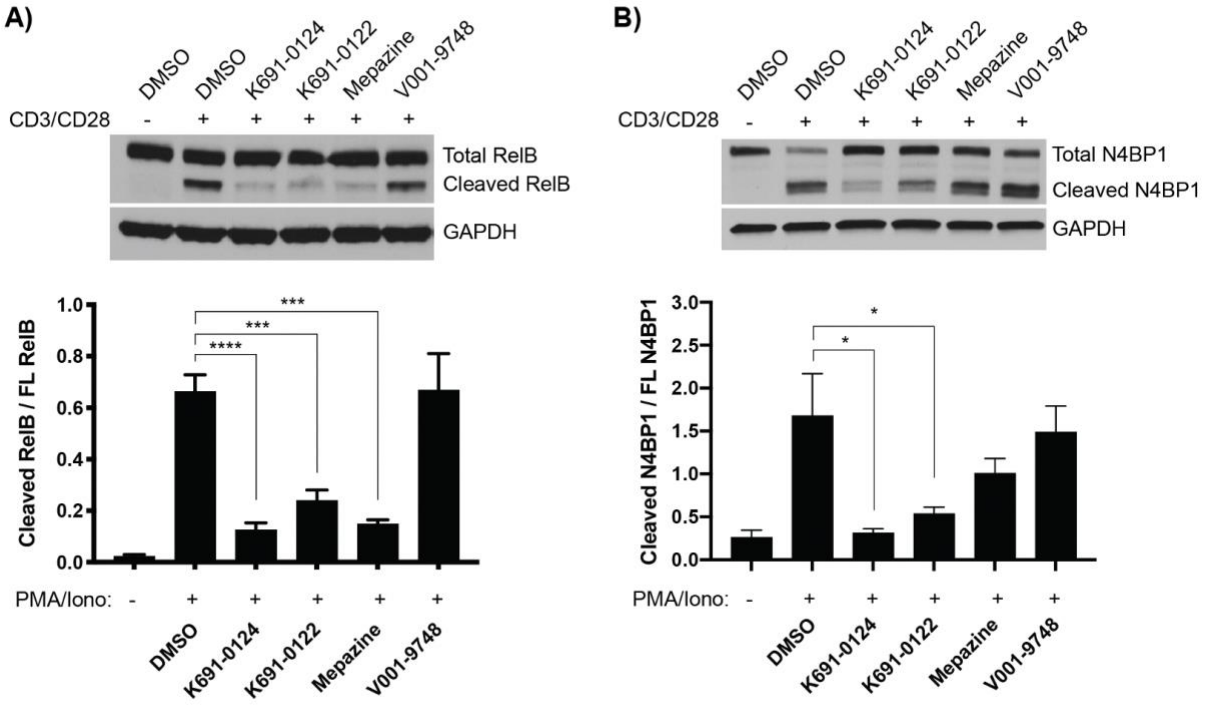

Figure 17. Compounds K691-0124 and K691-0122 inhibit MALT1 cleavage of its substrates, RelB and N4BP1, in Jurkat T cells.

Jurkat T cells were treated with compounds for 20 hours, then 5uM MG132 was added for 1 hour before stimulation with 5 ul/ml anti-CD3/CD28 for 1 hour. Treatment with compound K691-0124 or K691-0122 leads to reduced cleavage of RelB (A) and N4BP1 (B) in response to anti-CD3/CD28 stimulation. MALT1 protease inhibitor, mepazine, is shown as a positive control, and compound V001-9748 is shown as a negative control. Quantification of the ratio of cleaved band / full-length band is shown below. Statistical analysis was performed using one-way ANOVA and Dunnett test to correct for multiple comparisons in GraphPad Prism software (mean ± SEM; N = 4; * $p < 0.05$, *** $p < 0.001$, **** $p < 0.0001$).

In addition to being a protease, MALT1 is also a scaffold protein. MALT1 binds the ubiquitin ligase TRAF6, which modifies itself, Bcl10, and NEMO by K63-linked polyubiquitin chains to phosphorylate the IkB kinase (IKK) complex (81, 85, 86, 156-160). The IKK complex, consisting of the catalytic kinase subunits IKKα (IKK1) and IKKβ (IKK2) and the regulatory

component NEMO/IKKγ, phosphorylates the inhibitor of kappa B (IkB) inhibitory proteins, targeting them for ubiquitin-dependent degradation by proteasome, and releasing NF-kB dimer for nuclear translocation for DNA binding and target gene transcription (161, 162). In order for the IKK complex to become activated, IKKα needs to be phosphorylated on Ser 176 and 180, and IKKβ needs to be phosphorylated on Ser 177 and 181, which is mediated by TRAF6 ubiquitin ligase and TAK1 kinase, which in turn depends on oligomerized Bcl10-MALT1 complex after antigen receptor ligation (156, 163, 164). Thus, if these compounds truly inhibit Bcl10-MALT1 interaction and hence MALT1 function, the scaffold activity of MALT1 is also expected to be impaired, in addition to the protease activity. Thus, the phosphorylation of either IkB or the IKK complex is an established surrogate marker for MALT1 scaffold activity (82, 116, 165-167). Jurkat T cells were treated with 1uM K691-0124 or 1uM K691-0122 for 16 hours, while the cells in the control group were incubated with an equal volume of DMSO (0.05%) for 16h. After 16h treatment, the Jurkat T cells were stimulated with CD3/CD28 for 0, 5, 10, 15, or 20 minutes, then probed for phosphorylation of IKKα/β by Western blot analysis. Cells treated with either K691-0124 or K691-0122 exhibited significantly dampened phosphorylation of IKKα/β over the total IKK. These compounds further show that they are specifically disrupting only the MALT1 scaffold-dependent activity, as the TCR-ligation induced, yet MALT1-independent ERK phosphorylation is unaffected. Quantification of Western blot band intensity by ImageJ and statistically significant difference between control DMSO and treatment group for each stimulation timepoint is shown (Figure 16A, B).

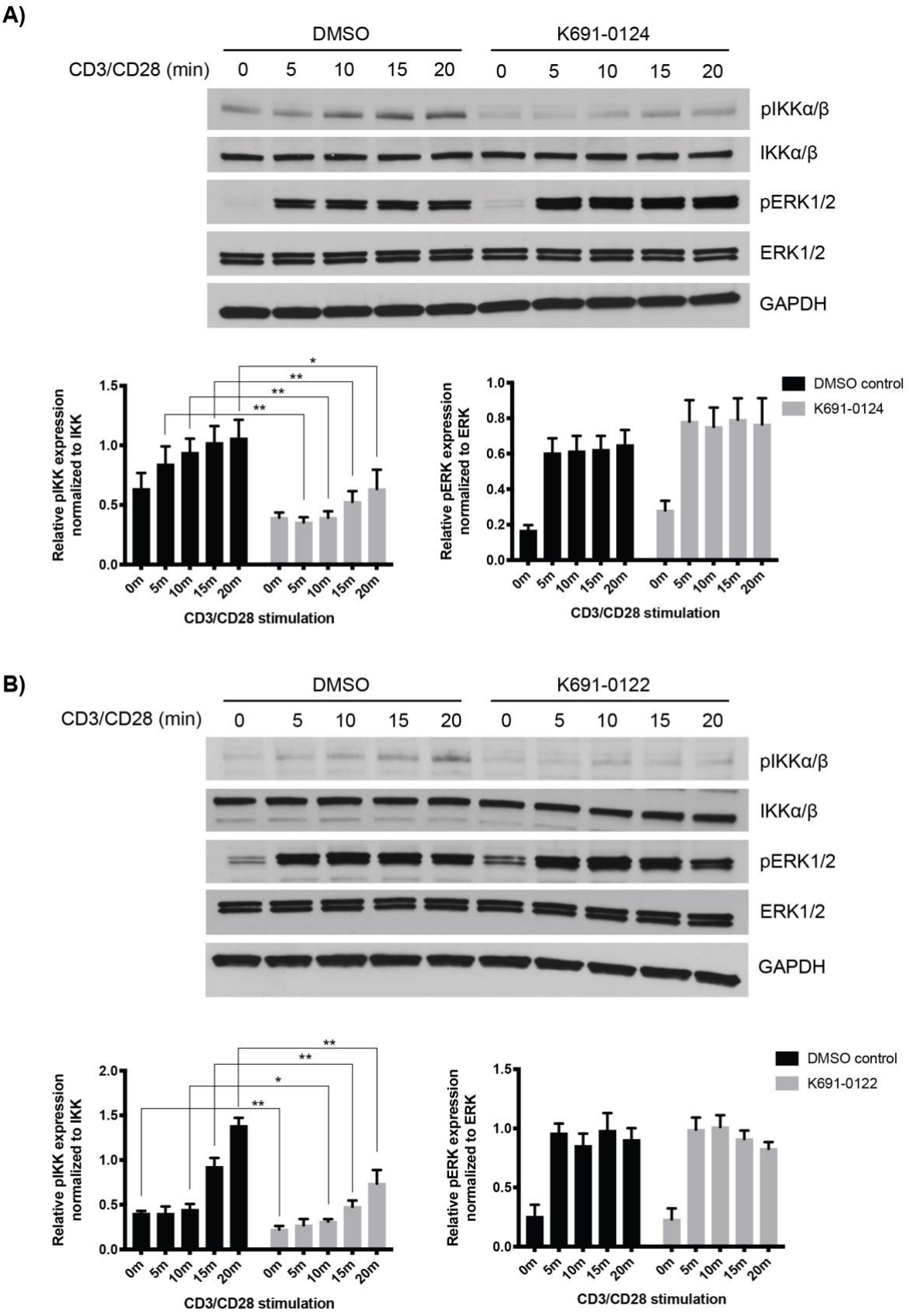
A)
DMSO
K691-0124
CD3/CD28 (min)
0 5 10 15 20 0 5 10 15 20
pIKKα/β
IKKα/β
pERK1/2
ERK1/2
GAPDH
Relative pIKK expression normalized to IKK
Relative pERK expression normalized to ERK
DMSO control
K691-0124
0m 5m 10m 15m 20m 0m 5m 10m 15m 20m
CD3/CD28 stimulation
B)
DMSO
K691-0122
CD3/CD28 (min)
0 5 10 15 20 0 5 10 15 20
pIKKα/β
IKKα/β
pERK1/2
ERK1/2
GAPDH
Relative pIKK expression normalized to IKK
Relative pERK expression normalized to ERK
DMSO control
K691-0122
0m 5m 10m 15m 20m 0m 5m 10m 15m 20m
CD3/CD28 stimulation

Figure 18. Compounds K691-0124 and K691-0122 impair MALT1 scaffolding activity by inhibiting phosphorylation of IKK in Jurkat T cells stimulated with CD3/CD28.

Jurkat T cells were treated with compounds for 20 hours, then stimulated with 5 ul/ml anti-CD3/CD28 for 0, 5, 10, 15, and 20 minutes. Treatment with compound K691-0124 (A) or K691-0122 (B) leads to reduced anti-CD3/CD28-induced phosphorylation of IKK. However, neither compound affects the phosphorylation of ERK, which is TCR-ligation induced, yet MALT1-independent, showing specificity. Quantification of the ratio of phospho-IKK / total IKK as well as the ratio of phospho-ERK / total ERK are shown below. Statistical analysis was performed using unpaired t-test comparing each stimulation timepoint in GraphPad Prism software (mean ± SEM; N = 5; * $p < 0.05$, ** $p < 0.01$).

Table 3. NF-kB activating mutations present in DLBCL cell lines used

DLBCL subtype	Cell line	CD79A/B (104)	MYD88 (27)	CARD11 (168)	TNFAIP3 (169)	TAK1 (169)
ABC (MALT1-dependent)	TMD8	Y196H$_{HET}$	L265P	WT	WT	WT
	OCI-LY3	WT	L265P	L251P	Hem del	WT
GCB (MALT1-independent)	OCI-LY1	WT	WT	WT	WT	WT
	OCI-LY7	WT	WT	WT	WT	WT

3.8 Compounds K691-0124 and K691-0122 selectively suppress the growth of ABC DLBCL cells, but do not affect the growth of GCB DLBCL cells.

Finally, we tested the selective killing ability of these two lead compounds. Starting with a low number of DLBCL cells, they were treated with a single 1uM dose of either K691-0124, K691-0122, or Mepazine, or 5uM Mepazine and allowed to proliferate undisturbed for 12 days. Samples were taken on days 7, 10, and 12 and cell numbers counted using the trypan blue dye exclusion method. The two MALT1-dependent ABC DLBCL cell lines, OCI-Ly3 and TMD8, both displayed inhibition of colony expansion after 12 days by both K691-0124 and K691-0122. Compound K691-0124 showed higher potency in suppressing cell growth, compared to K691-0122 and Mepazine at the same 1uM dose. Compound K691-0122, in turn, was more potent in suppressing cell growth than Mepazine at the same 1uM dose. In contrast, the two MALT1-independent GCB DLBCL cell lines, OCI-Ly1 and OCI-Ly7, did not show any significant changes in cell growth trend compared to the DMSO control group (Figure 20). After 10 days of no media change, OCI-Ly7 cells, including the DMSO control group, had mostly died at the day 12 count. Only data up to day 10 count is shown for OCI-Ly7.

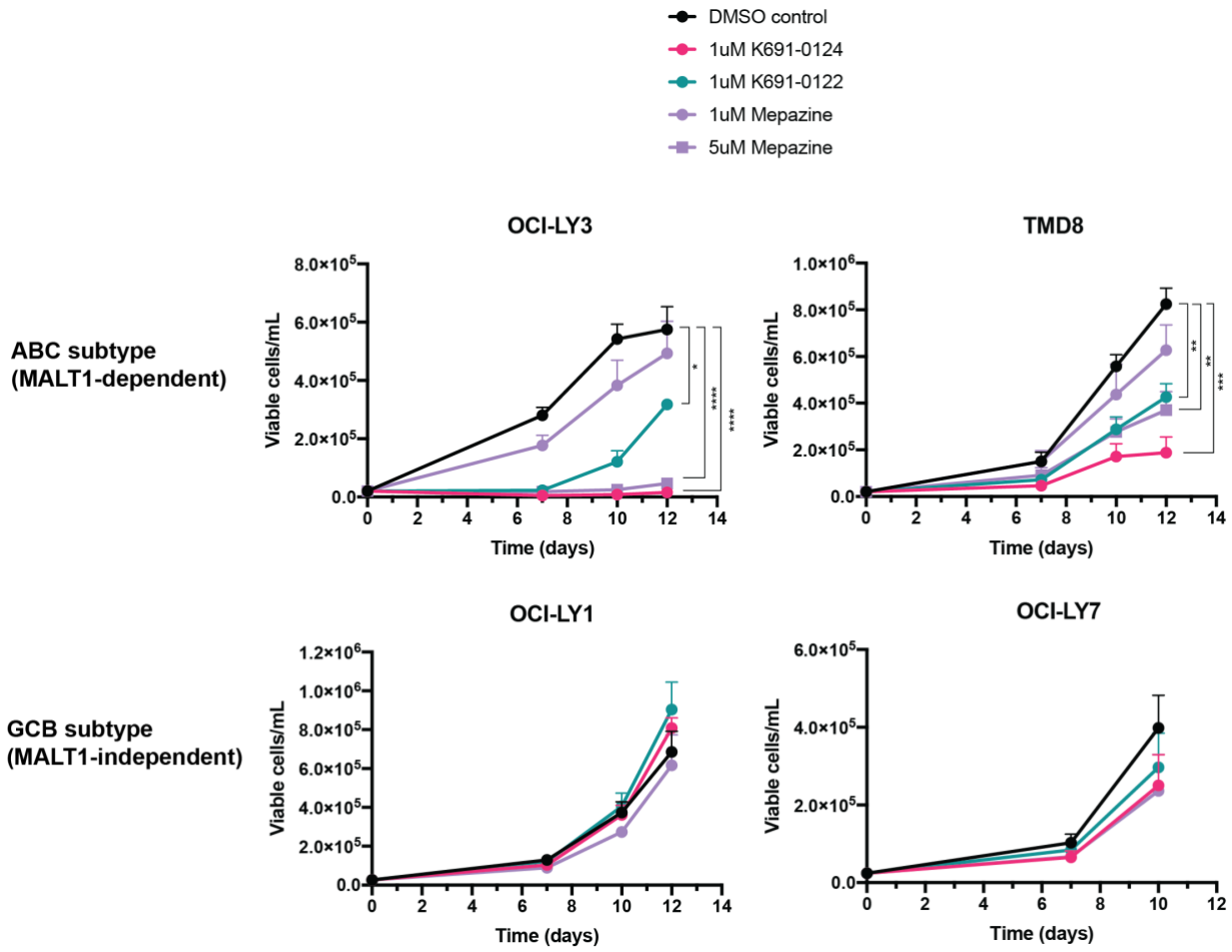

Figure 19. Compound K691-0124 and K691-0122 selectively suppress ABC DLBCL cell colony expansion, but does not affect the growth of GCB ABDLCL cells.

DLBCL cell lines are treated with a single initial dose of 1uM K691-0124, K691-0122, Mepazine, or 5uM mepazine for 12 days and cell number is counted at days 7, 10, and 12 using trypan blue dye. Data are mean ± SEM of 3-6 independent experiments. Statistical analysis was performed using one-way ANOVA at day 12 and Dunnett test to correct for multiple comparisons in GraphPad Prism software (* $p < 0.05$, ** $p < 0.01$, *** $p < 0.001$, **** $p < 0.0001$).

Next, we wanted to explore the mechanism of the observed cell growth suppression by the two lead compounds in more detail, beyond viability. To this end, we specifically tested for the ability of DLBCL cells to divide and proliferate. First, we treated ABC and GCB DLBCL cells

with 1uM K691-0124 or 1uM Mepazine for a short period (3 days) and longer period (6 days), and examined cell divisions using a dye dilution method by flow cytometry (CellTrace Violet, Invitrogen) on viable cells at days 0, 3, and 6. Compound K691-0124 blocked cell division at day 6 in OCI-Ly3 cells, similar to Mepazine, whereas OCI-Ly1 cell division was not affected by either compound, corroborating the ABC DLBCL-selective effects on cell proliferation exerted by K691-0124 (Figure 21). The effect of compound K691-0122 on DLBCL cell division is currently being tested.

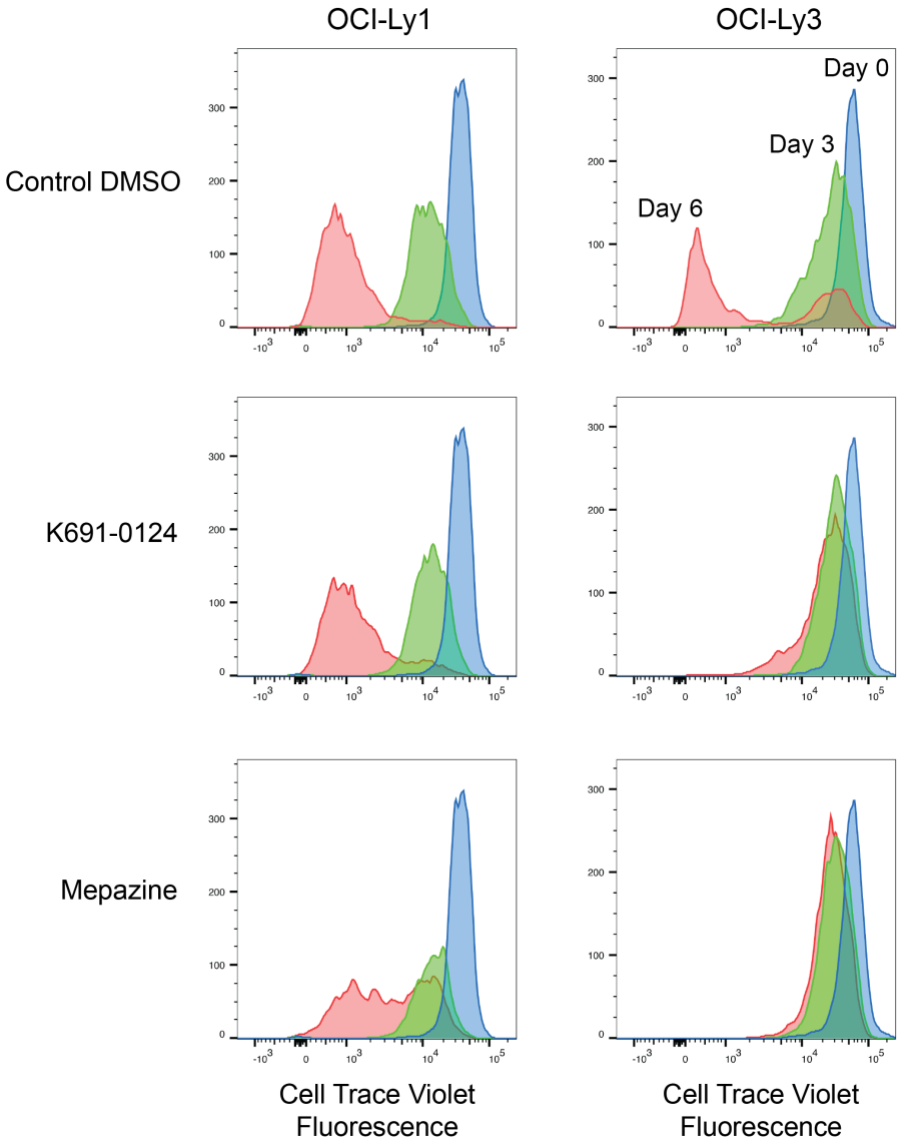

Figure 20. Compound K691-0124 arrests ABC DLBCL cell proliferation without affecting GCB DLBCL cell proliferation.

CellTrace Violet was used as a cell division tracking dye for OCI-Ly3 and OCI-Ly1 cells treated with 1uM compound K691-0124, where the intensity of the staining decreases with each round of cell division. At days 0, 3, and 6 after staining, CellTrace Violet fluorescence was measured by flow cytometry and analyzed by FlowJo. While K691-0124 does not affect the proliferation of the MALT1-independent OCI-Ly1 cells, it blocks the proliferation of MALT1-dependent OCI-Ly3 cells, compared to DMSO. Mepazine is included as a positive control.

We also indirectly assessed DLBCL cytotoxicity by measuring the levels of ATP bioluminescence as a proxy for metabolic health (170) after 0, 48, and 96 hours of treatment with 1uM K691-0124, 1uM K691-0122, or 1-10uM Mepazine. After 48 hours of treatment, none of the 1uM compound groups affected ATP levels in TMD8, OCI-Ly3, or OCI-Ly1 cells. By 96 hours, however, compounds K691-0124 and K691-0122 showed reduced levels of ATP and metabolic viability, compared to same dose Mepazine treatment in both ABC DLBCL cell lines. The GCB DLBCL cell line, OCI-Ly1, did not show reduction in ATP levels after 96 hours of treatment with K691-0124 or K691-0122 (Figure 22).

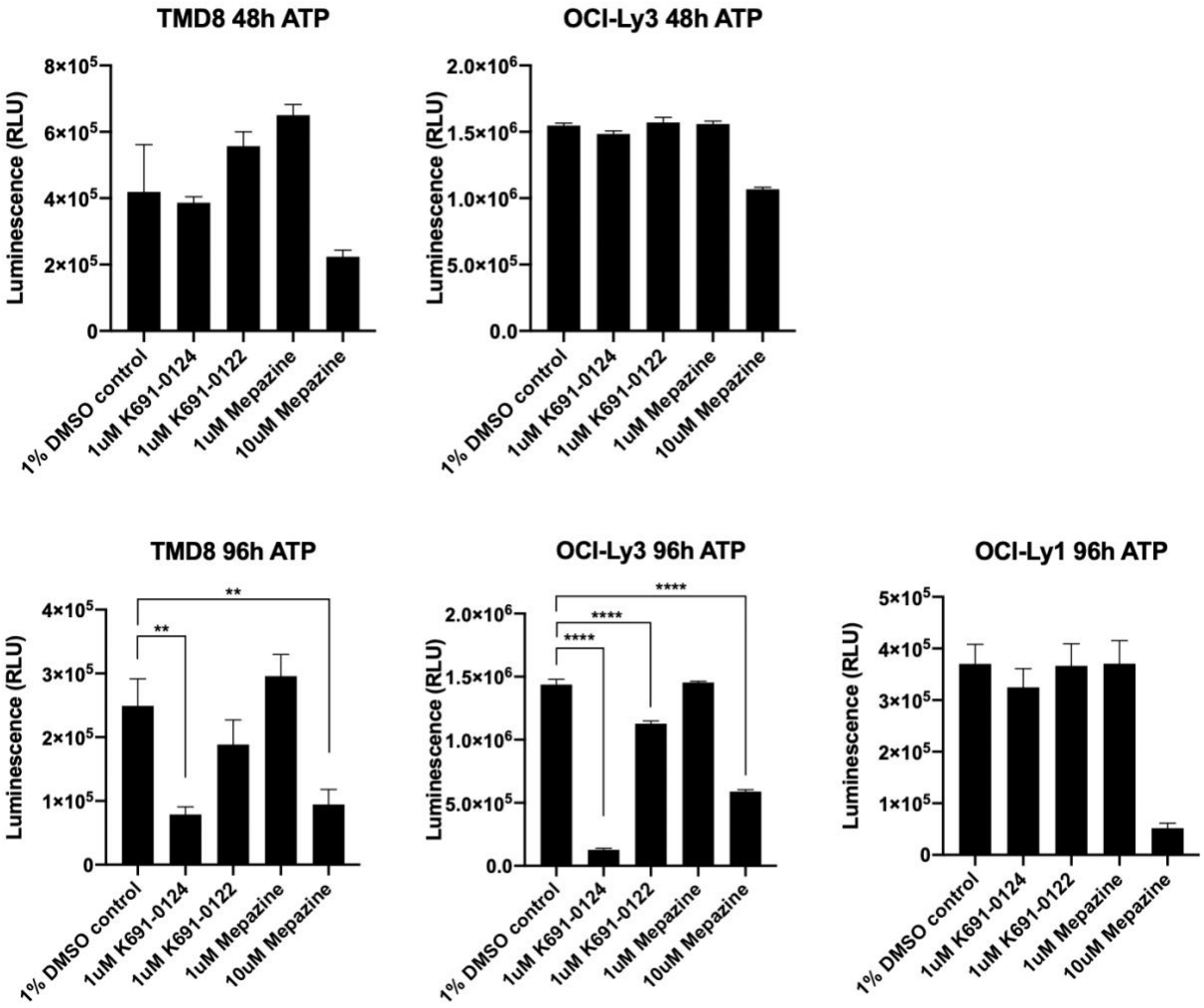

Figure 21. Compounds K691-0124 and K691-0122 are selectively toxic to ABC DLBCL cells.

ATP bioluminescence levels were measured after 48 hours and after 96 hours of treatment with 1uM K691-0124, 1uM K691-0122, or 1-10uM Mepazine in TMD8, OCI-Ly3, and OCI-Ly1 cells. Data are mean ± SEM with 6 biologic replicates. Statistical analysis was performed using one-way ANOVA and Dunnett test to correct for multiple comparisons in GraphPad Prism software (** $p < 0.01$, **** $p < 0.0001$).

Of note, treatment of DLBCL cells with 10uM Mepazine nonspecifically reduced metabolic viability of both ABC and GCB DLBCL cells, and 1uM Mepazine was not effective at reducing metabolic viability of ABC DLBCL cells. Compounds K691-0124 and K691-0122

display more potent and selective toxicity to ABC DLBCL cells, compared to Mepazine, which blocks only the protease arm of MALT1.

Next, we directly tested for the ability of our lead compounds to induce apoptosis and enhance ABC DLBCL cell death to eradicate tumor cells. ABC and GCB DLBCL cells were treated with 1uM K691-0124 or 1uM Mepazine for 6 days, and apoptotic cells were detected by Annexin V and Sytox blue dead cell DNA staining for flow cytometry. For the GCB DLBCL cell line, OCI-Ly1, the majority of cells were limited to the lower left Q4 with Annexin-/Sytox- for control DMSO, K691-0124, and Mepazine groups, confirming that K691-0124 does not induce apoptosis in MALT1-independent OCI-Ly1 cells. On the other hand, ABC DLBCL cell line, OCI-Ly3, displayed higher number of cells in the early apoptosis (Q3) and late apoptosis (Q2) stages, similar to Mepazine (Figure 23).

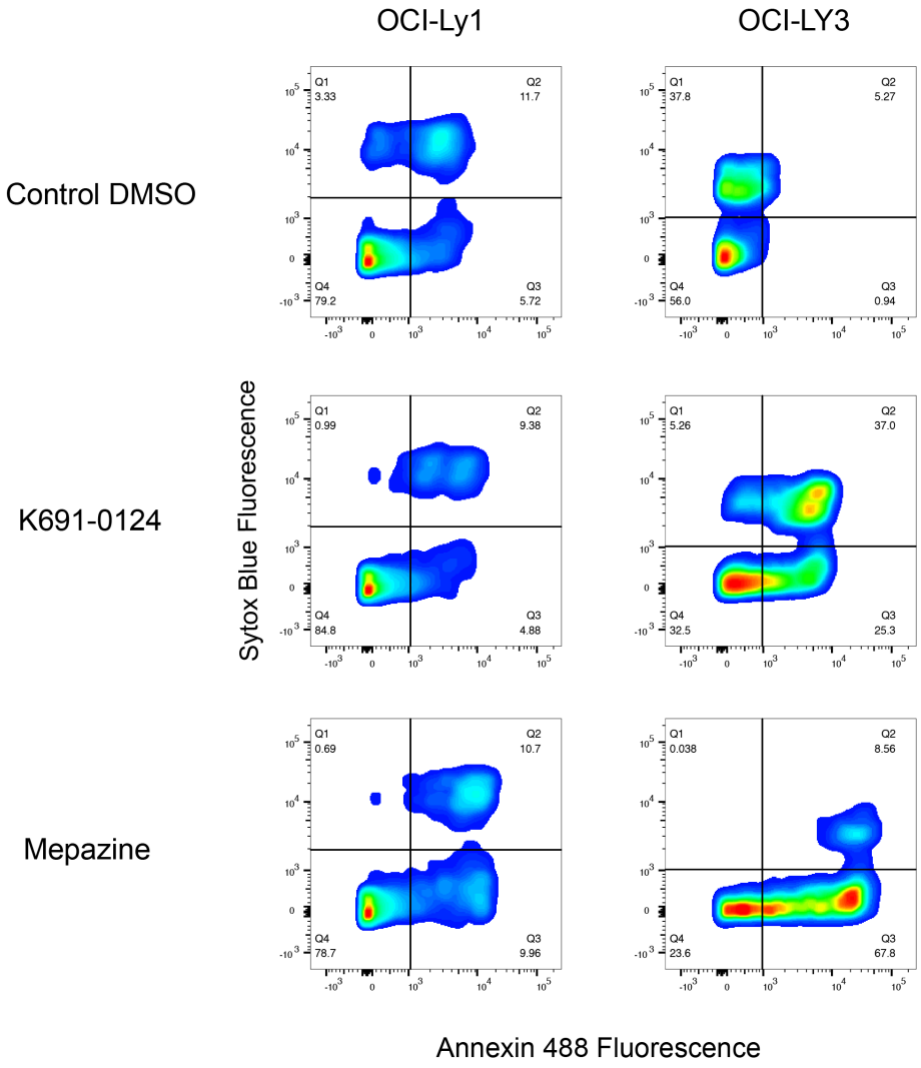

Figure 22. Compound K691-0124 selectively induces apoptosis in ABC DLBCL cells.

DLBCL cell lines were incubated with 1uM K691-0124 or Mepazine for 6 days. Cells were labeled with Annexin V-FITC and Sytox Blue dead cell stain for flow cytometry. K691-0124 does not induce apoptosis in OCI-Ly1 cells, compared to DMSO. Higher proportion of apoptotic OCI-Ly3 cells is observed in early apoptosis (Q3) and late apoptosis (Q3) quadrants when treated with K691-0124.

3.9 Pharmacokinetic study of compound K691-0124

Pharmacokinetics (PK) is the study of the rates of absorption, distribution, metabolism, and excretion of a drug and its metabolites in the body in order to evaluate the dosing and frequency regimen of a potential drug to maintain target efficacy. As a favorable PK profile is vital to the therapeutic success of a drug, a preliminary in vivo PK study of compound K691-0124 was performed by Touchstone Biosciences lab. There were no abnormal clinical symptoms in three mice observed during the 24 hours of the preliminary in vivo PK study to evaluate the clearance of compound K691-0124. LC-MS/MS was performed to analyze the plasma collected at multiple time points (5, 15, and 30 minutes, and 1, 2, 4, 6, 8, and 24 hours) after intraperitoneal injection of compound K691-0124. Non-compartmental PK modeling was used to fit the pharmacokinetic data. From the concentration vs. time curve in the semi-log scale (Figure 24), a linear regression was performed on the terminal linear phase. The elimination rate constant was determined from the slope of the line. The area under the plasma concentration vs. time curve was calculated using the linear trapezoidal rule. The following key pharmacokinetic parameters for extravascular administration of the test compound were measured:

- Maximum concentration (C_{max}) and time of maximum concentration (t_{max}): The peak concentration of test compound in the matrix (e.g. plasma) and the time at which the maximum concentration is reached.
- Area under the plasma concentration-time curve (AUC): AUC is the definite integral in the concentration-time curve and a measure of overall drug exposure. The noncompartmental model estimates AUC parameters using linear trapezoidal approximation of the integral.

  AUC = $\int_0^\infty C(t)dt$, where C(t) = plasma concentration at time t

- Terminal half-life ($t_{1/2}$): The time required to clear 50% of the drug from the matrix (e.g. plasma) after reaching pseudo-equilibrium.
- Mean residence time (MRT): The estimated time the drug molecule spends in the body as measured in the plasma. MRT is a function of the steady-state volume of distribution and time-averaged clearance. The concept behind MRT calculation is that each drug molecule spends a different amount of time in the body, with some molecules staying in the body for a short time and others lasting longer. MRT can be calculated by the following formula:

  MRT = AUMC / AUC, where AUMC = $\int_0^\infty tC(t)dt$

  (AUMC is the area under the moment curve, representing concentration vs. time plotted against time. AUMC can also be estimated from the sum of the area of each trapezoid multiplied by time.)

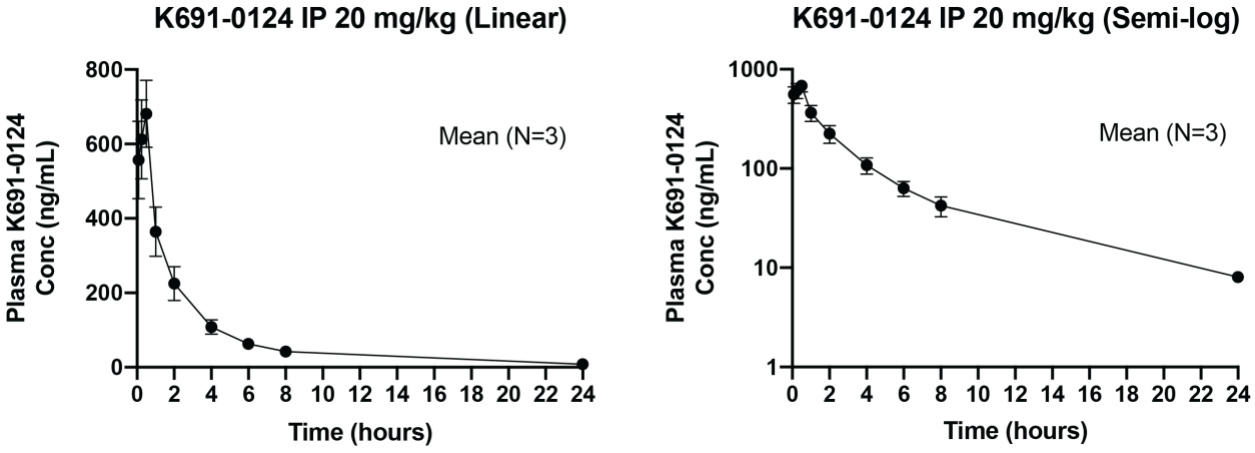

Figure 23. In vivo pharmacokinetic profile of compound K691-0124.

Following intraperitoneal injection of 20 mg/kg of K691-0124, the test compound rapidly reached a mean peak plasma concentration, C_{max} of 681 ng/mL within 30 minutes (t_{max}). After reaching C_{max}, the plasma concentration of the compound declined in a multiphasic manner with

the last measurable concentration C_{last}, of 8.06 ng/mL at hour 24. The compound exhibited a moderate terminal half-life of 6.33 hours. Total systemic exposure (AUC_{inf}) was 1921 hour * ng/mL. Mean residence time (MRT) was approximately 5 hours. Complete PK data of each animal and mean parameters are summarized in Table 4.

Table 4 In vivo pharmacokinetic parameters of 20 mg/kg of compound K691-0124

	Animal #					
	1	**2**	**3**	**Mean (N=3)**	**SD**	**CV%**
$t_{1/2}$ (hr)	6.06	6.16	6.76	**6.33**	0.38	6.01
t_{max} (hr)	0.5	0.5	0.5	**0.5**	0	0
C_{max} (ng/mL)	596	775	671	**681**	89.9	13.2
C_{max}/D (ng/mL)	29.8	38.8	33.6	**34**	4.49	13.2
t_{last} (hr)	24	24	24	**24**	0	0
C_{last} (ng/mL)	9.14	7.17	7.87	**8.06**	1	12.4
AUC_{last} (hr*ng/mL)	1991	1953	1602	**1849**	214	11.6
AUC_{inf} (hr*ng/mL)	2070	2016	1678	**1921**	212	11.1
AUC_{inf}/D (hr*ng/mL)	104	101	83.9	**96.1**	10.6	11.1
MRT_{inf} (hr)	5.45	4.48	5.29	**5.07**	0.52	10.3

3.10 Compound K691-0124 suppresses the growth of ABC DLBCL in vivo.

In light of our *in vitro* observation that our two lead compounds selectively suppress MALT1-dependent ABC DLBCL cells (Figure 19), we next examined the impact of compound K691-01244 on lymphoma growth *in vivo*. To test the in vivo efficacy of compound K691-0124, we used a mouse xenograft model of ABC DLBCL. To determine whether compound K691-0124 can suppress ABC DLBCL in vivo, we subcutaneously injected 10 million TMD8 cells suspended

in 50% Matrigel into the right flank region of 8-week-old NOD-SCID male mice, as previously reported (109, 110). Once tumors reached an average volume of 100 mm^3 [calculated using the formula: (smallest $diameter^2$ x largest diameter)/2], mice were randomized to receive daily IP injection of 50 mg/kg of the test compound or equivalent volume of vehicle DMSO (50 ul) for 12 days (Figure 24). Based on the results of preliminary PK study discussed previously, we deemed that 50 mg/kg/day of the compound will provide sufficient daily drug exposure. One day after the last IP injection, tumors were harvested for histologic analysis. The heart, lungs, liver, and kidneys sections were stained with H&E to assess for any drug toxicity.

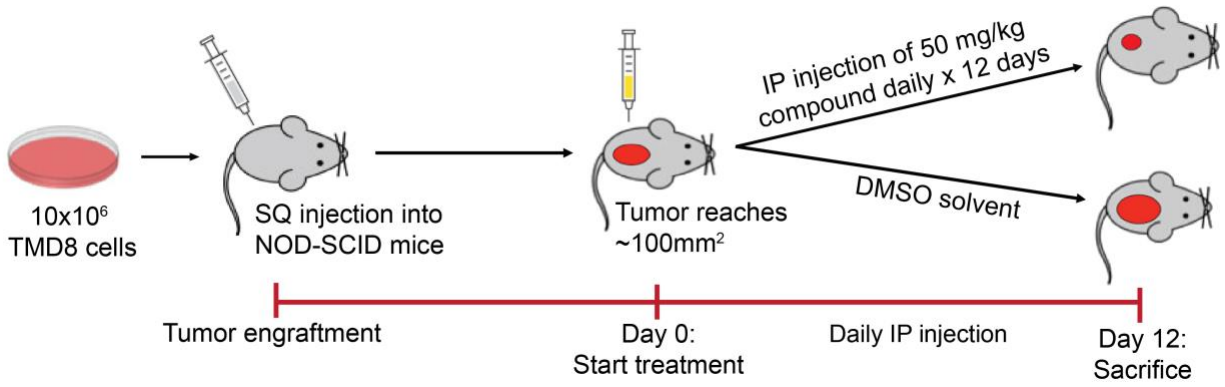

Figure 24. Schematic diagram of in vivo testing of compounds in ABC DLBCL xenograft model.

TMD8 cells resuspended in Matrigel were transplanted into the flank of NOD/SCID mice on day 0. Once tumors reached an average volume of 100 mm^3 within one week, mice were randomized into control (N = 8) and treatment (N = 8) groups, and daily IP injection of compound K691-0124 was initiated for 12 days.

The size of the xenograft tumor as well as the weight of the mice were measured three times a week during the two weeks of IP injection of compound or DMSO. The growth of the ABC DLBCL tumors with K691-0124 treatment was significantly suppressed, compared to the growth of tumors with DMSO treatment. Treatment with K691-0124 led to significantly reduced

tumor weight and volume (Figure 25A, B). Mice treated with K691-0124 showed a small but statistically significant reduction in body weight after 12 days of compound administration (Figure 25C). No abnormal clinical signs or indicators of sickness was observed during 12 days of treatment.

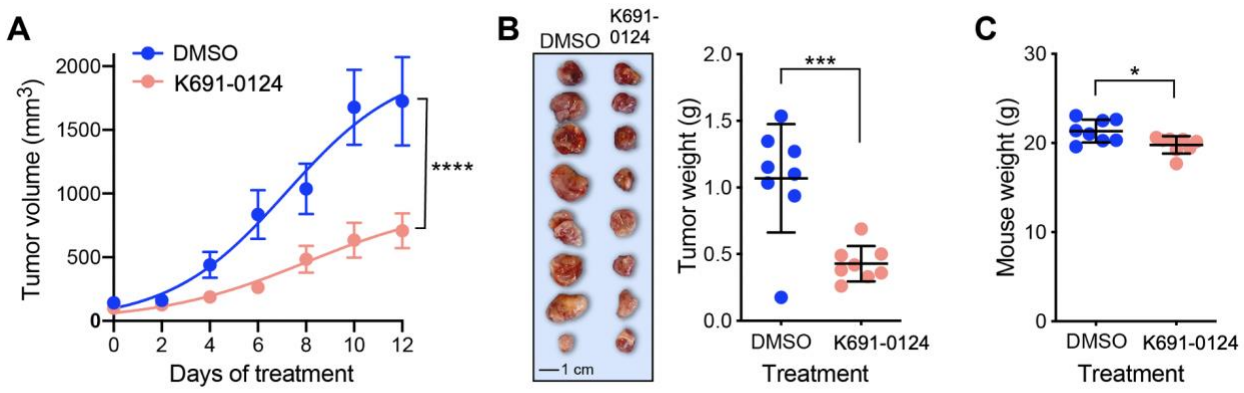

Figure 25. Compound K691-0124 suppresses ABC DLBCL tumor in vivo.

Treatment of mice with K691-0124 leads to significantly reduced tumor volume (A) and weight (B) in a xenograft model of ABC DLBCL. NOD/SCID mice were inoculated with TMD8 cells (10 x 10_6). Tumors were measured three times weekly with calipers, and tumor weight was determined 24 hours after the 12_{th} day of compound injection. Resected tumors from DMSO control group (N = 8) and K691-0124 group (N = 8) are shown in (B). Two-way ANOVA and Sidak's multiple comparison tests were performed to show tumor growth difference between DMSO control and K691-0124 groups. Unpaired t-test was performed for tumor weight and mouse body weight. (* $p < 0.05$, *** $p < 0.001$, **** $p < 0.0001$).

H&E stained heart, lung, liver, and kidney tissues in mice treated with 50 mg/kg K691-0124 daily for 12 days showed no histologic abnormality or signs of tissue damage. Testing of compound K691-0122 in this TMD8 xenograft model, as well as testing the effects of both compounds in an additional ABC DLBCL (OCI-Ly3) xenograft model, as well as in GCB DLBCL

(OCI-LY1) xenograft model are planned. Moreover, testing for synergistic effect of our lead compounds in combination with chemotherapeutics or with maintenance therapy with immunomodulatory agents such as lenalidomide in a xenograft model will inform therapeutic strategies for clinical trials.

4.0 Discussion

4.1 Conclusions

In conclusion, we have identified small molecule compounds K691-0124 and K691-0122 that block the interaction between Bcl10 and MALT1 proteins within the CBM complex, thereby inhibiting the activation of the effector protein MALT1 and effectively blocking both arms of MALT1 function (Figure 24). This novel class of Bcl10-MALT1 PPI inhibitors demonstrates profound inhibitory effects on 1) TCR-induced MALT1-dependent expression of IL-2, which promotes proliferation and survival of activated T cells, 2) constitutive secretion of pathogenic NF-kB target cytokines IL-6 and IL-10, which are negative prognostic factors in DLBCL, 3) MALT1 protease-mediated cleavage of RelB and N4BP1, 4) MALT1 scaffold-mediated phosphorylation of IKKα/β, and 5) proliferation of ABC DLBCL cells by inducing apoptosis without affecting the growth of MALT1-independent GCB DLBCL cells, and lastly displays a favorable PK profile in vivo.

Dysregulation of MALT1 function as a consequence of upstream driver mutations is an underlying cause of a number of T- and B-cell malignancies, as aberrant activation of MALT1 acts as a critical hub that directs inappropriate survival, proliferation, and anti-apoptotic signals toward oncogenesis. Despite this knowledge of MALT1 as a pathogenic driver of ABC DLBCL and increasing number of other hematologic malignancies mentioned previously, current standard treatment regimens do not include agents to specifically target MALT1. Thus, there is a clear unmet need for the development of MALT1-specific targeted therapies. Although there is no commercial MALT1 inhibitor in market, a Phase I clinical trial of an experimental MALT1

inhibitor, JNJ-67856633, recently launched (NCT03900598) (171), and there has been a growing interest and effort in developing MALT1 inhibitors by targeting its obvious protease activity.

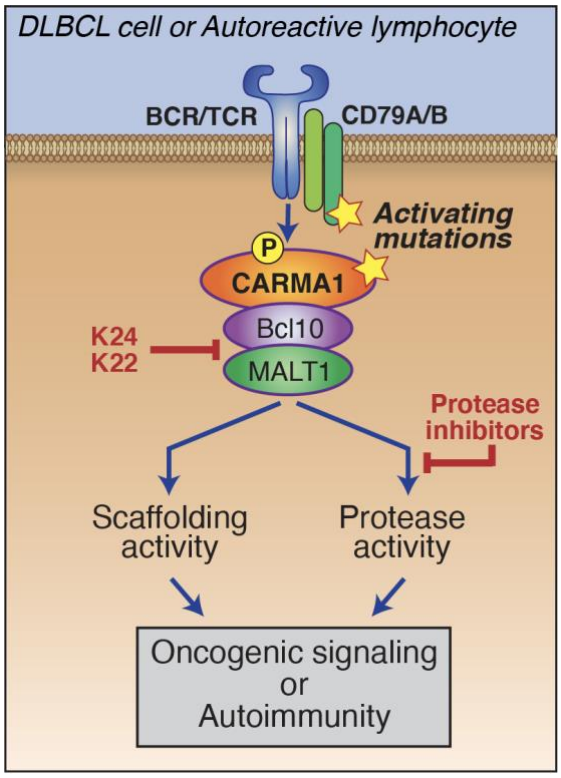

Figure 26. Schematic of sites of action in the CBM signaling pathway by Bcl10-MALT1 PPI inhibitors vs. MALT1 protease inhibitors.

MALT1 is the key effector protein in the CBM signaling pathway an exhibits two activities (scaffolding and protease) that drive oncogenesis in lymphoma and dysregulated inflammation in certain autoimmune diseases. Existing compounds that inhibit MALT1 protease activity are partially therapeutic in preclinical models, and cause incomplete and unbalanced inhibition of MALT1 activity that results in undesirable immune dysfunction. By targeting the Bcl10-MALT1 interaction that is necessary for MALT1 activation, our lead compounds, K691-0124 and K691-0122, block both arms of MALT1 activity.

Compared to Mepazine, a MALT1 protease inhibitor that has been preclinically developed, which is incompletely effective as it blocks only one of the two actions of MALT1 (the protease

activity of MALT1, but not the scaffolding activity), we show that our new class of Bcl10-MALT1 PPI-targeting compounds display higher potency and specificity by disrupting both functions of MALT1.

Despite the potent cellular effects with IC50s in downstream signaling that range from 0.013uM to 1uM, we have been intrigued by the fact that the effective dose of the compounds in cells is significantly less than the measured in vitro IC50 concentration at which 50% inhibition of Bcl10-MALT1 interaction is observed. This phenomenon has been seen in another MALT1 protease inhibitor, MI-2, developed by Fontan et al (109). The growth inhibition GI50 for MI-2 in multiple DLBCL cell lines were < 1uM, lower than its in vitro IC50 of 5.84 uM obtained from in vitro MALT1 protease cleavage assay. They have speculated that this is likely explained by the irreversible binding of MI-2 to MALT1, but also could be due to intracellular accumulation of the compound, as they observe up to 30-fold increase in MI-2 intracellular concentration in experiments where cells are exposed to certain initial doses of MI-2 and then cellular concentration of the compound measured by LC-MS two hours later. It is certainly possible that our PPI inhibitors behave similarly as an irreversible inhibitor. The terminal groups of K691-0124 containing the 1,3-dioxolane moiety and the terminal group of K691-0122 containing the anisole group could potentially modify the groove within the MALT1 Ig1-Ig2 domain covalently. The dioxolane ring of 1,3-benzodioxole group in K691-0124 may have to be deprotected by hydrolysis first, whereas the methoxy group of anisole in K691-0122 can readily react. This may also explain why K691-0124, despite showing higher *cellular* potency compared to K691-0122, has a much higher in vitro IC50 in the ELISA-based assay. In a cell-free environment, the carbonyl protecting group of K691-0124 may impede or delay prerequisite reactions that need to occur in order to competitively bind MALT1, decreasing its apparent availability. But in a cellular environment, the

carbonyl protecting group may confer the advantage of intracellular stability until the compound can cross the cell membrane and reach the target reactive site, increasing its apparent availability compared to the unprotected methoxybenzene group of K691-0122. Alternative explanation for the lower cellular effective dose may lie in the nature of the Bcl1-MALT1 interaction. As mentioned in the introduction, Bcl10 and MALT1 are thought to stabilize each other through the interaction itself. Knocking out Bcl10 or MALT1 reduces MALT1 or Bcl10 protein levels, respectively (132) and deletions of MALT1 domains that contribute to binding Bcl1 or mutations and deletions of Bcl10 residues that are critical to binding MALT1 impair the level of expression (69, 73, 75). Given that the stability of Bcl10 and MALT1 proteins depend on its interaction, our compounds may cause the degradation of both Bcl10 and MALT1 in cells by blocking their interaction, leading to higher cellular potency, compared to *in vitro* potency. The level of Bcl10 and MALT1 proteins in ABC DLBCL cells will be probed after treatment with our compounds to test this hypothesis.

The iterative process of structure-activity relationship (SAR) study, in vitro and in vivo efficacy analyses, and comprehensive pharmacological evaluations will be performed to continue developing these two lead molecules into clinical-grade compounds toward effective treatment of aggressive ABC DLBCL.

4.2 Future Directions

4.2.1 Validate the ability of compounds to block endogenous Bcl10-MALT1 interactions *in situ*.

We plan to further validate these two candidate compounds in a more physiologic context, by testing their ability to disrupt endogenous Bcl10-MALT1 complexes within cells. To this end, we will utilize proximity ligation assay (PLA), which precisely identifies protein-protein interactions only when these interactions occur in extremely close proximity, at < 40 nm (165, 172, 173). We have performed preliminary PLA experiments that probe for endogenous control protein-protein interactions, including CARMA1-Bcl10 and Bcl10-MALT1 interactions, in ABC DLBCL cells, and quantified PLA signals over number of cells (Figure 25, Appendix Figure 8). Further optimization to increase the PLA signal of control Bcl10-MALT1 interaction by testing primary antibody dilution, total reaction volume, and amplification duration is underway. Ultimately, we plan to test the effect of our lead compounds on endogenous Bcl10-MALT1 interaction in ABC DLBCL cell lines in situ.

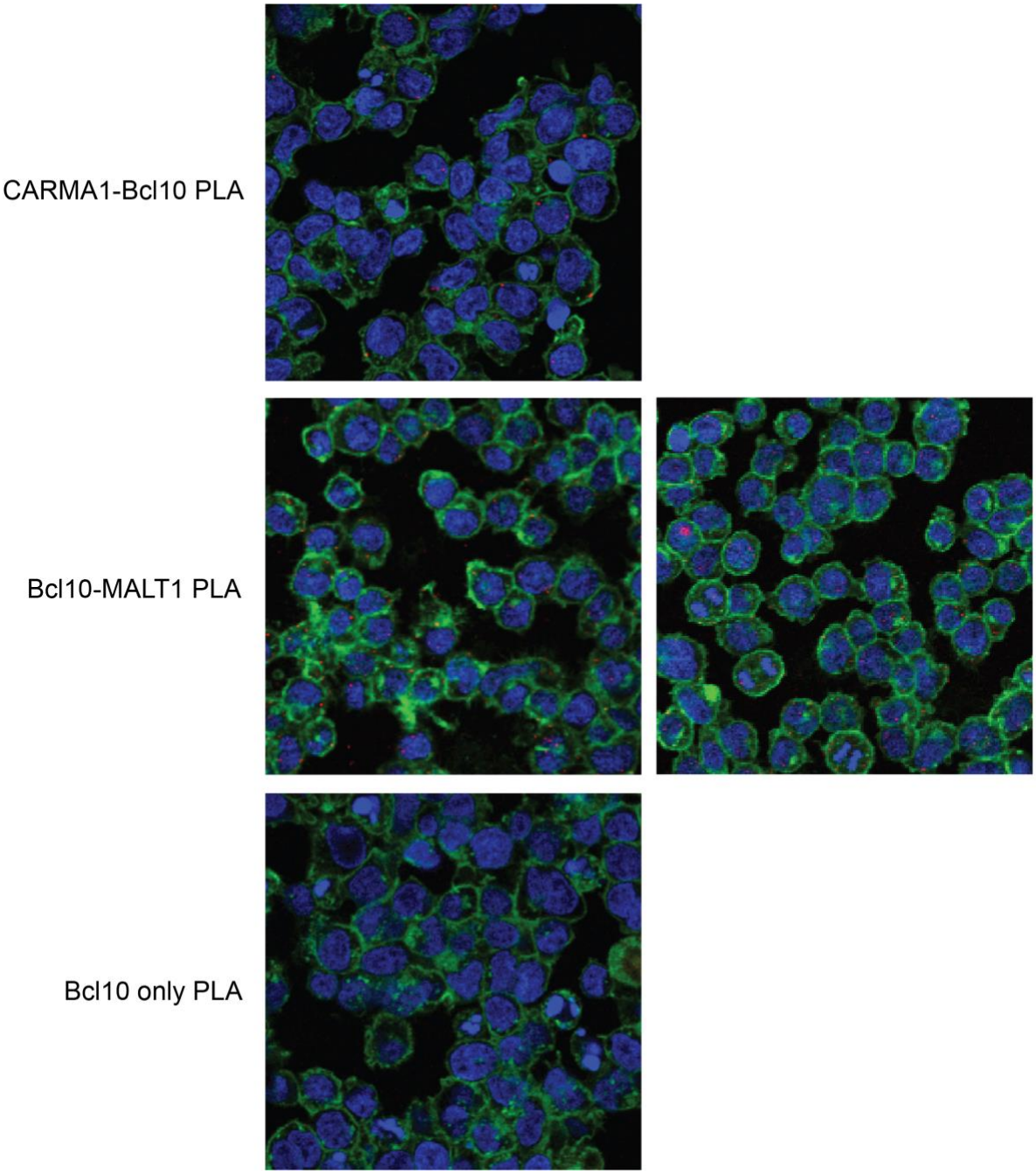

Figure 27. Proximity ligation assay (PLA) development for endogenous Bcl10-MALT1 interaction in TMD8 cells.

Confocal images of PLA spots are visible in red, indicating positive interactions of CARMA1-Bcl10 and Bcl10-MALT1. A negative control with anti-MALT1 primary antibody omitted shows minimal PLA probe background (Bcl10 only PLA).

4.2.2 Experimental evaluation of direct MALT1 target engagement by compounds.

Importantly, we have to verify target engagement by both of our compounds. As our design and development of these compounds were predicated on the in silico modeling of Bcl10-MALT1 interaction, we need to experimentally test the predicted model of how these compounds achieve its in vitro effects. To this end, cellular thermal shift assay (CETSA) will be used. CETSA evaluates drug-protein interaction in cell lysates, based on ligand-induced changes in protein thermal stability. Equilibrium binding of ligands to protein usually increases protein thermal stability (i.e. protein melting temperature) by an amount proportional to the concentration and affinity of the ligand. However, binding of ligands have been observed to destabilize proteins in multiple cases, seen by reduction of protein melting temperature. A ligand may bind to the native (N) and/or unfolded (U) protein. If the ligand binds to the native form of the protein more strongly than to the unfolded state, then the protein is stabilized by the ligand, shifting the protein melting temperature up. If the ligand binds to the unfolded protein more strongly than to the native protein, then the protein is destabilized by the ligand, shifting the protein melting temperature down. The assay involves heating intact cells to different temperatures and quantifying the level of target protein in the soluble fraction by western blotting. A protein melting curve generated from CETSA quantifies the target engagement. A preliminary CETSA experiment of endogenous proteins in HEK293 cells with limited heating temperature range shown below in Figure 26 is inconclusive, and needs to be repeated with a wider temperature range.

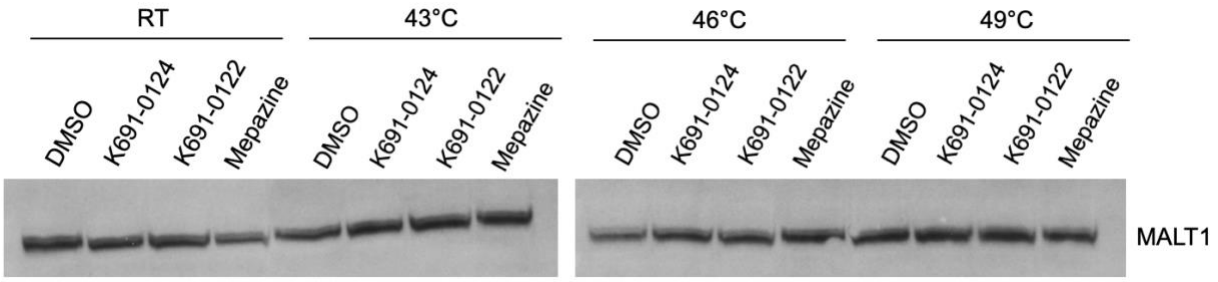

Figure 28. CETSA in HEK293 cells to evaluate MALT1 engagement by compounds.

A complicating factor in evaluating MALT1 engagement by the compounds again lies in the nature of the Bcl10-MALT1 interaction. Bcl10 and MALT1 are thought to stabilize each other through the interaction itself, as disrupting the interaction or knocking down one partner leads to degradation of its binding partner (132). With this consideration, we also plan to perform CETSA in HepG2 Bcl10 KO cell line that the Lucas lab has made in order to assess compound binding of MALT1 without the confounding factor of Bcl10 displacement leading to MALT1 destabilization.

4.2.3 Resolving the potentially context-dependent Bcl10-MALT1 binding mechanism to reconcile the conflicting reports of the putative Bcl10-binding domain of MALT1.

It will be important to address the conflicting reports of whether DD and Ig1-Ig2 domains of MALT1 is necessary and sufficient to bind Bcl10. Although our SPR data along with co-immunoprecipitation studies done by others (69, 74, 75) all indicate that Ig1-Ig2 domains without DD is sufficient to bind Bcl10, and that DD alone without the Ig domains cannot bind Bcl10, the direct interface at which MALT1 binds Bcl10 has been reported to be the DD according to a cryo-EM study (72). Schlauderer et al has also shown that a V81R mutation in the DD completely

abrogates Bcl10 binding. Moreover, FRET analysis by Langel et al (69) strongly suggests that MALT1 DD directly or indirectly contributes to stabilizing the Bcl10-MALT1 interaction in vivo. We also performed site-directed mutagenesis where several negatively charged residues within the MALT1 Ig1-Ig2 domains were mutated to positively charged Lysine residues, and these MALT1 Ig mutants, along with MALT1 DD V81R mutant, were co-immunoprecipitated with Bcl10, as shown in Figure 27. Although the co-IP needs to be repeated and confirmed, residues 220 and 224 in the Ig1-Ig2 are shown to be critical for Bcl10 binding (Figure 27).

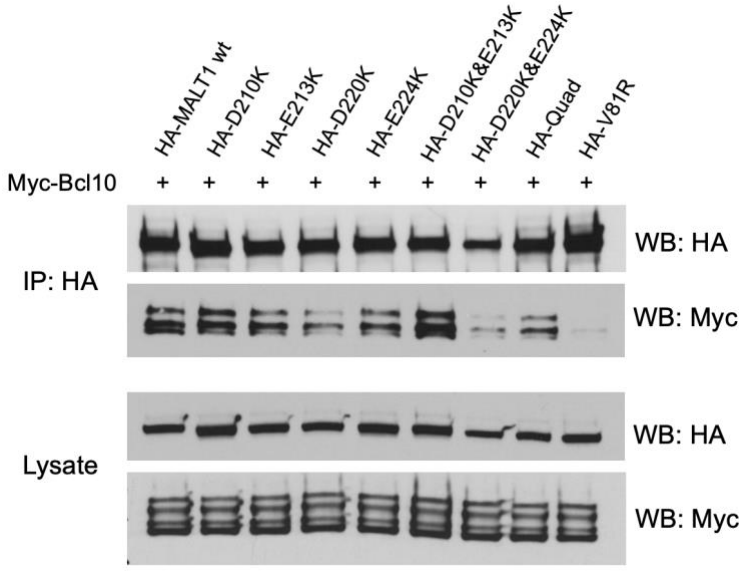

Figure 29. Point mutations within the MALT1 Ig1-Ig2 domains and DD disrupt Bcl10 binding.

Negatively charged residues within the MALT1 Ig1-Ig2 domain were mutated to a positively charged lysine residue. MALT1 DD point mutant V81R that has been previously described to completely abolish Bcl10 binding was included as a control. Mutation of MALT1 residues D220 and E224 in the Ig1-Ig2 domain led to reduced Bcl10 binding in co-immunoprecipitation analysis.

Taken together, it is reasonable to conclude that both the DD and the Ig domains of MALT1 contribute significantly to Bcl10 binding. While DD is reported to be the physical interface of

interaction with Bcl10, there is strong evidence that the Ig domains are necessary to facilitate and stabilize the specific conformation of the Bcl10 CARD and MALT1 DD that is required for interaction. We plan to perform alanine scanning mutagenesis in the MALT1 Ig1-Ig2 domains on a larger scale to elucidate which residues specifically contribute to Bcl10 binding.

However, it will still be necessary to reconcile how the Ig domain by itself seems to be able to bind Bcl10 while lacking the reported physical interface. We hypothesize that the endogenous constitutive Bcl10-MALT1 interaction at the resting, unstimulated state prior to receptor ligation and incorporation into oligomeric filament is different from the induced Bcl10 oligomer-MALT1 oligomer interactions within the filamentous structure, as illustrated in Figure 28. Since the level of local protein concentration has a strong influence on filament assembly, previous studies where Bcl10 and MALT1 proteins were overexpressed only capture protein-protein interactions in the context of an oligomerized higher-order structure. In contrast, endogenous MALT1 has been shown to constitutively associate with endogenous Bcl10 in cells without stimulation (74). Previous studies have also shown that endogenous Bcl10 displays a diffuse cytosolic distribution, whereas overexpression of Bcl10 induces filament formation demonstrated by fluorescence microscopy (65, 66). Moreover, when only MALT1 with two different tags were expressed without Bcl10 overexpression, MALT1 did not show association with each other in co-immunoprecipitation analysis (73). Thus, in an unstimulated cellular environment with endogenous or near-endogenous protein concentration, Bcl10-MALT1 interaction appears to be between monomeric units. Thus, to study the potentially distinct mechanism of resting Bcl10-MALT1 dimeric interaction, we have made Bcl10 oligomerization mutants, R42E and E53R (70, 72) in order to recapitulate an endogenous environment where oligomerization cannot be induced. While these mutations in Bcl10 CARD abrogate Bcl10-Bcl10 oligomerization, Bcl10-MALT1

interaction has been shown to be retained (70, 72). We also have in our toolkit CARMA1-deficient Jurkat T cells, JPM50.6 (50), in which Bcl10 and MALT1 theoretically cannot form filaments. Using these systems that are free of Bcl10 oligomerization, we plan to first examine whether MALT1 DD or MALT1 Ig1-Ig2 is able to bind monomeric Bcl10 by co-IP. Schlauderer et al has also shown that MALT1 DD mutant V81R is unable to bind Bcl10 in MALT1 KO Jurkat cells in both resting and PMA/ionomycin stimulated states. Thus, even in the context of resting Bcl10-MALT1 interaction, DD seems to be indispensable for binding Bcl10. We will also perform co-IP to test the ability of MALT1 Ig1-Ig2 mutants to bind monomeric Bcl10. Ultimately, solving the crystal structure of dimeric Bcl10-MALT1 complex at resting state will be crucial to definitively address this hypothesis.

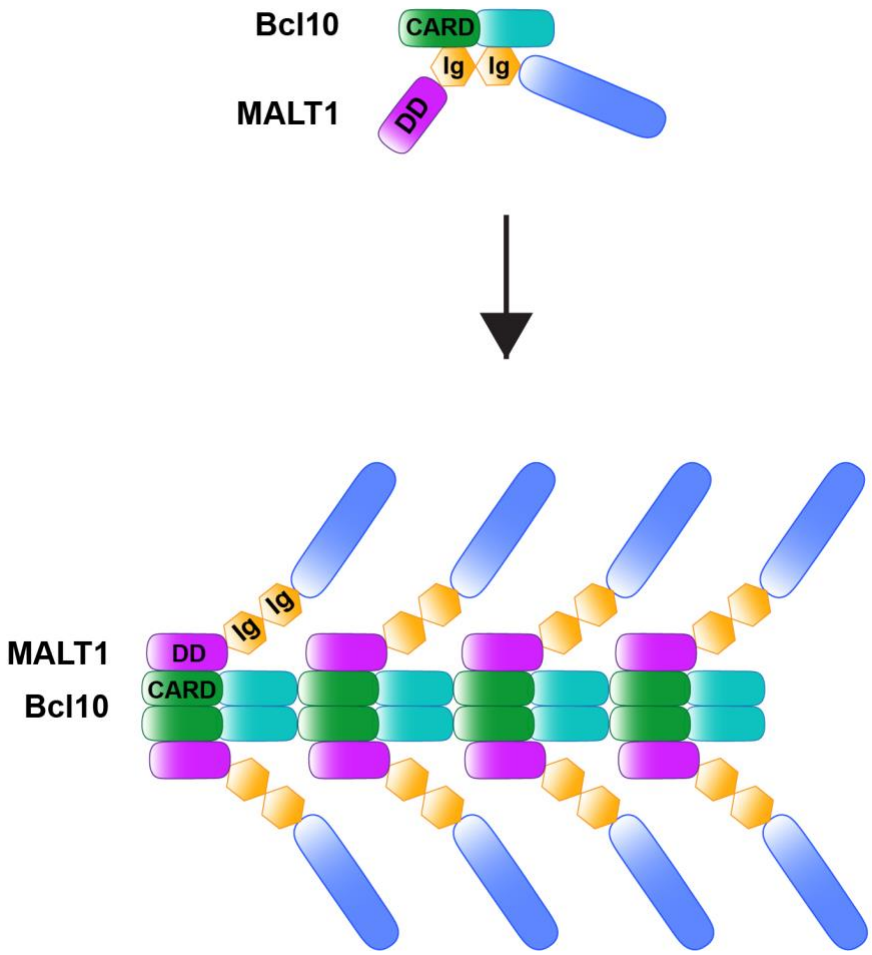

Figure 30. Hypothesized model of adaptable Bcl10-MALT1 interaction mechanisms in the process of oligomerization and filament formation.

4.2.4 In vitro assessment of toxicity and ADME properties of lead compounds

In vitro pharmacological profiling in early drug discovery process is critical for identifying undesirable off-target activity profiles and reduce safety-related drug attrition. Approximately 75% of all adverse drug reactions are reported to be dose-dependent, and can be predicted from the

pharmacologic profile of the candidate compound (174, 175). The pharmacologic profile of a candidate compound includes primary and secondary effects. Primary effects represent the potency of the compound as it relates to its action at its intended target, and secondary effects represent off-target interactions leading to undesirable side effects (176). Thus, evaluation of secondary pharmacologic profiles of our candidates is crucial to reduce the risk of adverse drug reactions. To this end, a commercial panel of 47 targets that are distinct from our intended therapeutic target will be tested to identify any potential undesirable off-target activities by our compounds. The panel will test a broad range of targets, including GPCRs, kinases, non-kinase enzymes, neurotransmitter transporters, ion channels, and nuclear receptors. Moreover, a commercial ADME panel will be used to determine compound solubility, permeability, protein binding, intrinsic clearance, and lipophilicity for comprehensive assessment of the pharmacokinetic properties of our lead compounds. As the absorption of oral drugs require movement of the compound across the intestinal epithelial barrier, intestinal permeability is critical for determining in vivo absorption and evaluating the bioavailability of a compound. The Caco-2 human colon adeno-carcinoma cell line that resembles the epithelial lining of the human small intestine will be used to test drug transport and permeability. The extent of a compound's reversible and saturable binding to plasma or serum proteins determines drug distribution and elimination. Thus, the in vitro plasma/serum protein binding will be used to predict in vivo hepatic clearance. Metabolic stability, which determines how rapidly a compound is metabolized in the liver, and thus predicts oral bioavailability, will be evaluated in a human liver microsome model. Compound solubility will be simulated in gastric fluid and intestinal fluid.

Evaluating the off-target profile and pharmacokinetic properties of lead compounds early in development through these predictive assays will allow us to make informed decisions on

improving compound safety and pharmacokinetic properties, as we continue to progress our lead compounds further into development.

4.3 The role of MALT1 inhibitors in refining rational treatment strategies for ABC DLBCL in the era of precision oncology

In this era of precision medicine where targetable driver mutations and pathway addictions are pinpointed through molecular profiling in clinical practice, challenges still remain in translating these discoveries into clinical grade drugs. The main source of clinical trial failures of investigational drugs has been and remains an inability to demonstrate efficacy or safety (177). Advancing effective and safe drugs through clinical trials remain difficult, as the specificity and selectivity of one novel compound often does not withstand the complexity of tumor biology, where multiple redundancies and crosstalk between pathways can lead to rapidly acquired resistance.

As reviewed in detail in section 1.4, many promising drug candidates for ABC DLBCL have failed to progress in clinical trials mainly due to suboptimal tolerability or failure to meet the primary endpoint of a statistically significant improvement in progression-free survival (PFS) in patients with ABC DLBCL. Thus, to improve the odds of success through clinical trials, rigorous vetting of the drug-like properties (e.g. solubility, permeability, metabolic stability, transporter effects) of early-stage compounds in preclinical models is critical in evaluating and refining ADME and toxicity profiles of the compounds.

Considering clinical trials, we would select patients expected to benefit from MALT1 blockade by screening patient tumors for CARMA1 or CD79A/B driver mutations. Our MALT1

inhibitors would not be expected to be efficacious in ABC DLBCL tumors with mutations downstream of MALT1, including A20 homozygous deletion and TAK1 mutation. Thus, targeted sequencing of recurrently mutated alleles in patients will be central for the rational deployment of MALT1 therapeutics. We envision pairing a molecular diagnostic "companion" test with the therapeutic application of our MALT1 inhibitor, in combination with the current front-line treatment of R-CHOP or an immunomodulatory agent.

Given the complex heterogeneity in the mutational landscape within ABC DLBCL, a single agent targeting a single driver mutation or activated pathway is unlikely to have a durable effect. A rational combination of targeted therapies against cooperating mutations as well as immunomodulatory agents will likely be necessary to overcome drug resistance mechanisms and exert durable effects. Thus, testing our lead compounds in combination with an immunomodulatory drug, lenalidomide, as well as with R-CHOP in *in vivo* models is part of our future directions. Moreover, there is evidence that targeting both MALT1 and MYD88 to terminate the cooperating BCR and TLR signaling pathways in ABC DLBCL cell lines is more toxic that targeting either one alone (27, 99). Recurrent MYD88 mutation occurs in about 30% of ABC DLBCL, often overlapping with MALT1-dependent mutations. Thus, a combination of these agents that target cooperating BCR-NF-kB and TLR-NF-kB signaling axes may exert synergistic and more effective anti-cancer effects, compared to either one by itself.

4.4 The broad therapeutic potential of Bcl10-MALT1 interaction inhibitor beyond ABC DLBCL

As previously discussed in detail, we have learned that MALT1 protease activity is essential for the normal immunosuppressive function of Tregs from studying MALT1 protease-dead mice that develop multiorgan inflammation and destructive autoimmunity. When only the protease arm of MALT1 is defective and Treg development is blunted, the preserved MALT1 scaffold mediates T cell activation and generation of effector T cells without the counterbalancing suppression by the Tregs, leading to autoimmunity. However, mice treated with chemical MALT1 protease inhibitors do not exhibit severe autoimmune side effects, at least in the short-term. This discrepancy in side effects compared to the MALT1 PD genetic model is consistent with the observation that T cells have different signaling requirements during development and at naïve and effector stages. Long-term MALT1 protease inhibitor treatment study will be necessary to monitor potential spontaneous autoimmune phenotype as in the MALT1 PD genetic model. Additionally, complete MALT1 KO mice where both the protease and scaffold functions of MALT1 are lost, both Treg development as well as T cell activation and differentiation into Teff are impaired, leading to immune suppression.

Multiple studies have demonstrated that pharmacologic inhibition of MALT1 holds great promise for the treatment of autoimmune disorders. A MALT1 protease inhibitor, mepazine has been shown to attenuate the severity of multiple sclerosis in EAE mouse model (54); mepazine and another protease inhibitor, MI-2, have both been shown to prevent the development of experimental colitis (178); and another MALT1 protease inhibitor, MLT-827, developed by Novartis (166), has been shown to reduce psoriatic skin disease in mice with CARD14-induced psoriasis (179).

We believe that our Bcl10-MALT1 PPI inhibitors that block both the scaffolding and protease activities of MALT1 in its entirety to suppress both effector T cells and regulatory T cells are particularly well-suited to treat Th17-mediated autoimmune diseases, such as multiple sclerosis, psoriasis, ulcerative colitis, and rheumatoid arthritis, where complete suppression of autoinflammatory immune response is desired. To this end, we have also proposed to test our compounds in an EAE mouse model of multiple sclerosis (Figure 30).

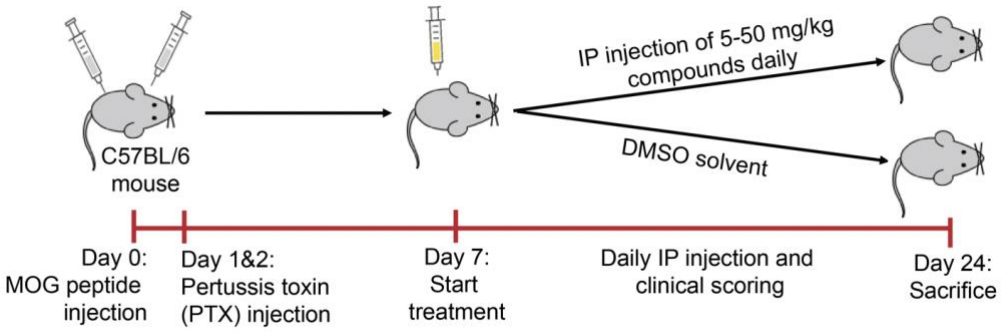

Figure 31. Schematic diagram of in vivo testing of compounds in EAE mouse model of multiple sclerosis.

Moreover, a recent study by DiPilato et al (180) reported that the deletion of CARMA1 in Tregs leads to production of IFN-γ in the tumor microenvironment, generating potent local anti-tumor activity. Treatment with MALT1 protease inhibitors, Mepazine and MI-2, in a melanoma model induced an inflammatory phenotype in Tregs with increased IFN-γ and TNF, and elevated expression of MHC-I and PD-L1 on tumor cells. Thus, small molecule inhibitors of MALT1 holds great promise as a part of solid tumor therapeutic, by inducing an inflammatory phenotype in Tregs to prime the tumor microenvironment for immune checkpoint therapy.

The complex interplay between the immunogenic and tolerogenic functions of MALT1 has great implications for the use of MALT1 inhibitors as a therapeutic for different pathologies. Investigating the exact mechanisms of protective and pathologic immune responses by MALT1 inhibition in immunocompetent mouse models will be critical. Targeting different components of MALT1 function will be an important consideration for therapeutic strategies in the contexts of autoimmune disorders, immunodeficiency diseases, solid tumors, and cancers of the immune system. The challenge will lie in striking the right balance in sufficiently tampering overactive CBM signaling while minimizing compromises to host defense mechanisms.

Appendix A Supplemental Figures

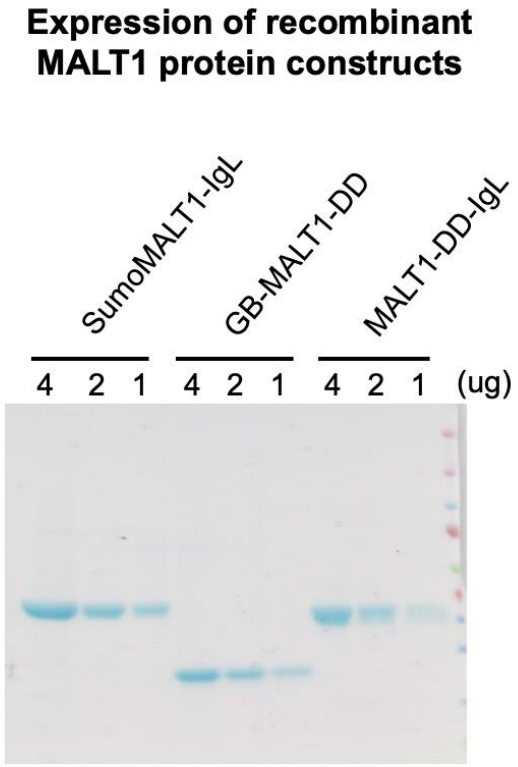

Appendix Figure 1. Expression of purified recombinant MALT1 domain constructs used for surface plasmon resonance.

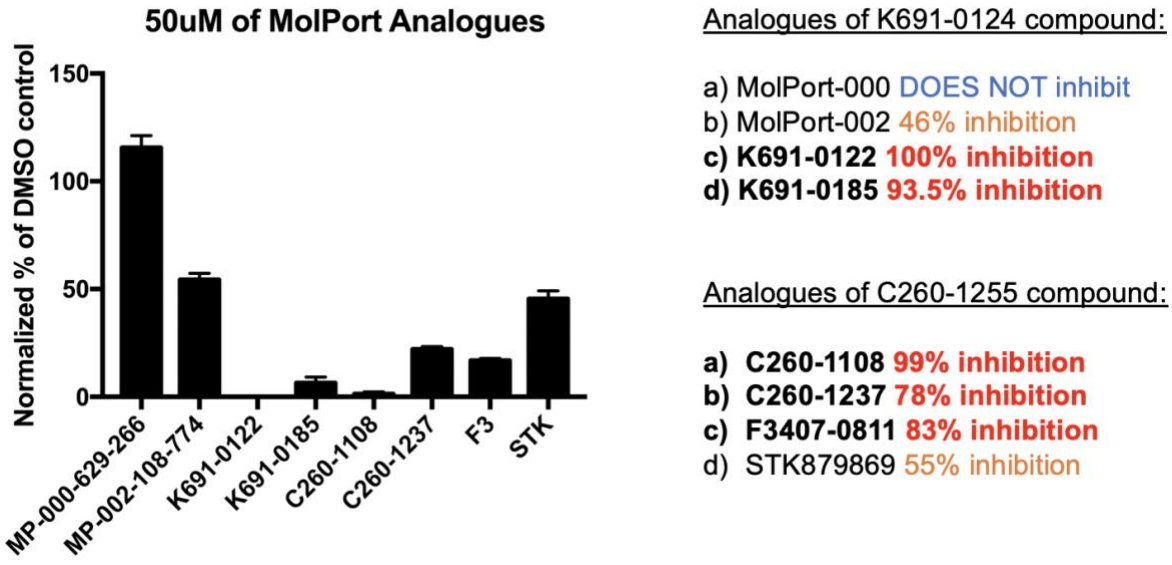

Appendix Figure 2. Effects of additional compounds derived from two screening hits (K691-0124 and C260-1255) on Bcl10-MALT1 interaction in vitro.

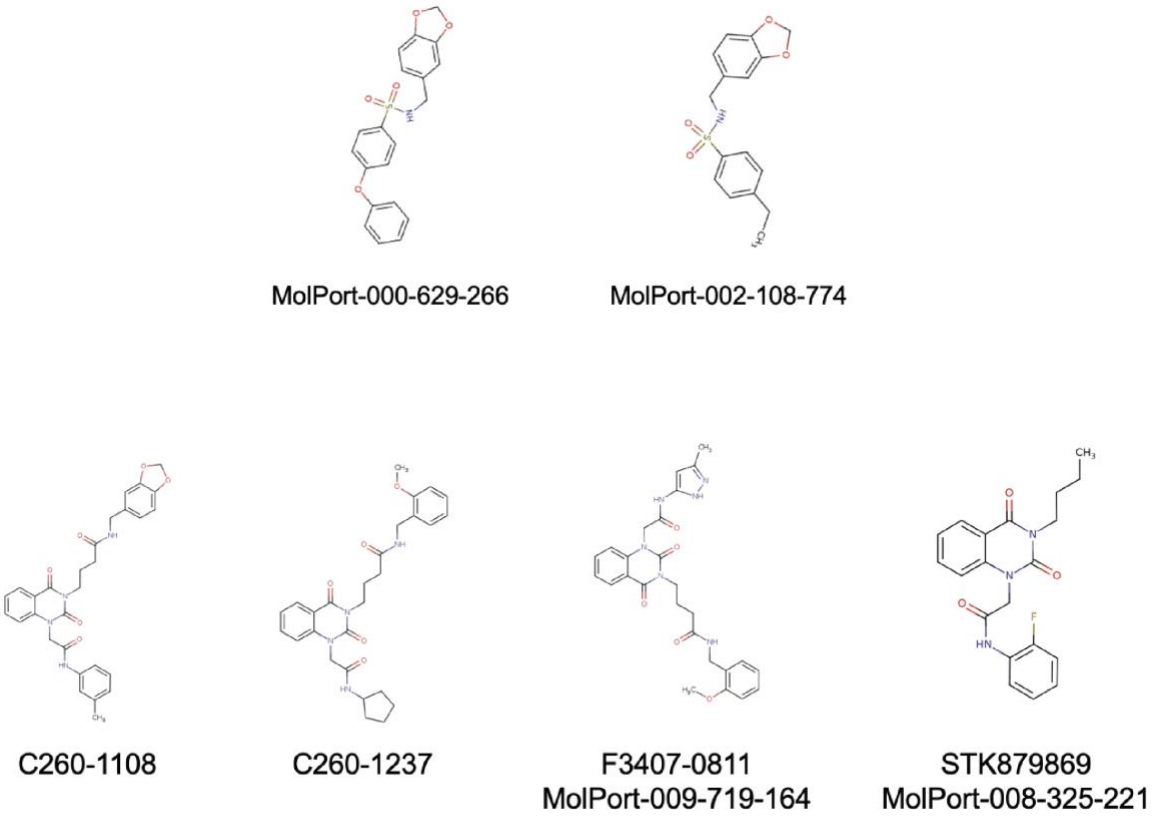

Appendix Figure 3. Structures of analogue compounds derived from two screening hits, K691-0124 and C260-1255.

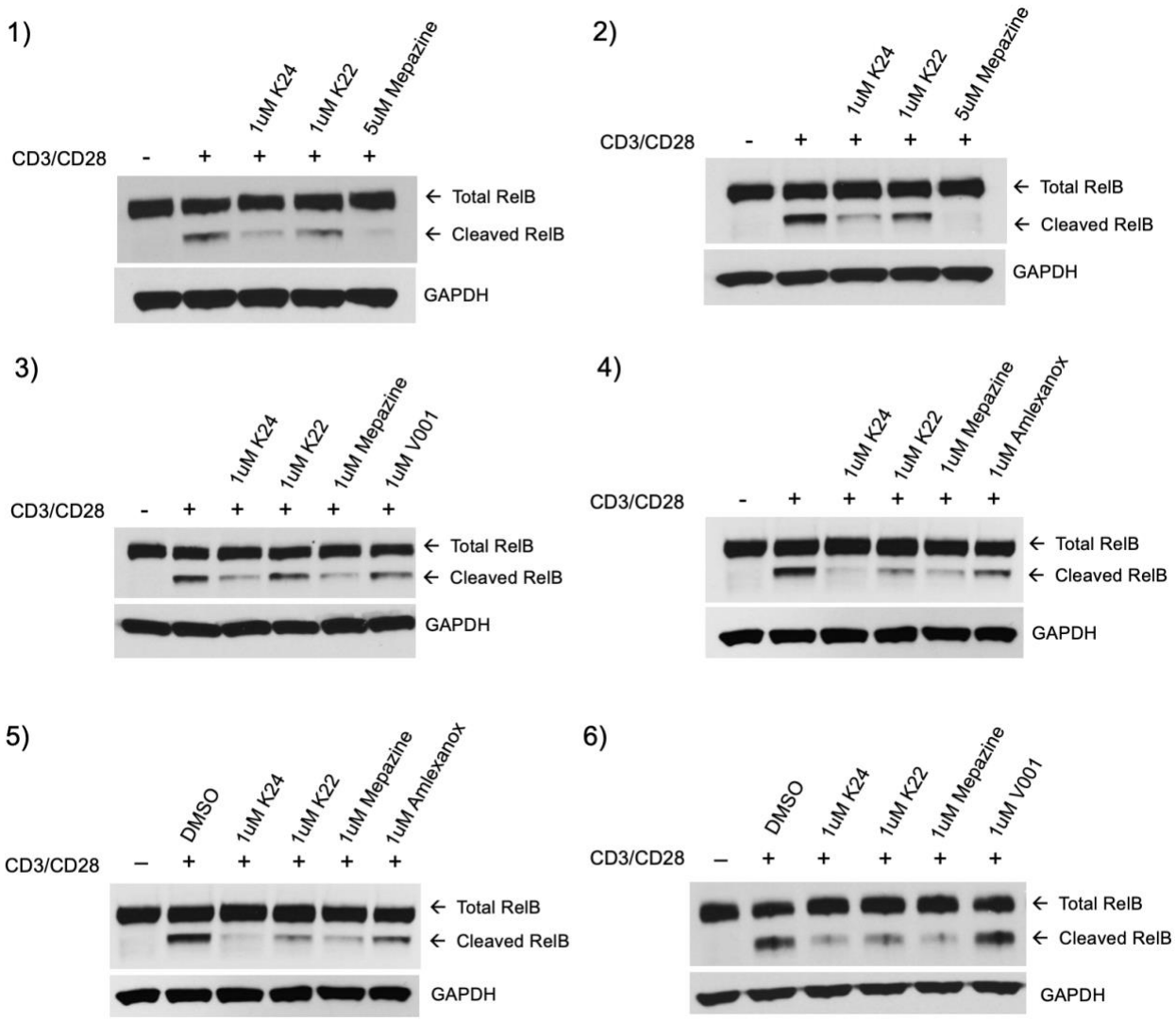

Appendix Figure 4. Repeat Western blot analyses of cleavage of RelB by MALT1 in Jurkat T cells.

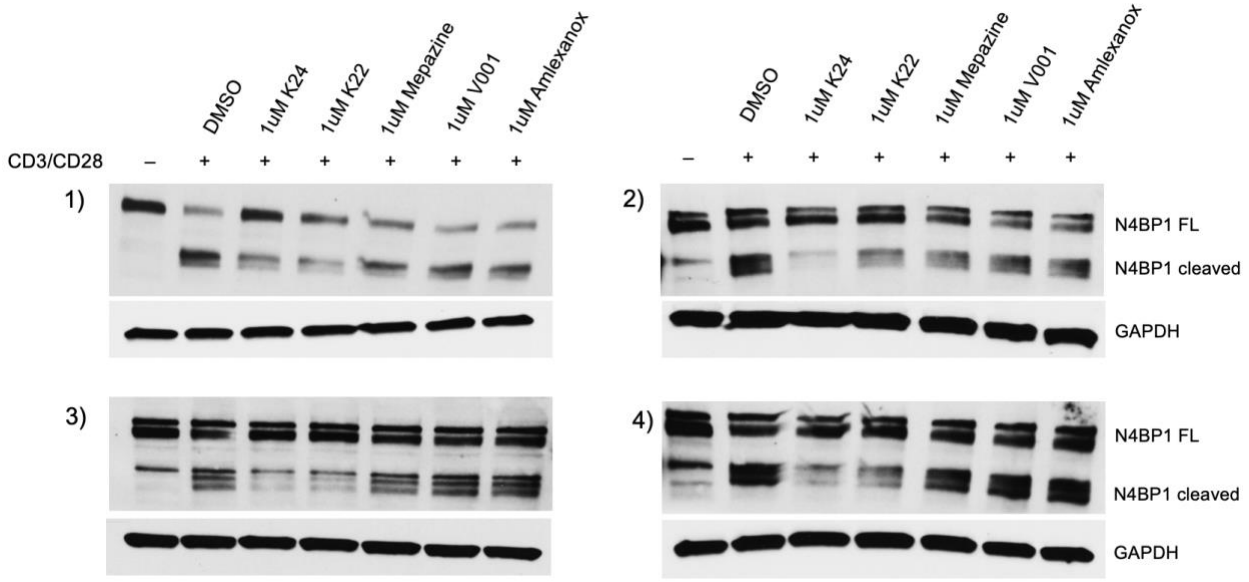

Appendix Figure 5. Repeat Western blot analyses of cleavage of N4BP1 by MALT1 in Jurkat T cells stimulated with CD3/CD28.

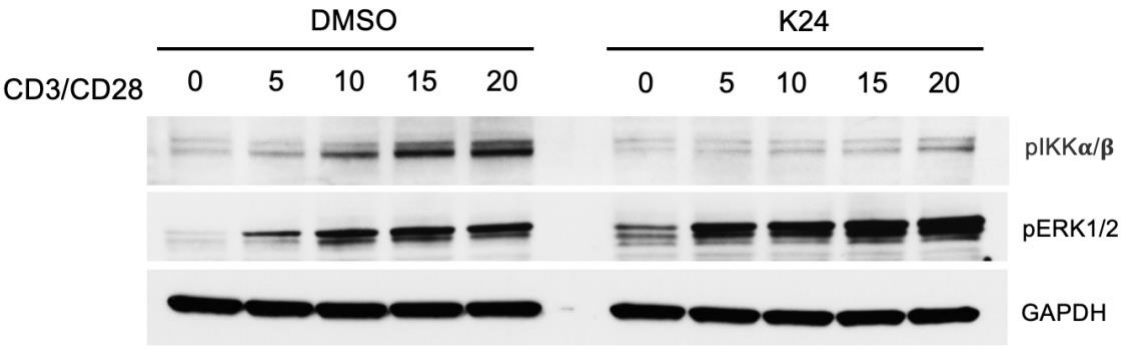
DMSO
K24
CD3/CD28
0
5
10
15
20
0
5
10
15
20
pIKKα/β
pERK1/2
GAPDH

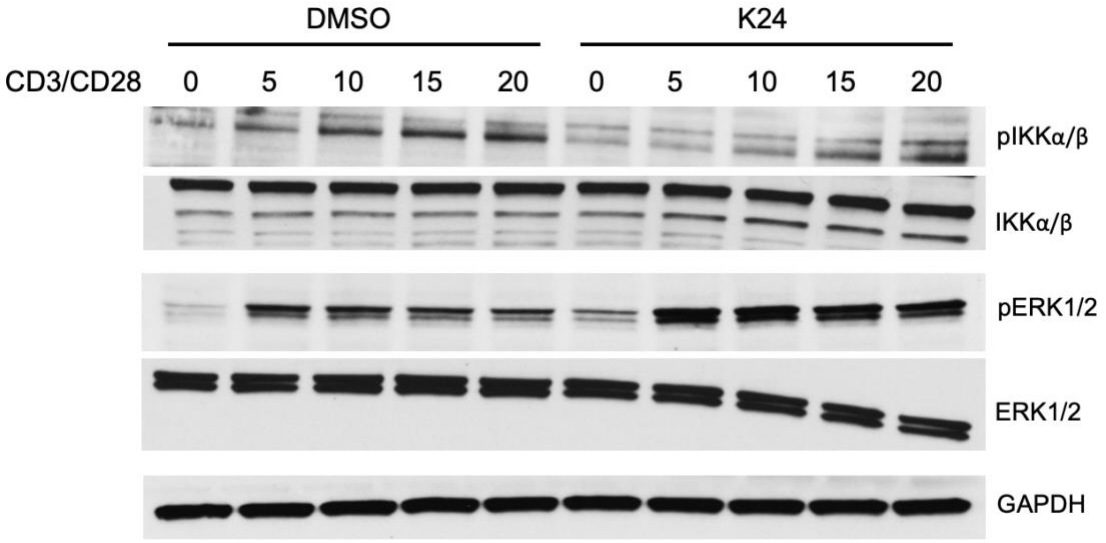
DMSO
K24
CD3/CD28
0
5
10
15
20
0
5
10
15
20
pIKKα/β
IKKα/β
pERK1/2
ERK1/2
GAPDH

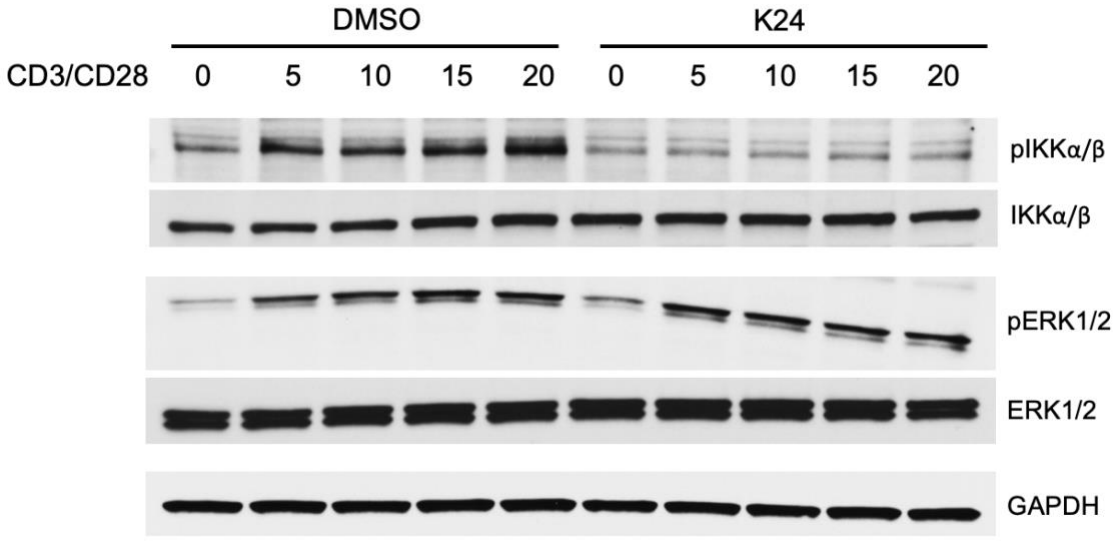
DMSO
K24
CD3/CD28
0
5
10
15
20
0
5
10
15
20
pIKKα/β
IKKα/β
pERK1/2
ERK1/2
GAPDH

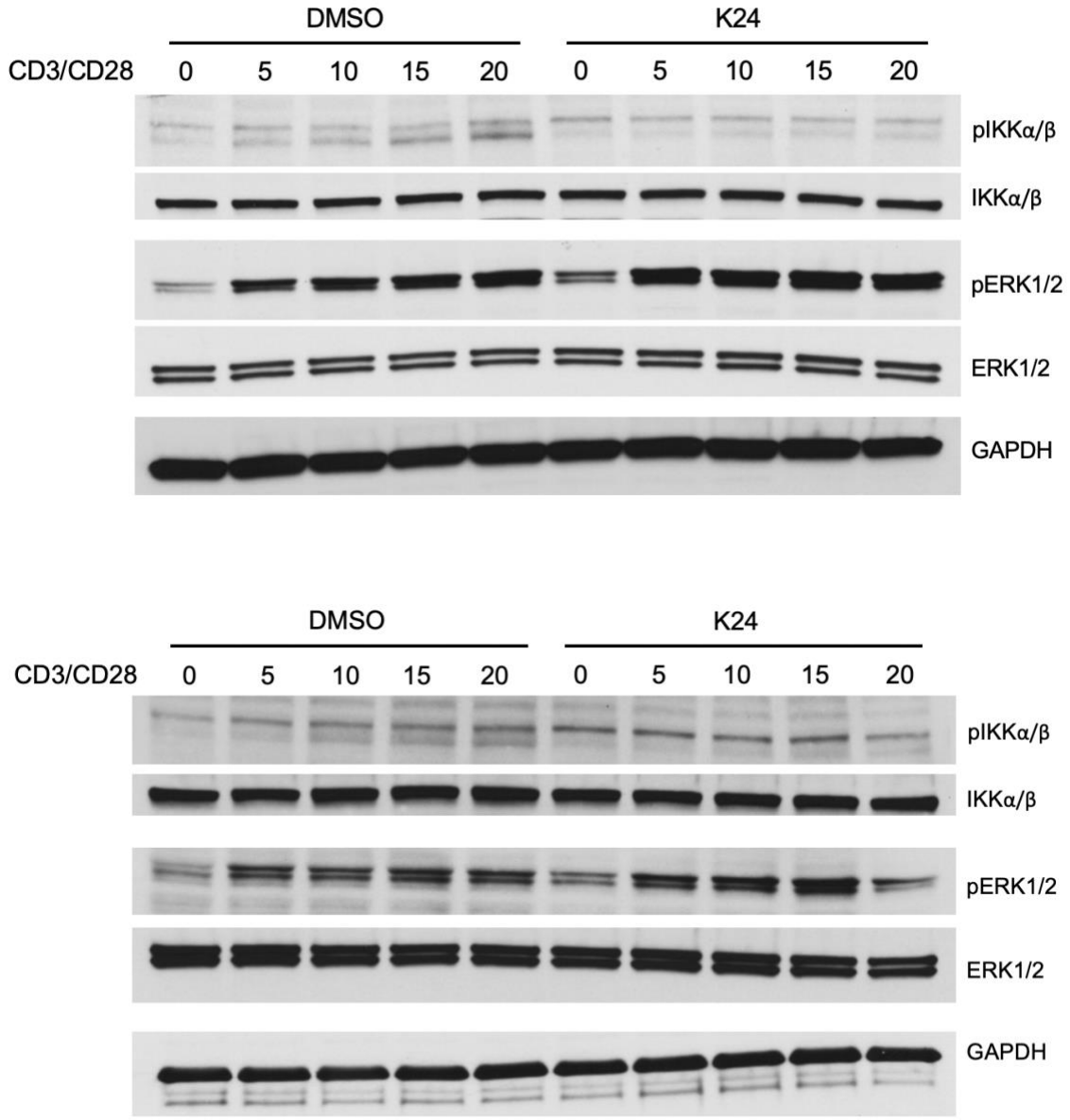

Appendix Figure 6. Repeat Western blot analyses of the effect of compound K691-0124 on the phosphorylation of IKK and ERK relative to total IKK and ERK in Jurkat T cells stimulated with CD3/CD28.

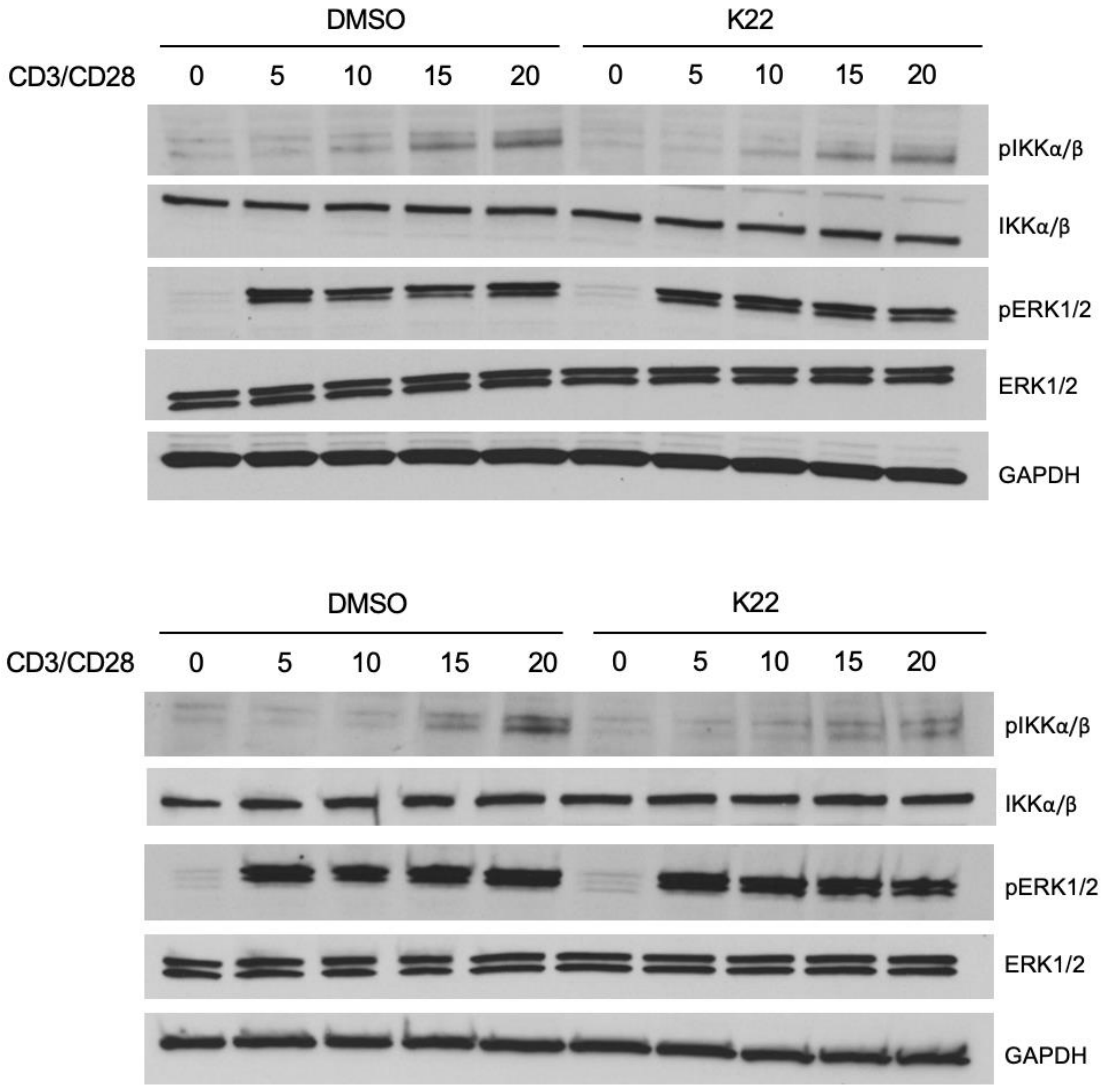
DMSO
K22
CD3/CD28
0
5
10
15
20
0
5
10
15
20
pIKKα/β
IKKα/β
pERK1/2
ERK1/2
GAPDH
DMSO
K22
CD3/CD28
0
5
10
15
20
0
5
10
15
20
pIKKα/β
IKKα/β
pERK1/2
ERK1/2
GAPDH

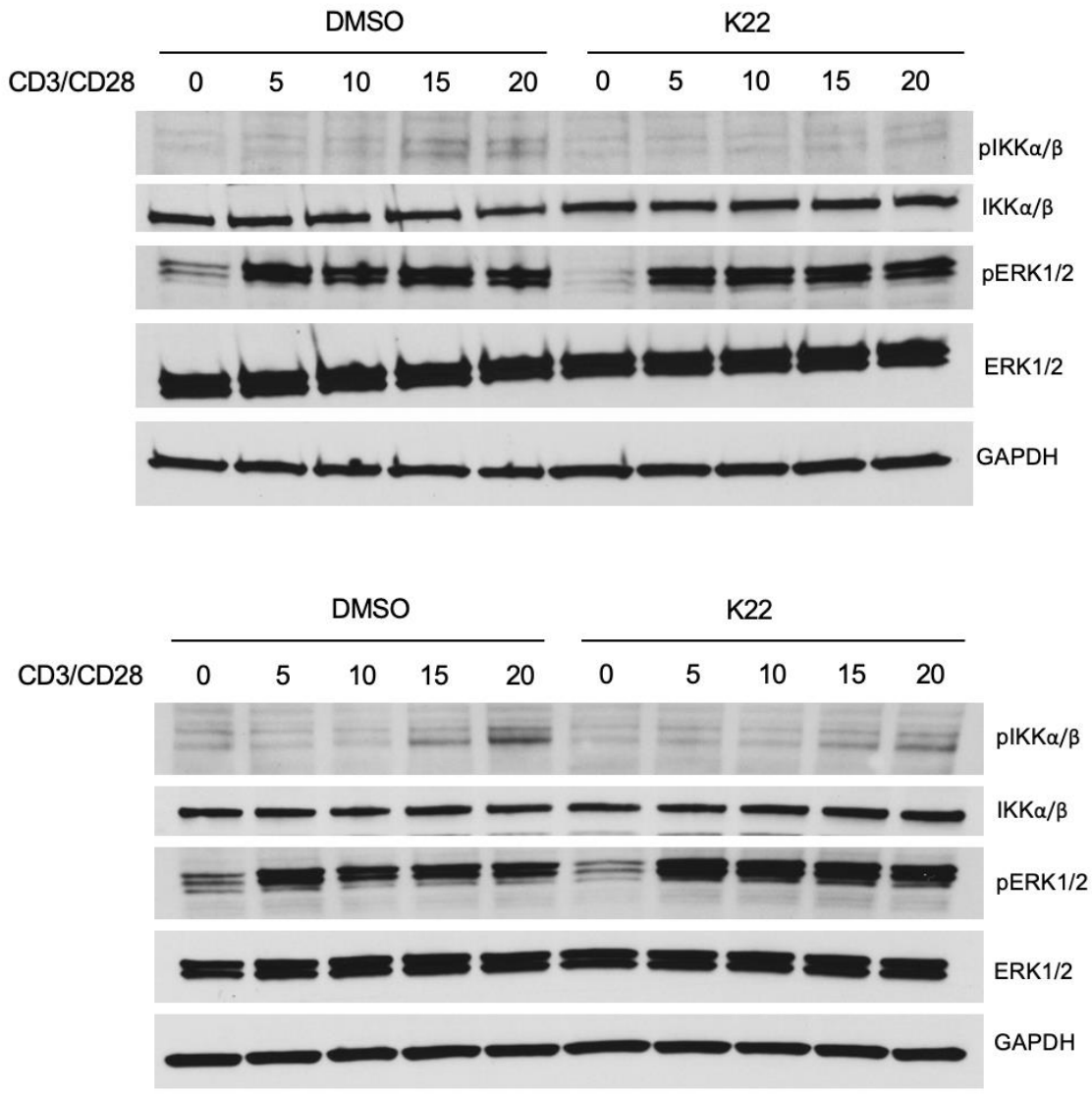

Appendix Figure 7. Repeat Western blot analyses of the effect of compound K691-0122 on the phosphorylation of IKK and ERK relative to total IKK and ERK in Jurkat T cells stimulated with CD3/CD28.

Bcl10only	Cell number	PLA spots	PLA signal/cell	Mean PLA signal/cell	STDEV
	117	4	0.0342	0.0199	0.0130
	113	1	0.0088		
	60	1	0.0167		
	Cell number	PLA spots	PLA signal/cell	Mean PLA signal/cell	STDEV
Carma1Bcl10	112	201	1.7946	2.0836	0.2636
	69	148	2.1449		
	90	208	2.3111		
Bcl10Malt1	Cell number	PLA spots	PLA signal/cell	Mean PLA signal/cell	STDEV
	132	21	0.1591	0.2536	0.0706
	109	32	0.2936		
	96	35	0.3646		
	131	33	0.2519		
	134	28	0.2090		
	111	27	0.2432		

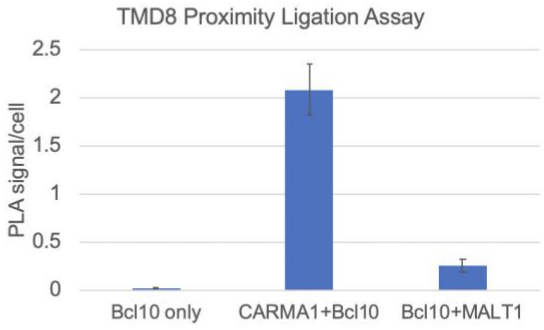

Appendix Figure 8. Quantification of PLA signals for CARMA1-Bcl10 and Bcl10-MALT1 interactions in TMD8 cells using CellProfiler.

Bibliography

1. Siegel RL, Miller KD, and Jemal A. Cancer statistics, 2020. *CA Cancer J Clin.* 2020;70(1):7-30.

2. Ran X, and Gestwicki JE. Inhibitors of protein-protein interactions (PPIs): an analysis of scaffold choices and buried surface area. *Current opinion in chemical biology.* 2018;44:75-86.

3. Azzarito V, Long K, Murphy NS, and Wilson AJ. Inhibition of alpha-helix-mediated protein-protein interactions using designed molecules. *Nat Chem.* 2013;5(3):161-73.

4. Bolanos-Garcia VM, Wu Q, Ochi T, Chirgadze DY, Sibanda BL, and Blundell TL. Spatial and temporal organization of multi-protein assemblies: achieving sensitive control in information-rich cell-regulatory systems. *Philos Trans A Math Phys Eng Sci.* 2012;370(1969):3023-39.

5. Cesa LC, Mapp AK, and Gestwicki JE. Direct and Propagated Effects of Small Molecules on Protein-Protein Interaction Networks. *Front Bioeng Biotechnol.* 2015;3:119.

6. Ekambaram P, Lee JL, Hubel NE, Hu D, Yerneni S, Campbell PG, et al. The CARMA3-Bcl10-MALT1 Signalosome Drives NFkappaB Activation and Promotes Aggressiveness in Angiotensin II Receptor-Positive Breast Cancer. *Cancer Res.* 2018;78(5):1225-40.

7. McAuley JR, Bailey KM, Ekambaram P, Klei LR, Kang H, Hu D, et al. MALT1 is a critical mediator of PAR1-driven NF-κB activation and metastasis in multiple tumor types. *Oncogene.* 2019.

8. Pan D, Jiang C, Ma Z, Blonska M, You MJ, and Lin X. MALT1 is required for EGFR-induced NF-kappaB activation and contributes to EGFR-driven lung cancer progression. *Oncogene.* 2016;35(7):919-28.

9. Jiang T, Grabiner B, Zhu Y, Jiang C, Li H, You Y, et al. CARMA3 is crucial for EGFR-Induced activation of NF-kappaB and tumor progression. *Cancer Res.* 2011;71(6):2183-92.

10. Pan D, Zhu Y, Zhou Z, Wang T, You H, Jiang C, et al. The CBM Complex Underwrites NF-kappaB Activation to Promote HER2-Associated Tumor Malignancy. *Mol Cancer Res.* 2016;14(1):93-102.

11. Coiffier B, Lepage E, Briere J, Herbrecht R, Tilly H, Bouabdallah R, et al. CHOP chemotherapy plus rituximab compared with CHOP alone in elderly patients with diffuse large-B-cell lymphoma. *N Engl J Med.* 2002;346(4):235-42.

12. Rosenwald A, Wright G, Chan WC, Connors JM, Campo E, Fisher RI, et al. The use of molecular profiling to predict survival after chemotherapy for diffuse large-B-cell lymphoma. *N Engl J Med.* 2002;346(25):1937-47.

13. Wright G, Tan B, Rosenwald A, Hurt EH, Wiestner A, and Staudt LM. A gene expression-based method to diagnose clinically distinct subgroups of diffuse large B cell lymphoma. *Proceedings of the National Academy of Sciences of the United States of America.* 2003;100(17):9991-6.

14. Alizadeh AA, Eisen MB, Davis RE, Ma C, Lossos IS, Rosenwald A, et al. Distinct types of diffuse large B-cell lymphoma identified by gene expression profiling. *Nature.* 2000;403(6769):503-11.

15. Pfeifer M, Grau M, Lenze D, Wenzel SS, Wolf A, Wollert-Wulf B, et al. PTEN loss defines a PI3K/AKT pathway-dependent germinal center subtype of diffuse large B-cell lymphoma. *Proceedings of the National Academy of Sciences of the United States of America.* 2013;110(30):12420-5.

16. Ngo VN, Davis RE, Lamy L, Yu X, Zhao H, Lenz G, et al. A loss-of-function RNA interference screen for molecular targets in cancer. *Nature.* 2006;441(7089):106-10.

17. Lamason RL, McCully RR, Lew SM, and Pomerantz JL. Oncogenic CARD11 mutations induce hyperactive signaling by disrupting autoinhibition by the PKC-responsive inhibitory domain. *Biochemistry.* 2010;49(38):8240-50.

18. Nacinovic-Duletic A, Stifter S, Dvornik S, Skunca Z, and Jonjic N. Correlation of serum IL-6, IL-8 and IL-10 levels with clinicopathological features and prognosis in patients with diffuse large B-cell lymphoma. *Int J Lab Hematol.* 2008;30(3):230-9.

19. Hashwah H, Bertram K, Stirm K, Stelling A, Wu CT, Kasser S, et al. The IL-6 signaling complex is a critical driver, negative prognostic factor, and therapeutic target in diffuse large B-cell lymphoma. *EMBO Mol Med.* 2019;11(10):e10576.

20. Lam LT, Wright G, Davis RE, Lenz G, Farinha P, Dang L, et al. Cooperative signaling through the signal transducer and activator of transcription 3 and nuclear factor-{kappa}B pathways in subtypes of diffuse large B-cell lymphoma. *Blood.* 2008;111(7):3701-13.

21. Ferch U, Kloo B, Gewies A, Pfander V, Duwel M, Peschel C, et al. Inhibition of MALT1 protease activity is selectively toxic for activated B cell-like diffuse large B cell lymphoma cells. *The Journal of experimental medicine.* 2009;206(11):2313-20.

22. Matsumoto R, Wang D, Blonska M, Li H, Kobayashi M, Pappu B, et al. Phosphorylation of CARMA1 plays a critical role in T Cell receptor-mediated NF-kappaB activation. *Immunity.* 2005;23(6):575-85.

23. Shinohara H, Yasuda T, Aiba Y, Sanjo H, Hamadate M, Watarai H, et al. PKC beta regulates BCR-mediated IKK activation by facilitating the interaction between TAK1 and CARMA1. *The Journal of experimental medicine.* 2005;202(10):1423-31.

24. Rueda D, and Thome M. Phosphorylation of CARMA1: the link(er) to NF-kappaB activation. *Immunity.* 2005;23(6):551-3.

25. Dai B, Grau M, Juilland M, Klener P, Horing E, Molinsky J, et al. B-cell receptor-driven MALT1 activity regulates MYC signaling in mantle cell lymphoma. *Blood.* 2017;129(3):333-46.

26. Rahal R, Frick M, Romero R, Korn JM, Kridel R, Chan FC, et al. Pharmacological and genomic profiling identifies NF-kappaB-targeted treatment strategies for mantle cell lymphoma. *Nat Med.* 2014;20(1):87-92.

27. Ngo VN, Young RM, Schmitz R, Jhavar S, Xiao W, Lim KH, et al. Oncogenically active MYD88 mutations in human lymphoma. *Nature.* 2011;470(7332):115-9.

28. Kataoka K, Nagata Y, Kitanaka A, Shiraishi Y, Shimamura T, Yasunaga J, et al. Integrated molecular analysis of adult T cell leukemia/lymphoma. *Nat Genet.* 2015;47(11):1304-15.

29. Saba NS, Wong DH, Tanios G, Iyer JR, Lobelle-Rich P, Dadashian EL, et al. MALT1 Inhibition Is Efficacious in Both Naive and Ibrutinib-Resistant Chronic Lymphocytic Leukemia. *Cancer Res.* 2017;77(24):7038-48.

30. da Silva Almeida AC, Abate F, Khiabanian H, Martinez-Escala E, Guitart J, Tensen CP, et al. The mutational landscape of cutaneous T cell lymphoma and Sezary syndrome. *Nat Genet.* 2015;47(12):1465-70.

31. Wang L, Ni X, Covington KR, Yang BY, Shiu J, Zhang X, et al. Genomic profiling of Sezary syndrome identifies alterations of key T cell signaling and differentiation genes. *Nat Genet.* 2015;47(12):1426-34.

32. Vallois D, Dobay MP, Morin RD, Lemonnier F, Missiaglia E, Juilland M, et al. Activating mutations in genes related to TCR signaling in angioimmunoblastic and other follicular helper T-cell-derived lymphomas. *Blood.* 2016;128(11):1490-502.

33. Buchbinder D, Stinson JR, Nugent DJ, Heurtier L, Suarez F, Sukumar G, et al. Mild B-cell lymphocytosis in patients with a CARD11 C49Y mutation. *J Allergy Clin Immunol.* 2015;136(3):819-21 e1.

34. Brohl AS, Stinson JR, Su HC, Badgett T, Jennings CD, Sukumar G, et al. Germline CARD11 Mutation in a Patient with Severe Congenital B Cell Lymphocytosis. *J Clin Immunol.* 2015;35(1):32-46.

35. Snow AL, Xiao W, Stinson JR, Lu W, Chaigne-Delalande B, Zheng L, et al. Congenital B cell lymphocytosis explained by novel germline CARD11 mutations. *The Journal of experimental medicine.* 2012;209(12):2247-61.

36. Ruland J, Duncan GS, Wakeham A, and Mak TW. Differential requirement for Malt1 in T and B cell antigen receptor signaling. *Immunity.* 2003;19(5):749-58.

37. Ruefli-Brasse AA, French DM, and Dixit VM. Regulation of NF-kappaB-dependent lymphocyte activation and development by paracaspase. *Science.* 2003;302(5650):1581-4.

38. Mc Guire C, Wieghofer P, Elton L, Muylaert D, Prinz M, Beyaert R, et al. Paracaspase MALT1 deficiency protects mice from autoimmune-mediated demyelination. *Journal of immunology.* 2013;190(6):2896-903.

39. Brustle A, Brenner D, Knobbe CB, Lang PA, Virtanen C, Hershenfield BM, et al. The NF-kappaB regulator MALT1 determines the encephalitogenic potential of Th17 cells. *The Journal of clinical investigation.* 2012;122(12):4698-709.

40. Gewies A, Gorka O, Bergmann H, Pechloff K, Petermann F, Jeltsch KM, et al. Uncoupling Malt1 threshold function from paracaspase activity results in destructive autoimmune inflammation. *Cell Rep.* 2014;9(4):1292-305.

41. Jaworski M, Marsland BJ, Gehrig J, Held W, Favre S, Luther SA, et al. Malt1 protease inactivation efficiently dampens immune responses but causes spontaneous autoimmunity. *The EMBO journal.* 2014;33(23):2765-81.

42. Bornancin F, Renner F, Touil R, Sic H, Kolb Y, Touil-Allaoui I, et al. Deficiency of MALT1 paracaspase activity results in unbalanced regulatory and effector T and B cell responses leading to multiorgan inflammation. *Journal of immunology.* 2015;194(8):3723-34.

43. Yu JW, Hoffman S, Beal AM, Dykon A, Ringenberg MA, Hughes AC, et al. MALT1 Protease Activity Is Required for Innate and Adaptive Immune Responses. *PloS one.* 2015;10(5):e0127083.

44. Molinero LL, Cubre A, Mora-Solano C, Wang Y, and Alegre ML. T cell receptor/CARMA1/NF-kappaB signaling controls T-helper (Th) 17 differentiation. *Proceedings of the National Academy of Sciences of the United States of America.* 2012;109(45):18529-34.

45. Jeltsch KM, Hu D, Brenner S, Zoller J, Heinz GA, Nagel D, et al. Cleavage of roquin and regnase-1 by the paracaspase MALT1 releases their cooperatively repressed targets to promote T(H)17 differentiation. *Nature immunology.* 2014;15(11):1079-89.

46. Staal J, Driege Y, Bekaert T, Demeyer A, Muyllaert D, Van Damme P, et al. T-cell receptor-induced JNK activation requires proteolytic inactivation of CYLD by MALT1. *The EMBO journal.* 2011;30(9):1742-52.

47. Sun Z, Arendt CW, Ellmeier W, Schaeffer EM, Sunshine MJ, Gandhi L, et al. PKC-theta is required for TCR-induced NF-kappaB activation in mature but not immature T lymphocytes. *Nature.* 2000;404(6776):402-7.

48. Ruland J, Duncan GS, Elia A, del Barco Barrantes I, Nguyen L, Plyte S, et al. Bcl10 is a positive regulator of antigen receptor-induced activation of NF-kappaB and neural tube closure. *Cell.* 2001;104(1):33-42.

49. Hara H, Wada T, Bakal C, Kozieradzki I, Suzuki S, Suzuki N, et al. The MAGUK family protein CARD11 is essential for lymphocyte activation. *Immunity.* 2003;18(6):763-75.

50. Wang D, You Y, Case SM, McAllister-Lucas LM, Wang L, DiStefano PS, et al. A requirement for CARMA1 in TCR-induced NF-kappa B activation. *Nature immunology.* 2002;3(9):830-5.

51. Egawa T, Albrecht B, Favier B, Sunshine MJ, Mirchandani K, O'Brien W, et al. Requirement for CARMA1 in antigen receptor-induced NF-kappa B activation and lymphocyte proliferation. *Current biology : CB.* 2003;13(14):1252-8.

52. Hailfinger S, Nogai H, Pelzer C, Jaworski M, Cabalzar K, Charton JE, et al. Malt1-dependent RelB cleavage promotes canonical NF-kappaB activation in lymphocytes and lymphoma cell lines. *Proceedings of the National Academy of Sciences of the United States of America.* 2011;108(35):14596-601.

53. Uehata T, Iwasaki H, Vandenbon A, Matsushita K, Hernandez-Cuellar E, Kuniyoshi K, et al. Malt1-induced cleavage of regnase-1 in CD4(+) helper T cells regulates immune activation. *Cell.* 2013;153(5):1036-49.

54. Mc Guire C, Elton L, Wieghofer P, Staal J, Voet S, Demeyer A, et al. Pharmacological inhibition of MALT1 protease activity protects mice in a mouse model of multiple sclerosis. *Journal of neuroinflammation.* 2014;11:124.

55. International Multiple Sclerosis Genetics C, Wellcome Trust Case Control C, Sawcer S, Hellenthal G, Pirinen M, Spencer CC, et al. Genetic risk and a primary role for cell-mediated immune mechanisms in multiple sclerosis. *Nature.* 2011;476(7359):214-9.

56. Mahanivong C, Chen HM, Yee SW, Pan ZK, Dong Z, and Huang S. Protein kinase C alpha-CARMA3 signaling axis links Ras to NF-kappa B for lysophosphatidic acid-induced urokinase plasminogen activator expression in ovarian cancer cells. *Oncogene.* 2008;27(9):1273-80.

57. Rehman AO, and Wang CY. CXCL12/SDF-1 alpha activates NF-kappaB and promotes oral cancer invasion through the Carma3/Bcl10/Malt1 complex. *Int J Oral Sci.* 2009;1(3):105-18.

58. Li Z, Qu L, Dong Q, Huang B, Li H, Tang Z, et al. Overexpression of CARMA3 in non-small-cell lung cancer is linked for tumor progression. *PloS one.* 2012;7(5):e36903.

59. Rawlings DJ, Sommer K, and Moreno-Garcia ME. The CARMA1 signalosome links the signalling machinery of adaptive and innate immunity in lymphocytes. *Nat Rev Immunol.* 2006;6(11):799-812.

60. Jattani RP, Tritapoe JM, and Pomerantz JL. Cooperative Control of Caspase Recruitment Domain-containing Protein 11 (CARD11) Signaling by an Unusual Array of Redundant Repressive Elements. *The Journal of biological chemistry.* 2016;291(16):8324-36.

61. Jattani RP, Tritapoe JM, and Pomerantz JL. Intramolecular Interactions and Regulation of Cofactor Binding by the Four Repressive Elements in the Caspase Recruitment Domain-containing Protein 11 (CARD11) Inhibitory Domain. *The Journal of biological chemistry.* 2016;291(16):8338-48.

62. Bertin J, Wang L, Guo Y, Jacobson MD, Poyet JL, Srinivasula SM, et al. CARD11 and CARD14 are novel caspase recruitment domain (CARD)/membrane-associated guanylate kinase (MAGUK) family members that interact with BCL10 and activate NF-kappa B. *The Journal of biological chemistry.* 2001;276(15):11877-82.

63. Gaide O, Martinon F, Micheau O, Bonnet D, Thome M, and Tschopp J. Carma1, a CARD-containing binding partner of Bcl10, induces Bcl10 phosphorylation and NF-kappaB activation. *FEBS letters.* 2001;496(2-3):121-7.

64. Chan W, Schaffer TB, and Pomerantz JL. A quantitative signaling screen identifies CARD11 mutations in the CARD and LATCH domains that induce Bcl10 ubiquitination and human lymphoma cell survival. *Mol Cell Biol.* 2013;33(2):429-43.

65. Yan M, Lee J, Schilbach S, Goddard A, and Dixit V. mE10, a novel caspase recruitment domain-containing proapoptotic molecule. *The Journal of biological chemistry.* 1999;274(15):10287-92.

66. Guiet C, and Vito P. Caspase recruitment domain (CARD)-dependent cytoplasmic filaments mediate bcl10-induced NF-kappaB activation. *The Journal of cell biology.* 2000;148(6):1131-40.

67. Koseki T, Inohara N, Chen S, Carrio R, Merino J, Hottiger MO, et al. CIPER, a novel NF kappaB-activating protein containing a caspase recruitment domain with homology to Herpesvirus-2 protein E10. *The Journal of biological chemistry.* 1999;274(15):9955-61.

68. Rossman JS, Stoicheva NG, Langel FD, Patterson GH, Lippincott-Schwartz J, and Schaefer BC. POLKADOTS are foci of functional interactions in T-Cell receptor-mediated signaling to NF-kappaB. *Molecular biology of the cell.* 2006;17(5):2166-76.

69. Langel FD, Jain NA, Rossman JS, Kingeter LM, Kashyap AK, and Schaefer BC. Multiple protein domains mediate interaction between Bcl10 and MALT1. *The Journal of biological chemistry.* 2008;283(47):32419-31.

70. Qiao Q, Yang C, Zheng C, Fontan L, David L, Yu X, et al. Structural architecture of the CARMA1/Bcl10/MALT1 signalosome: nucleation-induced filamentous assembly. *Molecular cell.* 2013;51(6):766-79.

71. David L, Li Y, Ma J, Garner E, Zhang X, and Wu H. Assembly mechanism of the CARMA1-BCL10-MALT1-TRAF6 signalosome. *Proceedings of the National Academy of Sciences of the United States of America.* 2018;115(7):1499-504.

72. Schlauderer F, Seeholzer T, Desfosses A, Gehring T, Strauss M, Hopfner KP, et al. Molecular architecture and regulation of BCL10-MALT1 filaments. *Nature communications.* 2018;9(1):4041.

73. Lucas PC, Yonezumi M, Inohara N, McAllister-Lucas LM, Abazeed ME, Chen FF, et al. Bcl10 and MALT1, independent targets of chromosomal translocation in malt lymphoma,

cooperate in a novel NF-kappa B signaling pathway. *The Journal of biological chemistry.* 2001;276(22):19012-9.

74. Uren AG, O'Rourke K, Aravind LA, Pisabarro MT, Seshagiri S, Koonin EV, et al. Identification of paracaspases and metacaspases: two ancient families of caspase-like proteins, one of which plays a key role in MALT lymphoma. *Molecular cell.* 2000;6(4):961-7.

75. Wegener E, Oeckinghaus A, Papadopoulou N, Lavitas L, Schmidt-Supprian M, Ferch U, et al. Essential role for IkappaB kinase beta in remodeling Carma1-Bcl10-Malt1 complexes upon T cell activation. *Molecular cell.* 2006;23(1):13-23.

76. Wiesmann C, Leder L, Blank J, Bernardi A, Melkko S, Decock A, et al. Structural determinants of MALT1 protease activity. *J Mol Biol.* 2012;419(1-2):4-21.

77. Cabalzar K, Pelzer C, Wolf A, Lenz G, Iwaszkiewicz J, Zoete V, et al. Monoubiquitination and activity of the paracaspase MALT1 requires glutamate 549 in the dimerization interface. *PloS one.* 2013;8(8):e72051.

78. Rebeaud F, Hailfinger S, Posevitz-Fejfar A, Tapernoux M, Moser R, Rueda D, et al. The proteolytic activity of the paracaspase MALT1 is key in T cell activation. *Nature immunology.* 2008;9(3):272-81.

79. Thome M. Multifunctional roles for MALT1 in T-cell activation. *Nat Rev Immunol.* 2008;8(7):495-500.

80. Coornaert B, Baens M, Heyninck K, Bekaert T, Haegman M, Staal J, et al. T cell antigen receptor stimulation induces MALT1 paracaspase-mediated cleavage of the NF-kappaB inhibitor A20. *Nature immunology.* 2008;9(3):263-71.

81. Juilland M, and Thome M. Holding All the CARDs: How MALT1 Controls CARMA/CARD-Dependent Signaling. *Frontiers in immunology.* 2018;9:1927.

82. Duwel M, Welteke V, Oeckinghaus A, Baens M, Kloo B, Ferch U, et al. A20 negatively regulates T cell receptor signaling to NF-kappaB by cleaving Malt1 ubiquitin chains. *Journal of immunology.* 2009;182(12):7718-28.

83. Klein T, Fung SY, Renner F, Blank MA, Dufour A, Kang S, et al. The paracaspase MALT1 cleaves HOIL1 reducing linear ubiquitination by LUBAC to dampen lymphocyte NF-kappaB signalling. *Nature communications.* 2015;6:8777.

84. Yu JW, Jeffrey PD, Ha JY, Yang X, and Shi Y. Crystal structure of the mucosa-associated lymphoid tissue lymphoma translocation 1 (MALT1) paracaspase region. *Proceedings of the National Academy of Sciences of the United States of America.* 2011;108(52):21004-9.

85. Sun L, Deng L, Ea CK, Xia ZP, and Chen ZJ. The TRAF6 ubiquitin ligase and TAK1 kinase mediate IKK activation by BCL10 and MALT1 in T lymphocytes. *Molecular cell.* 2004;14(3):289-301.

86. Oeckinghaus A, Wegener E, Welteke V, Ferch U, Arslan SC, Ruland J, et al. Malt1 ubiquitination triggers NF-kappaB signaling upon T-cell activation. *The EMBO journal.* 2007;26(22):4634-45.

87. Baens M, Bonsignore L, Somers R, Vanderheydt C, Weeks SD, Gunnarsson J, et al. MALT1 auto-proteolysis is essential for NF-kappaB-dependent gene transcription in activated lymphocytes. *PloS one.* 2014;9(8):e103774.

88. Ginster S, Bardet M, Unterreiner A, Malinverni C, Renner F, Lam S, et al. Two Antagonistic MALT1 Auto-Cleavage Mechanisms Reveal a Role for TRAF6 to Unleash MALT1 Activation. *PloS one.* 2017;12(1):e0169026.

89. Douanne T, Gavard J, and Bidere N. The paracaspase MALT1 cleaves the LUBAC subunit HOIL1 during antigen receptor signaling. *Journal of cell science.* 2016;129(9):1775-80.

90. Yamasoba D, Sato K, Ichinose T, Imamura T, Koepke L, Joas S, et al. N4BP1 restricts HIV-1 and its inactivation by MALT1 promotes viral reactivation. *Nat Microbiol.* 2019;4(9):1532-44.

91. Roschewski M, Staudt LM, and Wilson WH. Diffuse large B-cell lymphoma-treatment approaches in the molecular era. *Nat Rev Clin Oncol.* 2014;11(1):12-23.

92. Lam LT, Davis RE, Pierce J, Hepperle M, Xu Y, Hottelet M, et al. Small molecule inhibitors of IkappaB kinase are selectively toxic for subgroups of diffuse large B-cell lymphoma defined by gene expression profiling. *Clinical cancer research : an official journal of the American Association for Cancer Research.* 2005;11(1):28-40.

93. Dunleavy K, Pittaluga S, Czuczman MS, Dave SS, Wright G, Grant N, et al. Differential efficacy of bortezomib plus chemotherapy within molecular subtypes of diffuse large B-cell lymphoma. *Blood.* 2009;113(24):6069-76.

94. Field-Smith A, Morgan GJ, and Davies FE. Bortezomib (Velcadetrade mark) in the Treatment of Multiple Myeloma. *Ther Clin Risk Manag.* 2006;2(3):271-9.

95. Gu JJ, Hernandez-Ilizaliturri FJ, Kaufman GP, Czuczman NM, Mavis C, Skitzki JJ, et al. The novel proteasome inhibitor carfilzomib induces cell cycle arrest, apoptosis and potentiates the anti-tumour activity of chemotherapy in rituximab-resistant lymphoma. *Br J Haematol.* 2013;162(5):657-69.

96. Holkova B, Kmieciak M, Bose P, Yazbeck VY, Barr PM, Tombes MB, et al. Phase 1 trial of carfilzomib (PR-171) in combination with vorinostat (SAHA) in patients with relapsed or refractory B-cell lymphomas. *Leuk Lymphoma.* 2016;57(3):635-43.

97. Wu L, Adams M, Carter T, Chen R, Muller G, Stirling D, et al. lenalidomide enhances natural killer cell and monocyte-mediated antibody-dependent cellular cytotoxicity of rituximab-treated CD20+ tumor cells. *Clinical cancer research : an official journal of the American Association for Cancer Research.* 2008;14(14):4650-7.

98. Hernandez-Ilizaliturri FJ, Reddy N, Holkova B, Ottman E, and Czuczman MS. Immunomodulatory drug CC-5013 or CC-4047 and rituximab enhance antitumor activity in a severe combined immunodeficient mouse lymphoma model. *Clinical cancer research : an official journal of the American Association for Cancer Research.* 2005;11(16):5984-92.

99. Yang Y, Shaffer AL, 3rd, Emre NC, Ceribelli M, Zhang M, Wright G, et al. Exploiting synthetic lethality for the therapy of ABC diffuse large B cell lymphoma. *Cancer cell.* 2012;21(6):723-37.

100. Zhang LH, Kosek J, Wang M, Heise C, Schafer PH, and Chopra R. Lenalidomide efficacy in activated B-cell-like subtype diffuse large B-cell lymphoma is dependent upon IRF4 and cereblon expression. *Br J Haematol.* 2013;160(4):487-502.

101. Nowakowski GS, Chiappella A, Witzig TE, Spina M, Gascoyne RD, Zhang L, et al. ROBUST: Lenalidomide-R-CHOP versus placebo-R-CHOP in previously untreated ABC-type diffuse large B-cell lymphoma. *Future oncology.* 2016;12(13):1553-63.

102. Vitolo U, Witzig TE, Gascoyne RD, Scott DW, Zhang Q, Jurczak W, et al. ROBUST: First report of phase III randomized study of lenalidomide/R-CHOP (R2-CHOP) vs placebo/R-CHOP in previously untreated ABC-type diffuse large B-cell lymphoma. *Hematological Oncology.* 2019;37(S2):36-7.

103. Young RM, and Staudt LM. Targeting pathological B cell receptor signalling in lymphoid malignancies. *Nat Rev Drug Discov.* 2013;12(3):229-43.

104. Davis RE, Ngo VN, Lenz G, Tolar P, Young RM, Romesser PB, et al. Chronic active B-cell-receptor signalling in diffuse large B-cell lymphoma. *Nature.* 2010;463(7277):88-92.

105. Younes A, Sehn LH, Johnson P, Zinzani PL, Hong X, Zhu J, et al. Randomized Phase III Trial of Ibrutinib and Rituximab Plus Cyclophosphamide, Doxorubicin, Vincristine, and Prednisone in Non-Germinal Center B-Cell Diffuse Large B-Cell Lymphoma. *J Clin Oncol.* 2019;37(15):1285-95.

106. Kim SW, Oleksyn DW, Rossi RM, Jordan CT, Sanz I, Chen L, et al. Protein kinase C-associated kinase is required for NF-kappaB signaling and survival in diffuse large B-cell lymphoma cells. *Blood.* 2008;111(3):1644-53.

107. Naylor TL, Tang H, Ratsch BA, Enns A, Loo A, Chen L, et al. Protein kinase C inhibitor sotrastaurin selectively inhibits the growth of CD79 mutant diffuse large B-cell lymphomas. *Cancer Res.* 2011;71(7):2643-53.

108. Hailfinger S, Lenz G, Ngo V, Posvitz-Fejfar A, Rebeaud F, Guzzardi M, et al. Essential role of MALT1 protease activity in activated B cell-like diffuse large B-cell lymphoma. *Proceedings of the National Academy of Sciences of the United States of America.* 2009;106(47):19946-51.

109. Fontan L, Yang C, Kabaleeswaran V, Volpon L, Osborne MJ, Beltran E, et al. MALT1 small molecule inhibitors specifically suppress ABC-DLBCL in vitro and in vivo. *Cancer cell.* 2012;22(6):812-24.

110. Fontan L, Qiao Q, Hatcher JM, Casalena G, Us I, Teater M, et al. Specific covalent inhibition of MALT1 paracaspase suppresses B cell lymphoma growth. *The Journal of clinical investigation.* 2018;128(10):4397-412.

111. Lim SM, Jeong Y, Lee S, Im H, Tae HS, Kim BG, et al. Identification of beta-Lapachone Analogs as Novel MALT1 Inhibitors To Treat an Aggressive Subtype of Diffuse Large B-Cell Lymphoma. *J Med Chem.* 2015;58(21):8491-502.

112. Nagel D, Spranger S, Vincendeau M, Grau M, Raffegerst S, Kloo B, et al. Pharmacologic inhibition of MALT1 protease by phenothiazines as a therapeutic approach for the treatment of aggressive ABC-DLBCL. *Cancer cell.* 2012;22(6):825-37.

113. Lehmann HE, and Ban TA. The history of the psychopharmacology of schizophrenia. *Can J Psychiatry.* 1997;42(2):152-62.

114. Sarwer-Foner GJ, and Koranyi EK. The clinical investigation of pacatal in open psychiatric settings. *Can Med Assoc J.* 1957;77(5):450-9.

115. Schlauderer F, Lammens K, Nagel D, Vincendeau M, Eitelhuber AC, Verhelst SH, et al. Structural analysis of phenothiazine derivatives as allosteric inhibitors of the MALT1 paracaspase. *Angewandte Chemie.* 2013;52(39):10384-7.

116. Quancard J, Klein T, Fung SY, Renatus M, Hughes N, Israel L, et al. An allosteric MALT1 inhibitor is a molecular corrector rescuing function in an immunodeficient patient. *Nat Chem Biol.* 2019;15(3):304-13.

117. Fontan L, Hatcher J, Scott D, Qiao Q, Us I, Du G, et al. Chemically Induced Degradation of MALT1 to Treat B-Cell Lymphomas. *Blood.* 2019;134(Supplement_1):2073-.

118. Juilland M, and Thome M. Role of the CARMA1/BCL10/MALT1 complex in lymphoid malignancies. *Curr Opin Hematol.* 2016;23(4):402-9.

119. Wu G, Chai J, Suber TL, Wu JW, Du C, Wang X, et al. Structural basis of IAP recognition by Smac/DIABLO. *Nature.* 2000;408(6815):1008-12.

120. Liu Z, Sun C, Olejniczak ET, Meadows RP, Betz SF, Oost T, et al. Structural basis for binding of Smac/DIABLO to the XIAP BIR3 domain. *Nature.* 2000;408(6815):1004-8.

121. LaCasse EC, Mahoney DJ, Cheung HH, Plenchette S, Baird S, and Korneluk RG. IAP-targeted therapies for cancer. *Oncogene.* 2008;27(48):6252-75.

122. Oltersdorf T, Elmore SW, Shoemaker AR, Armstrong RC, Augeri DJ, Belli BA, et al. An inhibitor of Bcl-2 family proteins induces regression of solid tumours. *Nature.* 2005;435(7042):677-81.

123. Borkin D, He S, Miao H, Kempinska K, Pollock J, Chase J, et al. Pharmacologic inhibition of the Menin-MLL interaction blocks progression of MLL leukemia in vivo. *Cancer cell.* 2015;27(4):589-602.

124. Illendula A, Pulikkan JA, Zong H, Grembecka J, Xue L, Sen S, et al. Chemical biology. A small-molecule inhibitor of the aberrant transcription factor CBFbeta-SMMHC delays leukemia in mice. *Science.* 2015;347(6223):779-84.

125. Li X, Colvin T, Rauch JN, Acosta-Alvear D, Kampmann M, Dunyak B, et al. Validation of the Hsp70-Bag3 protein-protein interaction as a potential therapeutic target in cancer. *Mol Cancer Ther.* 2015;14(3):642-8.

126. Makley LN, McMenimen KA, DeVree BT, Goldman JW, McGlasson BN, Rajagopal P, et al. Pharmacological chaperone for alpha-crystallin partially restores transparency in cataract models. *Science.* 2015;350(6261):674-7.

127. Nero TL, Morton CJ, Holien JK, Wielens J, and Parker MW. Oncogenic protein interfaces: small molecules, big challenges. *Nat Rev Cancer.* 2014;14(4):248-62.

128. Arkin MR, Tang Y, and Wells JA. Small-molecule inhibitors of protein-protein interactions: progressing toward the reality. *Chemistry & biology.* 2014;21(9):1102-14.

129. O'Shannessy DJ, Brigham-Burke M, Soneson KK, Hensley P, and Brooks I. Determination of rate and equilibrium binding constants for macromolecular interactions using surface plasmon resonance: use of nonlinear least squares analysis methods. *Anal Biochem.* 1993;212(2):457-68.

130. Finkel T, Duc J, Fearon ER, Dang CV, and Tomaselli GF. Detection and modulation in vivo of helix-loop-helix protein-protein interactions. *The Journal of biological chemistry.* 1993;268(1):5-8.

131. Qiu L, and Dhe-Paganon S. Oligomeric structure of the MALT1 tandem Ig-like domains. *PloS one.* 2011;6(9):e23220.

132. Klemm S, Gutermuth J, Hultner L, Sparwasser T, Behrendt H, Peschel C, et al. The Bcl10-Malt1 complex segregates Fc epsilon RI-mediated nuclear factor kappa B activation and cytokine production from mast cell degranulation. *The Journal of experimental medicine.* 2006;203(2):337-47.

133. Gehring T, Seeholzer T, and Krappmann D. BCL10 - Bridging CARDs to Immune Activation. *Frontiers in immunology.* 2018;9:1539.

134. Lipinski CA, Lombardo F, Dominy BW, and Feeney PJ. Experimental and computational approaches to estimate solubility and permeability in drug discovery and development settings. *Adv Drug Deliv Rev.* 2001;46(1-3):3-26.

135. Bickerton GR, Paolini GV, Besnard J, Muresan S, and Hopkins AL. Quantifying the chemical beauty of drugs. *Nat Chem.* 2012;4(2):90-8.

136. Mullard A. Re-assessing the rule of 5, two decades on. *Nat Rev Drug Discov.* 2018;17(11):777.

137. Shultz MD. Two Decades under the Influence of the Rule of Five and the Changing Properties of Approved Oral Drugs. *J Med Chem.* 2019;62(4):1701-14.

138. Ahuja D, Saenz-Robles MT, and Pipas JM. SV40 large T antigen targets multiple cellular pathways to elicit cellular transformation. *Oncogene.* 2005;24(52):7729-45.

139. Martin YC. A bioavailability score. *J Med Chem.* 2005;48(9):3164-70.

140. Gleeson MP. Generation of a set of simple, interpretable ADMET rules of thumb. *J Med Chem.* 2008;51(4):817-34.

141. Daina A, Michielin O, and Zoete V. SwissADME: a free web tool to evaluate pharmacokinetics, drug-likeness and medicinal chemistry friendliness of small molecules. *Sci Rep.* 2017;7:42717.

142. Lovering F, Bikker J, and Humblet C. Escape from flatland: increasing saturation as an approach to improving clinical success. *J Med Chem*. 2009;52(21):6752-6.

143. Ritchie TJ, Ertl P, and Lewis R. The graphical representation of ADME-related molecule properties for medicinal chemists. *Drug Discov Today.* 2011;16(1-2):65-72.

144. Veber DF, Johnson SR, Cheng HY, Smith BR, Ward KW, and Kopple KD. Molecular properties that influence the oral bioavailability of drug candidates. *J Med Chem.* 2002;45(12):2615-23.

145. Mendez-Lucio O, and Medina-Franco JL. The many roles of molecular complexity in drug discovery. *Drug Discov Today.* 2017;22(1):120-6.

146. Ertl P, and Schuffenhauer A. Estimation of synthetic accessibility score of drug-like molecules based on molecular complexity and fragment contributions. *J Cheminform.* 2009;1(1):8.

147. Arkin MR, Glicksman MA, Fu H, Havel JJ, and Du Y. In: Sittampalam GS, Grossman A, Brimacombe K, Arkin M, Auld D, Austin CP, et al. eds. *Assay Guidance Manual*. Bethesda (MD); 2004.

148. Maurer LM, Tomasini-Johansson BR, Ma W, Annis DS, Eickstaedt NL, Ensenberger MG, et al. Extended binding site on fibronectin for the functional upstream domain of protein F1 of Streptococcus pyogenes. *The Journal of biological chemistry.* 2010;285(52):41087-99.

149. Maurer LM, Ma W, Eickstaedt NL, Johnson IA, Tomasini-Johansson BR, Annis DS, et al. Ligation of the fibrin-binding domain by beta-strand addition is sufficient for expansion of soluble fibronectin. *The Journal of biological chemistry.* 2012;287(16):13303-12.

150. Dickson HM, Wilbur A, Reinke AA, Young MA, and Vojtek AB. Targeted inhibition of the Shroom3-Rho kinase protein-protein interaction circumvents Nogo66 to promote axon outgrowth. *BMC Neurosci.* 2015;16:34.

151. Meanwell NA. Improving Drug Design: An Update on Recent Applications of Efficiency Metrics, Strategies for Replacing Problematic Elements, and Compounds in Nontraditional Drug Space. *Chem Res Toxicol.* 2016;29(4):564-616.

152. Liao W, Lin JX, and Leonard WJ. Interleukin-2 at the crossroads of effector responses, tolerance, and immunotherapy. *Immunity.* 2013;38(1):13-25.

153. Nagel D, and Krappmann D. Detection of Recombinant and Cellular MALT1 Paracaspase Activity. *Methods in molecular biology.* 2015;1280:239-46.

154. Nagel D, Bognar M, Eitelhuber AC, Kutzner K, Vincendeau M, and Krappmann D. Combinatorial BTK and MALT1 inhibition augments killing of CD79 mutant diffuse large B cell lymphoma. *Oncotarget.* 2015;6(39):42232-42.

155. Afonina IS, Elton L, Carpentier I, and Beyaert R. MALT1 - a universal soldier: multiple strategies to ensure NF-kappaB activation and target gene expression. *FEBS J.* 2015;282(17):3286-97.

156. Delhase M, Hayakawa M, Chen Y, and Karin M. Positive and negative regulation of IkappaB kinase activity through IKKbeta subunit phosphorylation. *Science.* 1999;284(5412):309-13.

157. Mercurio F, Murray BW, Shevchenko A, Bennett BL, Young DB, Li JW, et al. IkappaB kinase (IKK)-associated protein 1, a common component of the heterogeneous IKK complex. *Mol Cell Biol.* 1999;19(2):1526-38.

158. Sun L, and Chen ZJ. The novel functions of ubiquitination in signaling. *Curr Opin Cell Biol.* 2004;16(2):119-26.

159. Paul S, Traver MK, Kashyap AK, Washington MA, Latoche JR, and Schaefer BC. T cell receptor signals to NF-kappaB are transmitted by a cytosolic p62-Bcl10-Malt1-IKK signalosome. *Sci Signal.* 2014;7(325):ra45.

160. Rosebeck S, Rehman AO, Lucas PC, and McAllister-Lucas LM. From MALT lymphoma to the CBM signalosome: three decades of discovery. *Cell cycle.* 2011;10(15):2485-96.

161. Hayden MS, and Ghosh S. NF-kappaB, the first quarter-century: remarkable progress and outstanding questions. *Genes Dev.* 2012;26(3):203-34.

162. Hayden MS, and Ghosh S. Signaling to NF-kappaB. *Genes Dev.* 2004;18(18):2195-224.

163. Karin M. How NF-kappaB is activated: the role of the IkappaB kinase (IKK) complex. *Oncogene.* 1999;18(49):6867-74.

164. Israel A. The IKK complex, a central regulator of NF-kappaB activation. *Cold Spring Harbor perspectives in biology.* 2010;2(3):a000158.

165. Phelan JD, Young RM, Webster DE, Roulland S, Wright GW, Kasbekar M, et al. A multiprotein supercomplex controlling oncogenic signalling in lymphoma. *Nature.* 2018;560(7718):387-91.

166. Bardet M, Unterreiner A, Malinverni C, Lafossas F, Vedrine C, Boesch D, et al. The T-cell fingerprint of MALT1 paracaspase revealed by selective inhibition. *Immunol Cell Biol.* 2018;96(1):81-99.

167. Gehring T, Erdmann T, Rahm M, Grass C, Flatley A, O'Neill TJ, et al. MALT1 Phosphorylation Controls Activation of T Lymphocytes and Survival of ABC-DLBCL Tumor Cells. *Cell Rep.* 2019;29(4):873-88 e10.

168. Lenz G, Davis RE, Ngo VN, Lam L, George TC, Wright GW, et al. Oncogenic CARD11 mutations in human diffuse large B cell lymphoma. *Science.* 2008;319(5870):1676-9.

169. Compagno M, Lim WK, Grunn A, Nandula SV, Brahmachary M, Shen Q, et al. Mutations of multiple genes cause deregulation of NF-kappaB in diffuse large B-cell lymphoma. *Nature.* 2009;459(7247):717-21.

170. Crouch SP, Kozlowski R, Slater KJ, and Fletcher J. The use of ATP bioluminescence as a measure of cell proliferation and cytotoxicity. *J Immunol Methods.* 1993;160(1):81-8.

171. Philippar U, Lu T, Vloemans N, Bekkers M, van Nuffel L, Gaudiano M, et al. DISCOVERY OF A NOVEL, POTENTIAL FIRST-IN-CLASS MALT1 PROTEASE INHIBITOR FOR THE TREATMENT OF B CELL LYMPHOMAS. *Hematological Oncology.* 2019;37(S2):128-.

172. Gustafsdottir SM, Schallmeiner E, Fredriksson S, Gullberg M, Soderberg O, Jarvius M, et al. Proximity ligation assays for sensitive and specific protein analyses. *Anal Biochem.* 2005;345(1):2-9.

173. Duarte JG, and Blackburn JM. Advances in the development of human protein microarrays. *Expert Rev Proteomics.* 2017;14(7):627-41.

174. Redfern WS, Wakefield ID, Prior H, Pollard CE, Hammond TG, and Valentin JP. Safety pharmacology--a progressive approach. *Fundam Clin Pharmacol.* 2002;16(3):161-73.

175. Smith DA, and Schmid EF. Drug withdrawals and the lessons within. *Curr Opin Drug Discov Devel.* 2006;9(1):38-46.

176. Bowes J, Brown AJ, Hamon J, Jarolimek W, Sridhar A, Waldron G, et al. Reducing safety-related drug attrition: the use of in vitro pharmacological profiling. *Nat Rev Drug Discov.* 2012;11(12):909-22.

177. Hwang TJ, Carpenter D, Lauffenburger JC, Wang B, Franklin JM, and Kesselheim AS. Failure of Investigational Drugs in Late-Stage Clinical Development and Publication of Trial Results. *JAMA Intern Med.* 2016;176(12):1826-33.

178. Liu W, Guo W, Hang N, Yang Y, Wu X, Shen Y, et al. MALT1 inhibitors prevent the development of DSS-induced experimental colitis in mice via inhibiting NF-kappaB and NLRP3 inflammasome activation. *Oncotarget.* 2016;7(21):30536-49.

179. Van Nuffel E, Staal J, Baudelet G, Haegman M, Driege Y, Hochepied T, et al. MALT1 targeting suppresses CARD14-induced psoriatic dermatitis in mice. *EMBO Rep.* 2020:e49237.

180. Di Pilato M, Kim EY, Cadilha BL, Prussmann JN, Nasrallah MN, Seruggia D, et al. Targeting the CBM complex causes Treg cells to prime tumours for immune checkpoint therapy. *Nature.* 2019;570(7759):112-6.